Sérgio Alves da Silva

Novel insights to develop and characterize aerobic granular sludge for wastewater treatment

UMinho | 2022

Universidade do Minho
Escola de Engenharia

Sérgio Alves da Silva

Novel insights to develop and characterize aerobic granular sludge for wastewater treatment

julho de 2022

Universidade do Minho
Escola de Engenharia

Sérgio Alves da Silva

Novel insights to develop and characterize aerobic granular sludge for wastewater treatment

Tese de Doutoramento
Doutoramento em Engenharia Química e Biológica

Trabalho efetuado sob a orientação da
Doutora Daniela Patrícia Bernardino Mesquita
e da
Professora Doutora Maria Madalena dos Santos Alves

julho de 2022

DIREITOS DE AUTOR E CONDIÇÕES DE UTILIZAÇÃO DO TRABALHO POR TERCEIROS

Este é um trabalho académico que pode ser utilizado por terceiros desde que respeitadas as regras e boas práticas internacionalmente aceites, no que concerne aos direitos de autor e direitos conexos.

Assim, o presente trabalho pode ser utilizado nos termos previstos na licença abaixo indicada.

Caso o utilizador necessite de permissão para poder fazer um uso do trabalho em condições não previstas no licenciamento indicado, deverá contactar o autor, através do RepositóriUM da Universidade do Minho.

Licença concedida aos utilizadores deste trabalho



Atribuição-NãoComercial-SemDerivações
CC BY-NC-ND

https://creativecommons.org/licenses/by-nc-nd/4.0/

AGRADECIMENTOS

Gostaria de agradecer à Doutora Daniela Mesquita e à prof. Doutora Madalena Alves. Daniela, obrigado por me teres colocado o desafio de realizar o doutoramento neste tema em particular, completamente novo para mim, e teres acreditado que seria capaz de o concluir com sucesso. Madalena, obrigado por teres concedido todas as oportunidade para crescer como investigador desde que cheguei ao grupo BRIDGE em 2010. A ambas, sou muito grato por todas as sugestões, recomendações e motivação para a realização deste trabalho. Em segundo lugar, gostaria de agradecer ao prof. Doutor Eugénio Ferreira e ao Doutor António Amaral, pelas valiosas colaborações ao longo deste doutoramento. Um agradecimento muito especial à Doutora Ângeles Val del Rio pela ajuda e ensinamentos sobre operação de reatores e processos de granulação. Não poderia deixar de agradecer à Doutora Diana Sousa, por me ter dado a oportunidade de entrar no mundo da investigação científica e que culminou na realização desta tese. À Doutora Ana Júlia Cavaleiro agradeço todos os teus ensinamentos e pensamento científico que sempre tentei colocar em prática na realização deste trabalho. Agradeço a todos os amigos e colegas de laboratório (LBA e LBSS) por todos os momentos de partilha, solidariedade e entreajuda. Gostaria de estender este agradecimento a todo o pessoal técnico do CEB pela disponibilidade e apoio. Obrigado Jorge, João, Cátia, Carla, Rita P., Débora, Ana Luísa e Rita M., pela vossa amizade e por todos os bons momentos passados dentro e fora do laboratório. Um agradecimento muito especial à Sónia e à Salomé pela vossa preciosa amizade. À minha família, a quem dedico esta tese, muito obrigado. Por fim, a ti Diana, quero agradecer-te por teres sido o meu suporte nos momentos de dúvida e incerteza. Obrigado pelo teu apoio e pela tua motivação.

This PhD was supported by the Portuguese Foundation for Science and Technology (FCT) through the grant SFRH/BD/122623/2016 and the exceptional grant for mitigation of the effects of covid-19 COVID/BD/151748/2021. Additionally, this study was supported by FCT under the scope of the strategic funding of UIDB/04469/2020 unit, and LABBELS - associate laboratory in biotechnology and bioengineering and microelectromechanical systems.

STATEMENT OF INTEGRITY

I hereby declare having conducted this academic work with integrity. I confirm that I have not used plagiarism or any form of undue use of information or falsification of results along the process leading to its elaboration.

I further declare that I have fully acknowledged the Code of Ethical Conduct of the University of Minho.

Novas perceções para desenvolver e caracterizar lama granular aeróbia para o tratamento de águas residuais

Sumário

A lama granular aeróbia (LGA) é uma nova tecnologia compacta que apresenta potencial de sustentabilidade em relação aos processos aeróbios convencionais. No entanto, o extenso período necessário para a formação dos grânulos, bem como a sua estabilidade a longo prazo, são ainda limitações para o estabelecimento mais amplo e robusto desta tecnologia. A caracterização e a avaliação de LGA tem suscitado interesse como forma de aumentar a nossa compreensão e controlo do processo. Nesta tese, métodos de análise quantitativa de imagens (AQI) foram usados para definir e quantificar as mudanças morfológicas das lamas durante o processo de granulação e avaliar a estabilidade dos grânulos sob condições operacionais específicas. Para tal, a granulação foi inicialmente monitorizada em dois reatores descontínuos sequenciais com diferentes cargas orgânicas e velocidades mínimas impostas de sedimentação da lama. Enquanto os padrões de estratificação e a morfologia dos pequenos grânulos iniciais revelaram o ponto de mudança da floculação para a granulação, a análise estatística multivariada dos dados da AQI revelou o estado de agregação das lamas e maturação dos grânulos, permitindo antecipar as propriedades de sedimentação das lamas. Além disso, uma relação complexa entre remoção de nutrientes e morfologia das lamas foi avaliada durante a granulação sob diferentes razões de carência química de oxigénio (CQO) e azoto (CQO/N), e dinâmicas de lavagem das lamas. Baixas eficiências de remoção de azoto, durante a formação dos grânulos aeróbios, favoreceram o desenvolvimento de *bulking* viscoso e filamentoso, o que prejudicou a granulação nos estágios iniciais do processo. A estabilidade e a atividade dos grânulos maduros, como consórcios microbianos para a bioaumentação (i.e., grânulos bioativos), foram avaliadas em sistemas de LGA apresentando baixa capacidade de remoção de nutrientes. A morfologia dos grânulos bioativos e grânulos inatos foram fundamentais para o sucesso da bioaumentação. A estabilidade das LGA é um problema limitante nestes sistemas. Portanto, a estabilidade dos grânulos maduros a longo prazo foi avaliada na presença de concentrações crescente de oleato. Os dados de AQI revelaram que a adsorção do oleato às LGA influenciou os padrões de distribuição dos grânulos, induzindo a lavagem seletiva dos grânulos menores devido à sua maior área de superfície específica. Além disso, a análise de componentes principais identificou as alterações morfológicas das LGA, induzidas pelo oleato, correlacionando-as com a diminuição do desempenho do reator. No geral, a AQI aumentou a nossa compreensão sobre a transição morfológica das lamas durante o processo de granulação, bem como a sua estabilidade sob condições operacionais definidas, destacando o potencial da AQI para monitorizar e regular sistemas de LGA.

Palavras-chave: reatores descontínuo sequencial, lama aeróbia, granulação, microscopia, análise quantitativa de imagens, análise estatística multivariada.

Novel insights to develop and characterize aerobic granular sludge for wastewater treatment

Summary

Aerobic granular sludge (AGS) is a novel compact technology presenting sustainability potential over conventional aerobic processes. However, a long start-up for granules formation and their long-term stability are still the main issues for a wider establishment of this technology. AGS characterization and evaluation have gained attention to improve our understanding and process control. In this thesis, quantitative image analysis (QIA) methods were used to define and quantify the morphological changes of sludge during granulation processes and evaluate the stability of granules under specified operating conditions. For this purpose, granulation was initially monitored in two sequencing batch reactors (SBR) at different organic loading rates (OLR) and minimal imposed sludge settling velocities (MISSV). While the stratification patterns and the morphology of the initial small granules revealed the turning point from flocculation to granulation, multivariate statistical analysis of the QIA data revealed the sludge aggregation and granules maturation status and anticipated the sludge settling properties. Moreover, a complex relationship between nutrient removal and sludge morphology was assessed during granulation under different chemical oxygen demand (COD)-to-nitrogen ratios (COD/N) and washout dynamics. Poor nitrogen removal efficiencies during the formation of aerobic granules favoured the development of viscous and filamentous bulking, which impaired the granulation process at the early stages. The stability and activity of mature granules as bioaugmenting microbial consortia (i.e., bioactive granules) were evaluated in AGS systems exhibiting poor nutrient removal capabilities. The morphology of the bioactive granules and innate AGS were fundamental for bioaugmentation success in AGS systems. The stability of AGS is a bottleneck of AGS systems. Thus, the long-term stability of mature granules was evaluated in the presence of increasing oleate concentration. QIA data revealed that oleate adsorption onto AGS influenced granules distribution patterns, inducing selective sludge washout of small granules owing to their larger specific surface area. Moreover, principal component analysis (PCA) revealed the morphological changes of the AGS due to oleate, which were correlated with decreasing reactor performance. Overall, QIA increased our understanding of the sludge morphological transition during the granulation process, as well as their stability under defined operating conditions, highlighting the potential of QIA to monitor and regulate AGS systems.

Keywords: sequencing batch reactors, aerobic sludge, granulation, microscopy, quantitative image analysis, multivariate statistical analysis.

TABLE OF CONTENTS

Chapter 1 CONTEXT, AIM AND THESIS OUTLINE 1
1.1. CONTEXT 1
1.2. AIM 3
1.3. THESIS OUTLINE 3
1.4. REFERENCES 4
Chapter 2 GENERAL INTRODUCTION 6
2.1. THE IMPORTANCE OF BIOLOGICAL WASTEWATER TREATMENT 6
2.2. ANAEROBIC DIGESTION SYSTEMS 7
2.3. CONVENTIONAL ACTIVATED SLUDGE SYSTEMS 9
2.4. AEROBIC GRANULAR SLUDGE SYSTEMS 11
2.4.1. Aerobic granules 12
2.4.2. Granulation process 13
2.4.3. Factors affecting aerobic granulation 14
2.4.4. Microbial groups for nutrient removal in aerobic granules 17
2.4.5. Monitoring AGS 18
2.5. QUANTITATIVE IMAGE ANALYSIS 21
2.5.1. Fundamentals of image analysis procedures 21
2.6. CHEMOMETRIC ANALYSIS 26
2.7. REFERENCES 27
Chapter 3 Monitoring morphological changes from activated sludge to aerobic granular sludge under distinct organic loading rates and increasing minimal imposed sludge settling velocities through quantitative image analysis 37
3.1. INTRODUCTION 38
3.2. MATERIAL AND METHODS 40
3.2.1. Reactors set-up and experimental conditions 40
3.2.2. Analytical methods 41
3.2.3. Quantitative image analysis 42
3.2.3.1. Image acquisition 42
3.2.3.2. Image processing and analysis 43
3.2.4. Multivariate statistical analysis 46
3.3. RESULTS 47

3.3.1. Sludge properties: solids concentration, settling properties and COD depletion 47
3.3.2. QIA as monitoring tool for sludge morphological changes in granulation 50
3.3.2.1. Aggregates distribution and filamentous content 50
3.3.2.2. Morphology characterization of granules with 200 μm ≤ deq ≤ 650 μm 51
3.3.3. Multivariate statistical analysis 52
3.3.3.1. PLS 52
3.3.3.2. PCA 53
3.4. DISCUSSION 55
3.5. CONCLUSION 59
3.6. REFERENCES 59
Chapter 4 Characterization of aerobic granular sludge formation under washout dynamics through quantitative image analysis: The influence of COD/N 63
4.1. INTRODUCTION 64
4.2. MATERIAL AND METHODS 65
4.2.1. Reactors setup and operating conditions 65
4.2.2. Analytical methods 67
4.2.3. Quantitative image analysis 67
4.2.3.1. Sludge sampling, image acquisition, processing and analysis 67
4.2.4. Multivariate statistical analysis 69
4.3. RESULTS 71
4.3.1. Sludge concentration and settling properties in SBR 71
4.3.2. COD and nutrients removal 73
4.3.3. Morphological properties 75
4.3.4. Effluent quality assessment 79
4.4. DISCUSSION 80
4.5. CONCLUSIONS 84
4.6. REFERENCES 84
Chapter 5 Improving nutrient removal efficiencies of aerobic granular sludge by bioaugmentation with bioactive granules: Accessing the impact on the granules' morphology through quantitative image analysis 87
5.1. INTRODUCTION 88
5.2. MATERIAL AND METHODS 89

5.2.1. Reactors setup and operation 89
5.2.2. Reactors inoculum and bioactive granules sludge source 90
5.2.3. Bioaugmentation 90
5.2.4. Analytical methods 92
5.2.5. Quantitative image analysis 92
5.2.5.1. Sludge sampling 92
5.2.5.2. Image acquisition, processing, and analysis 92
5.3. RESULTS 94
5.3.1. The effect of bioaugmentation on nutrient removal performance 94
5.3.2. The effect of bioaugmentation in sludge concentration and settling properties 97
5.3.3. Granules distribution and morphology 98
5.4. DISCUSSION 104
5.4.1. The influence of granules morphology on the bioaugmentation efficacy 104
5.4.2. The influence of bioactive granules in the morphological stability of AGS 105
5.5. CONCLUSIONS 107
5.6. REFERENCES 107
Chapter 6 The effect of LCFA on the performance and stability of aerobic granular sludge in a sequencing batch reactor 111
6.1. INTRODUCTION 112
6.2. MATERIAL AND METHODS 113
6.2.1. Experimental setup 113
6.2.2. Analytical methods 114
6.2.3. Quantitative image analysis 115
6.2.3.1. Sludge sampling 115
6.2.3.2. Image acquisition, processing, and analysis 115
6.2.4. Principal Component Analysis 116
6.3. RESULTS 116
6.3.1. Organic matter and nutrients removal efficiencies 116
6.3.2. Sludge concentration and settling properties 120
6.3.3. Distribution and morphology of aerobic granular sludge 122
6.4. DISCUSSION 125
6.5. CONCLUSIONS 127

6.6. REFERENCES 127
Chapter 7 GENERAL CONCLUSION AND SUGGESTION FOR FUTURE WORKS 130
7.1. GENERAL CONCLUSION 130
7.2. SUGGESTION FOR FUTURE WORKS 131
SCIENTIFIC OUTPUTS 133
ANNEXE 134

LIST OF FIGURES

Figure 2.1 – Schematic representation of the AD of organic substrates in methanogenic environments. 8

Figure 2.2 – Schematic representation of the three levels of treatment in a WWTP. 10

Figure 2.3 – Typical cycle in a SBR for aerobic granules formation. 13

Figure 2.4 – Representation of the different aerobic, anoxic and anaerobic environments for organic matter, nitrogen and phosphorus removal in aerobic granules. Adapted from Wilén et al. (2018), and Winkler et al. (2013). 17

Figure 2.5 – Fundamental steps in quantitative image analysis procedures applied to biological processes. Adapted from Costa et al. (2013). 22

Figure 2.6 – Grey-scale signal brightness levels of a pixel at different bit depths. Adapted from Lambert and Waters (2014). 24

Figure 2.7 – Grey-scale image processing: the binary image generated from the original image segmentation. Images obtained during this work. 25

Figure 2.8 – Original image from activated sludge containing flocs and filaments (a). Distinct binary images containing flocs (b) and filaments (c). Labelled image identifying the flocs (green), filaments (red), and excluded object (blue) (d). Images obtained during this work. 26

Figure 3.1 – Aggregates observed in bright-field microscopy at 100x magnification in R1 (A-C) and R2 (D-F) at the end of stage I (day 27), stage II (day 38) and stage III (day 69). Granules observed in stereomicroscopy at 15x magnification in R1 (G-I) and R2 (J-L) at the end of stage I (day 27), stage II (day 38) and stage III (day 69). Scale corresponds to 100 μm and 1000 μm for 100x and 15x magnification, respectively. 43

Figure 3.2 – Original grey scale images acquired through bright-field microscopy with a 100x amplification (a, c) and stereomicroscopy with a 15x amplification (e) and respective final binary images (b, d, f). .. 44

Figure 3.3 – Sludge profiles of MLVSS (a), $VSS_{effluent}$ (b), SVI_{30}/SVI_5 ratio (c), SVI_5 (d), and SVI_{30} (e) in R1 (■) and R2 (□). Operational stages I, II and III. 48

Figure 3.4 – COD removal efficiencies (a) and $COD_{aeration}$ (b) in R1 (●) and R2 (○), during the operational stages I, II and III. 49

Figure 3.5 – The specific area of aggregates in the different size range: Deq < 200 µm (▲); 200 µm ≤ Deq ≤ 650 µm (◆) and Deq > 650 µm (●) in R1 (a) and R2 (b). Filaments length (c) in R1 (◆) and R2 (◇) with filaments content threshold of 7 mm μL^{-1} (—), according to Mesquita (2010). Operational stages I, II, III. 51

Figure 3.6 – The solidity (a), eccentricity (b), and convexity (c) of aggregates with 200 µm ≤ Deq ≤ 650 µm present in R1 (▲) and R2 (△), during the operational stages I, II and III. 52

Figure 3.7 – Correlation between observed and predicted SVI_5 (a) and SVI_{30} (b). Calibration (●) and validation (○) data set.....53

Figure 3.8 – PCA scores plot of the QIA dataset for PC1 vs PC2 (a) of R1 (●) and R2 (○). Variables loadings plot of the PC1 and PC2 (b). 54

Figure 4.1 – MLVSS (a), $VSS_{effluent}$ (b), F/M ratio (c), and SVI_{30}/SVI_5 (d) profiles in R1 (—○—), R2 (—□—), and R3 (—▲—). The settling time (ST) (—) applied throughout the reactors' operation. 72

Figure 4.2 – Removal efficiencies for COD (a), $N\text{-}NH_4^+$ (b), and $P\text{-}PO_4^{3-}$ (c) in R1 (—○—), R2 (—□—), and R3 (—▲—). The settling time (ST) (—) applied throughout the reactors' operation. 74

Figure 4.3 – $N\text{-}NO_3^-$ (a) and $N\text{-}NO_2^-$ (b) effluent concentration in R1 (—○—), R2 (—□—), and R3 (—▲—). The settling time (ST) (—) applied throughout the reactors' operation.....75

Figure 4.4 – TA_{Flocs}/Vol (a), $TA_{Granules}$/Vol (b), and TL/TA_{Flocs} (c) in R1 (—○—), R2 (—□—), and R3 (—▲—). The settling time (ST) (—) applied throughout the reactors' operation. 76

Figure 4.5 – Bright-field microscopy of flocs and filaments observed in R2 (a) and R3 (b) on day 84 and day 39, respectively. Stereomicroscopy from the granular fraction observed in R2 (c) and R3 (d) on day 79. Images of the AGS formed in R1 (e), R2 (f) and R3 (g) on day 129. 77

Figure 4.6 – Detailed evolution of the granules Deq (a), Area/Vol (b), and Volume/Vol (c) according to the size class: overall granules (—✳—), Gc1 (—○—), Gc2 (—●—), and Gc3 (—●—) during granulation (Gr) and maturation (Mt) periods in R1. The settling time (ST) (—) applied throughout the reactors' operation.....78

Figure 4.7 – Correlation between observed and predicted effluent concentration of: $P\text{-}PO_4^{3-}$ (a), $N\text{-}NH_4^+$ (b), $N\text{-}NO_2^-$ (c), and $N\text{-}NO_3^-$ (d). Training (●) and validation (○) data set. 80

Figure 5.1 – Images of the granules morphology. Bioactive granules (a). AGS used to inoculate: R1 (b), R2 and R3 (c). The scale bar equal to 5 mm. 91

Figure 5.2 – Effluent ammonium (✱), nitrite (Δ) and nitrate (◆) concentration profiles in: R1 (a), R2 (b) and R3 (c). Dashed arrow mark bioaugmentation day....95

Figure 5.3 – Influent (●) and effluent (○) phosphate concentration profiles in: R1 (a), R2 (b) and R3(c). Dashed arrow mark bioaugmentation day. 96

Figure 5.4 – MLVSS (●), MLVSS/MLSS (○), SVI_5 (◆), SVI_{30} (Δ) and SVI_{30}/SVI_5 (✱) profiles: in R1 (a,b), R2 (c,d) and R3 (e,f). Dashed arrow mark bioaugmentation day....98

Figure 5.5 – Area and number distribution profiles for granules with Deq < 1000 µm (○) and Deq ≥ 1000 µm (●) in: R1 (a,b), R2 (c,d) and R3 (e,f). Dashed arrow mark bioaugmentation day. 99

Figure 5.6 – The average Deq (●) and solidity (○) profiles of AGS in R1 (a). Dashed arrow mark bioaugmentation day. Red arrows marks the granules observation on day 21 and 63. Images of typical granules recognized by the software on day 21 (b-d) and on day 63 (e-g), acquired at 15x magnification. The scale is equal to 1mm.... 101

Figure 5.7 – MLVSS/TV (●) and convexity (□) profiles of AGS in R2 (a). Dashed arrow mark bioaugmentation day. Red arrows marks the granules observation on day 21, 39 and 63. Images of typical granules recognized by the software and the respective binary image created on day 21 (b,c), day 39 (d,e) and day 63 (f,g), acquired at 15x magnification. The scale is equal to 1mm. 102

Figure 5.8 – The solidity (○) and convexity (□) profiles of AGS in R3 (a). Dashed arrow mark bioaugmentation day. Red arrows marks the granules observation on day 32 and 63. Images of typical granules recognized by the software and the respective binary image created on day 32 (b,c) and on day 63 (d,e), acquired at 15x magnification. The scale is equal to 1mm.... 103

Figure 6.1 – Original image (a) of granules, and the binary image (b) created.... 116

Figure 6.2 – Concentration profiles during the SBR operation: Oleate (a), soluble COD (b), $P\text{-}PO_4^{3-}$ (c) and $N\text{-}NH_4^+$ (d). Oleate concentration in the reactor (■) and in the feed (—). Soluble COD, $P\text{-}PO_4^{3-}$ and $N\text{-}NH_4^+$ concentration in the influent (○) and effluent (●). Soluble COD and $P\text{-}PO_4^{3-}$ at the beginning of the aeration phase (- -△- -).... 118

Figure 6.3 – Concentration profiles of soluble COD (a), P-PO_4^{3-} (b), and N-NH_4^+ (c) during anaerobic feeding phase (AnP) and aeration phase (AP) in the SBR cycle analysis at day 126 (−●−) and day 147 (---○---). 119

Figure 6.4 – N-NO_2^- (◆) and N-NO_3^- (◇) concentrations in the effluent and oleate concentration in the feed (—) during SBR operation (a), and correlation analysis between nitrate concentration in the effluent and oleate concentration in the feed (b). 120

Figure 6.5 – Profiles during the SBR operation: MLSS (●) and MLVSS (○) concentration in the reactor (a), TSS (▲) and VSS (△) concentration in the effluent (b), SVI_5 (□) and SVI_{30} (■) (c), and SVI_{30}/SVI_5 (◇) ratio (d). Oleate concentration in the feed (—). 121

Figure 6.6 – AGS profile during SBR operation: $\%NB_{Gc1}$ (–○–), $\%NB_{Gc2}$ (–●–), and $\%NB_{Gc3}$ (–●–) (a), $TN_{granules}/Vol$ (–■–) and Deq_{ovr} (–□–) (b), and SA:V (–◆–) ratio (c). 122

Figure 6.7 – The $Conv_{ovr}$ (—▲—) of AGS during the SBR operation (a), and image of granules with protruding filaments at day 147 with 15x magnification (b). 123

Figure 6.8 – PCA of the dataset: scores (a) and loadings (b) plots of PC1 vs PC2. 124

LIST OF TABLES

Table 2.1 – Biogas potential from AD of different types of substrates. Adapted from Alves et al. (2009) 7

Table 2.2 – Comparison of AS and AGS characteristics for WWT. Adapted from Nancharaiah and Reddy (2018) 12

Table 2.3 - Main monitoring methods during granulation studies in SBR 20

Table 3.1 – Time of each phase during the SBR cycle, throughout the entire operation, and MISSV in the different operation stage 41

Table 3.2 – Variables selected for the second PLS with the highest VIP value for each reactor 47

Table 4.1 – The reactor's operating condition 66

Table 4.2 – The settling time and MISSV during SBR operation 66

Table 4.3 – The main component concentration in the synthetic feed 67

Table 4.4 – Minimum and maximum number of granules captured in each reactor 68

Table 4.5 – Set of independent variables (X) and respective VIP used in the PLS models for prediction of each target variable (Y) 70

Table 4.6 – PLS modelling results for each target variable 79

Table 5.1 – Acetate, ammonium and phosphate concentrations in the feed for each reactor 90

Table 5.2 – Characterization of bioactive granules and innate granules present in R1, R2 and R3, before bioaugmentation 91

Table 5.3 – COD concentrations and overall removal efficiency in each reactor 97

Table 6.1 – Oleate concentration in the influent throughout the SBR operation 114

Table A1 – QIA parameters determined from each sludge fraction 134

LIST OF SYMBOLS AND ABBREVIATIONS

AD	Anaerobic digestion
AGS	Aerobic granular sludge
AOB	Ammonium-oxidizing bacteria
Area, A	Area
$Area_{spec}$	Specific area
AS	Activated sludge
BMP	Bitmap
CAS	Conventional activated sludge
CCD	Charge-coupled device
CLSM	Confocal laser scanning microscopy
CMOS	Complementary metal-oxide-semiconductor
COD	Chemical oxygen demand
COD/N	COD-to-nitrogen ratio
Comp	Compactness
Conv	Convexity
Deq	Equivalent diameter
DO	Dissolved oxygen
Ecc	Eccentricity
EEA	European environment agency
EGSB	Expanded granular sludge blanket reactor
EPS	Extracellular polymeric substances
Ext	Extent
F/M	Food-to-microorganisms ratio
F_{cal}	Calibration factor
Fc	Flocs class
FF	Form factor
GAO	Glycogen-accumulating organism
Gc	Granules class
GC-FID	Gas chromatography with flame ionization detector
H/D	Height-to-diameter ratio
HRT	Hydraulic retention time
IA	Image analysis
JPEG	Joint Photographic Experts Group
L	Length
LCFA	Long-chain fatty acids
LPSA	Laser particle size analysis
LrgC	Largest concavity
MISSV	Minimal imposed sludge settling velocity
MLSS	Mixed liquor suspended solids

MLVSS	Mixed liquor volatile suspended solids
Nb	Number
$N\text{-}NH_4^+$	Ammonium nitrogen
$N\text{-}NO_2^-$	Nitrite
$N\text{-}NO_3^-$	Nitrate
NOB	Nitrite-oxidizing bacteria
OHO	Ordinary heterotroph organisms
OLR	Organic loading rate
P	Perimeter
PAO	Polyphosphate-accumulating organism
PBS	Phosphate buffered saline
PC	Principal components
PCA	Principal components analysis
PHA	Polyhydroxyalkanoates
PHB	Polyhydroxybutyrate
PLS	Partial least squares
$P\text{-}PO_4^{3-}$	Phosphate
QIA	Quantitative image analysis
RelArea	Ratio between hole and object area
RGB	Primary colours channels red, greed and blue
RMSEP	Root mean square error of prediction
Rob	Robustness
Round	Roundness
RPD	Residual predictive deviation
SA:V	Surface-area-to-volume ratio
SBR	Sequencing batch reactor
SEM	Scanning electron microscopy
SND	Simultaneous nitrification denitrification
Sol	Solidity
SRT	Sludge retention time
ST	Settling time
SVI	Sludge volume index
SVI_{30}	Sludge volume index at 30 min
SVI_5	Sludge volume index at 5 min
SVP-SB200	Sludge volume percentage with a size below 200 µm
TA	Total area
TIFF	Tagged Image File Format
TIN	Total inorganic nitrogen
TL	Total filaments length
TNb	Total number
TSS	Total suspended solids
TV	Total volume

UHF-NMR	Ultra-high-field nuclear magnetic resonance
VER	Volume exchange ratio
VFA	Volatile fatty acids
VIP	Variable importance in projection
Vol, v	Volume
VSS	Volatile suspended solids
W	Width
WWT	Wastewater treatment
WWTP	Wastewater treatment Plant

CHAPTER 1

CONTEXT, AIM AND THESIS OUTLINE

1.1. CONTEXT

In modern society, progress is commonly associated with environmental problems. Among these environmental concerns are the high amounts of wastewater produced associated with increasing activities in urban, industrial and agricultural sectors. Organic and inorganic compounds are commonly found in wastewater, including biological nutrients such as nitrogen and phosphorous, which are essential elements for living beings. However, increasing nutrient concentrations are found in watercourses, leading to the eutrophication of surface waters (Balasuriya et al., 2022). Eutrophication can seriously degrade the aquatic ecosystem due to oxygen depletion caused by the outgrowth and decomposition of algae and aquatic plants (Balasuriya et al., 2022). Hence, nutrient-rich wastewater must be treated before being safely discharged into the environment. Restrictive legislation has emerged to limit the levels of nutrients and other contaminants present in watercourses. Biological wastewater treatment (WWT) has become fundamental to keeping our natural water resources of the highest quality. Nevertheless, in order to achieve sustainable development, besides water recovery, biological WWT studies should focus on energy production and footprint reduction (Franca et al., 2018).

Biological treatment is considered the most environmental-friendly and cost-effective way to remove organic matter and nutrients from wastewater (Lemaire et al., 2008). Among biological processes, the activated sludge (AS) system is the most widely used in wastewater treatment plants (WWTP) (Franca et al., 2018). However, AS systems are no longer sustainable due to increasing land demand and energy requirements (Bengtsson et al., 2019; Nancharaiah and Sarvajith, 2019). Aerobic granular sludge (AGS) is presented as a promising compact technology with the potential to replace AS systems (Bengtsson et al., 2019; Pronk et al., 2015). AGS technology depends on establishing a self-immobilizing microbial community to form dense spherical aggregates with excellent settling characteristics in a process called granulation (de Kreuk and van Loosdrecht, 2004). Due to the granule's layered structure, both anoxic and aerobic microorganisms prevail in AGS systems, allowing the removal of organic matter and nutrients simultaneously in a single reactor, which contributes to its smaller footprint and lowers the energy

requirements (Bengtsson et al., 2019; Pronk et al., 2015). However, the mechanism behind the granulation process is still not completely elucidated. Moreover, deteriorating reactor performance is often observed in terms of sludge settling ability and nutrient removal associated with the sludge washout during the early stage of the granulation process. Long granulation periods and granules instability have been pointed to as the critical issues of AGS technology preventing its large-scale application (Lin et al., 2020).

The aerobic granulation process is a complex physicochemical and biological process of gradual morphological changes from flocs to granules affected by several operational parameters (Franca et al., 2018; Liu and Tay, 2004; Rollemberg et al., 2018). Furthermore, the operating condition favouring granulation might not be suitable for the stability of granules in long term operation (Liu and Tay, 2015, 2008). Granular stability is essential to provide high tolerance to toxic compounds associated with the treatment of industrial wastewaters. Unexpected changes in operational conditions can lead to the granules disruption and ultimately to the reactor failure in meeting the effluent requirements. Hence, monitoring the dynamic sludge changes under defined operating conditions in AGS systems is fundamental, increasing the knowledge about the granulation rates and stability of the aerobic granules. However, typical monitoring practices include determining the granule's size and morphological evaluation through visual inspection, which can be somewhat subjective and qualitative.

Quantitative image analysis (QIA) is a powerful tool to extract quantitative information from images, removing the subjectivity of image interpretation (Costa et al., 2013). In simple terms, images are made up of a large number of pixels, which after computer processing and analysis, can provide us with valuable quantitative information. Thus, QIA methods may bring new opportunities to biological WWT processes by overcoming the gaps in-process monitoring and control (Costa, 2008). In fact, QIA methods have been successfully applied to monitor the sludge morphological changes in both aerobic and anaerobic treatment processes (Costa et al., 2009; Mesquita et al., 2011). In AGS systems, the estimation of the sludge settling ability, density and effluent quality has been successfully achieved through QIA (Costa et al., 2022; Leal et al., 2022). However, these studies were performed with mature granules and studies addressing the morphological changes from flocs to granules during granulation process are still scarce. Gathering precise and quantitative morphological information about how the granulation process occurs under different operating conditions is relevant to predicting granulation rates, granules stability, and reactor performances.

The large amount of data provided by QIA demands the use of mathematical and statistical methods to treat and extract the most important information. Principal component analysis (PCA) and partial least squares (PLS) are the most widely used multivariate statistical analysis techniques in WWTP operation (Teppola et al., 1997). Besides simplifying high-dimensional and strongly correlated data by reducing it to a smaller dataset, PCA can be used to find correlation in a dataset with a large number of variables. On the other hand, PLS can be used to predict a set of dependent (or target) variables from a large set of independent (or predictors) variables. Therefore, monitoring the sludge morphology through QIA data coupled with multivariable statistical methods has the potential to optimize the biological treatment process, contributing to the predictive control of operational parameters in AGS systems.

1.2. AIM

This thesis aims to get novel insights into the development of AGS from AS in a sequencing batch reactor (SBR). QIA methodologies were used to monitor the morphological changes from flocs to granules during the reactor start-up, providing a new understanding of the granule's formation and stability. The research focused on the sludge morphological parameters sensitive to the granulation status, sludge settling properties and reactors performance using multivariate statistical methods. The bioaugmentation approach was also investigated to enhance the nutrient removal capability of mature granules. The stability of granules and reactor performance was also analysed in the presence of the most common unsaturated long-chain fatty acid (i.e., oleate) existing in wastewaters.

1.3. THESIS OUTLINE

This chapter introduces the subject of this thesis and its importance in the framework of AGS systems. The current knowledge about the aerobic granulation process in SBR, QIA methods and multivariate statistical analysis applied to biological WWT is reviewed in **Chapter 2**. In **Chapter 3**, QIA methods were used to monitor the sludge morphological changes from flocs to granules in two SBRs operated under different organic loading rates. The granulation status and the sludge settling properties were assessed in both reactors through PCA and PLS. In **Chapter 4**, the effect of nitrogen on the granulation rate was evaluated by QIA in three SBR operated under distinct ammonium nitrogen concentrations. The effluent quality in terms of phosphate, ammonium, nitrite and nitrate was estimated through PLS using

QIA data. The potential to enhance the nutrient removal capability of mature AGS using morphologically distinct bioactive granules was assessed in **Chapter 5**. The effect of oleate, the most common unsaturated long-chain fatty acid present in wastewaters, on granular stability, sludge settling properties, organic matter and nutrients removal efficiencies was evaluated in **Chapter 6**. In the final **Chapter 7**, the main conclusions of the work presented in this thesis are summarized, and future research is suggested.

1.4. REFERENCES

Balasuriya, B.T.G., Ghose, A., Gheewala, S.H., Prapaspongsa, T., 2022. Assessment of eutrophication potential from fertiliser application in agricultural systems in Thailand. Sci. Total Environ. 833, 154993. https://doi.org/10.1016/j.scitotenv.2022.154993

Bengtsson, S., Blois, M. De, Wilén, B., Gustavsson, D., 2019. A comparison of aerobic granular sludge with conventional and compact biological treatment technologies 3330. https://doi.org/10.1080/09593330.2018.1452985

Costa, J.C., 2008. Supervision of Transient Anaerobic Granular Sludge Process through Quantitative Image Analysis and Multivariate Statistical Techniques. PhD thesis, University of Minho. https://hdl.handle.net/1822/8504.

Costa, J.C., Alves, M.M., Ferreira, E.C., 2009. Principal component analysis and quantitative image analysis to predict effects of toxics in anaerobic granular sludge. Bioresour. Technol. 100, 1180–1185. https://doi.org/10.1016/j.biortech.2008.09.018

Costa, J.C., Mesquita, D.P., Amaral, A.L., Alves, M.M., Ferreira, E.C., 2013. Quantitative image analysis for the characterization of microbial aggregates in biological wastewater treatment: a review. Environ. Sci. Pollut. Res. 20, 5887–5912. https://doi.org/10.1007/s11356-013-1824-5

Costa, J.G., Paulo, A.M.S., Amorim, C.L., Amaral, A.L., Castro, P.M.L., Ferreira, E.C., Mesquita, D.P., 2022. Quantitative image analysis as a robust tool to assess effluent quality from an aerobic granular sludge system treating industrial wastewater. Chemosphere 291. https://doi.org/10.1016/j.chemosphere.2021.132773

de Kreuk, M.K., van Loosdrecht, M.C.M., 2004. Selection of slow growing organisms as a means for improving aerobic granular sludge stability. Water Sci. Technol. 49, 9–17. https://doi.org/10.2166/wst.2004.0792

Franca, R.D.G., Pinheiro, H.M., van Loosdrecht, M.C.M., Lourenço, N.D., 2018. Stability of aerobic granules during long-term bioreactor operation. Biotechnol. Adv. 36, 228–246. https://doi.org/10.1016/j.biotechadv.2017.11.005

Leal, C., del Río, A.V., Mesquita, D.P., Amaral, A.L., Ferreira, E.C., 2022. Prediction of sludge settleability, density and suspended solids of aerobic granular sludge in the presence of pharmaceutically active compounds by quantitative image analysis and chemometric tools. J. Environ. Chem. Eng. 10. https://doi.org/10.1016/j.jece.2022.107136

Lemaire, R., Webb, R.I., Yuan, Z., 2008. Micro-scale observations of the structure of aerobic microbial granules used for the treatment of nutrient-rich industrial wastewater. ISME J. 2, 528–541. https://doi.org/10.1038/ismej.2008.12

Lin, H., Ma, R., Hu, Y., Lin, J., Sun, S., Jiang, J., Li, T., Liao, Q., Luo, J., 2020. Reviewing bottlenecks in aerobic granular sludge technology : Slow granulation and low granular stability. Environ. Pollut. 263, 114638. https://doi.org/10.1016/j.envpol.2020.114638

Liu, Y., Tay, J.H., 2004. State of the art of biogranulation technology for wastewater treatment. Biotechnol. Adv. 22, 533–563. https://doi.org/10.1016/j.biotechadv.2004.05.001

Liu, Y.Q., Tay, J.H., 2015. Fast formation of aerobic granules by combining strong hydraulic selection pressure with overstressed organic loading rate. Water Res. 80, 256–266. https://doi.org/10.1016/j.watres.2015.05.015

Liu, Y.Q., Tay, J.H., 2008. Influence of starvation time on formation and stability of aerobic granules in sequencing batch reactors. Bioresour. Technol. 99, 980–985. https://doi.org/10.1016/j.biortech.2007.03.011

Mesquita, D.P., Amaral, A.L., Ferreira, E.C., 2011. Identifying different types of bulking in an activated sludge system through quantitative image analysis. Chemosphere 85, 643–652. https://doi.org/10.1016/j.chemosphere.2011.07.012

Nancharaiah, Y. V., Sarvajith, M., 2019. Aerobic granular sludge process: a fast growing biological treatment for sustainable wastewater treatment. Curr. Opin. Environ. Sci. Heal. 12, 57–65. https://doi.org/10.1016/j.coesh.2019.09.011

Pronk, M., de Kreuk, M.K., de Bruin, B., Kamminga, P., Kleerebezem, R., van Loosdrecht, M.C.M., 2015. Full scale performance of the aerobic granular sludge process for sewage treatment. Water Res. 84, 207–217. https://doi.org/10.1016/j.watres.2015.07.011

Rollemberg, S.L., Mendes Barros, A.R., Milen Firmino, P.I., Bezerra dos Santos, A., 2018. Aerobic granular sludge: Cultivation parameters and removal mechanisms. Bioresour. Technol. 270, 678–688. https://doi.org/10.1016/j.biortech.2018.08.130

Teppola, P., Mujunen, S.P., Minkkinen, P., 1997. Partial least squares modeling of an activated sludge plant: A case study. Chemom. Intell. Lab. Syst. 38, 197–208. https://doi.org/10.1016/S0169-7439(97)00055-5

CHAPTER 2

GENERAL INTRODUCTION

2.1. THE IMPORTANCE OF BIOLOGICAL WASTEWATER TREATMENT

The increased intensity of domestic, agricultural, and industrial activity has prompted concerns about the vast amounts of wastewater produced, which can have adverse environmental and economic consequences if not treated adequately. Most of these wastewater streams do not meet the basic quality requirements to be safely discharged into watercourses since they present a high concentration of organic matter and nutrients (i.e., nitrogen and phosphorus). Wastewater discharge without appropriate treatment can cause eutrophication of watercourses, a phenomenon that degrades aquatic habitats (Balasuriya et al., 2022).

Biological treatment systems are commonly used to remove organic matter and nutrients from wastewaters since they are considered the most ecologically friendly and cost-effective option (Lemaire et al., 2008). During biological wastewater treatment (WWT), decomposition of organic compounds proceeds either in the presence or absence of oxygen, that is, in aerobic or anaerobic environments. In these systems, mixed microbial communities consume pollutants contained in wastewater for growth. The majority of wastewater containing biodegradable compounds can be handled biologically under the right conditions. Aerobic treatment has been applied typically to low-strength effluents to obtain a high level of treatment efficiency, whereas anaerobic treatment has been used on effluents with a higher organic matter concentration (i.e., industrial wastewaters). Consequently, it is vital to comprehend the peculiarities of each biological process to ensure that the right environment is created and successfully managed to ensure appropriate treatment (Metcalf and Eddy, 2003).

2.2. ANAEROBIC DIGESTION SYSTEMS

Anaerobic digestion (AD) is a biological WWT process with the dual benefit of stabilizing waste materials and producing energy (Duarte et al., 2021). Thousands of large-scale systems are in operation around the world, mainly applied to organic industrial wastewaters, such as the agro-food, beverage and paper pulp industries (van Lier et al., 2015). Biogas, a valuable energy blend mainly composed of methane and carbon dioxide is the primary end-product of the AD process (Alves et al., 2009). Methane production relies on the substrate provided to the anaerobic system, with lipid degradation exhibiting the highest biogas potential (Table 2.1).

Table 2.1 – Biogas potential from AD of different types of substrates. Adapted from Alves et al. (2009)

Organic compound	**Methanogenic Reaction**	**Biogas ($L\ g^{-1}$)**	**Methane (%)**
Lipids	$C_{50}H_{90}O_6 + 24.4H_2O \rightarrow 34.75CH_4 + 15.25CO_2$	1.425	69.5
Carbohydrates	$C_6H_{10}O_5 + H_2O \rightarrow 3CH_4 + 3CO_2$	0.830	50.0
Proteins	$C_{16}H_{24}O_5N_4 + 14.5H_2O \rightarrow 8.25CH_4 + 3.75CO_2 + 4NH_4^+ + 4HCO_3^-$	0.921	68.8

The AD process can be divided into four main steps: hydrolysis, acidogenesis (or fermentation), acetogenesis, and methanogenesis (Figure 2.1). Briefly, the hydrolysis step converts proteins, carbohydrates and lipids contained in the complex substrates into their respective monomers through the action of extracellular enzymes excreted by fermentative bacteria, allowing these smaller molecules to pass through the cellular membrane. In the acidogenic step, hydrolysis products, such as amino acids, sugars and glycerol, are further degraded, producing volatile fatty acids (VFA) and alcohol intermediates. These intermediates can be further oxidized to acetate, hydrogen, and carbon dioxide by acetogenic bacteria (Schink, 1997). However, syntrophic relations with hydrogen utilizing bacteria are essential to maintain hydrogen at low concentrations, allowing the reaction to be thermodynamically feasible under standard conditions (Pereira, 2003). The final AD step is methanogenesis, where methane is produced by acetate- and hydrogen- consuming methanogenic archaea (i.e., acetoclastic and hydrogenotrophic methanogens).

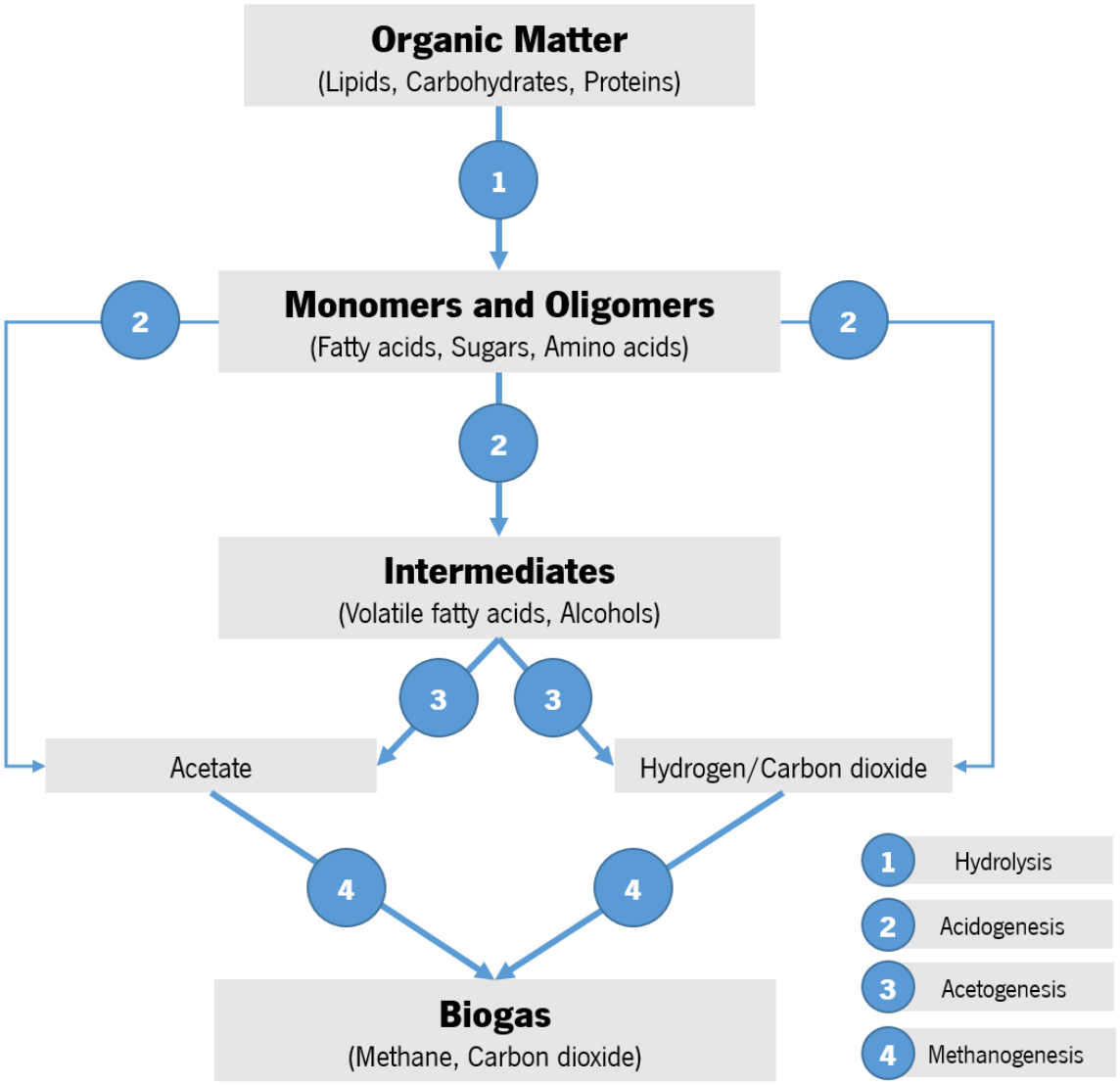


Figure 2.1 – Schematic representation of the AD of organic substrates in methanogenic environments.

However, the treatment of industrial wastewaters can be challenging. In fact, the hydrolysis step is considered a slow process for several complex organic substrates, and it can be the rate-limiting step in the whole degradation process (Costa et al., 2012). Nevertheless, several studies have been made to fasten this step, using different biological, physical and chemical pre-treatment strategies (Donkor et al., 2022; Preethi et al., 2022). On the other hand, the accumulation of intermediates and hydrolysis by-products are one of the leading causes of anaerobic digesters' distress and failure (Yuan and Zhu, 2016). For instance, long-chain fatty acids (LCFA) are produced through lipids hydrolysis and accumulate onto the biomass during continuous bioreactor operation (Silva et al., 2014). Methane production usually decreases following this phenomenon, and in later stages, biomass becomes overloaded with the accumulated LCFA, resulting in a decrease in microbial activity and the ceasing of methane production

(Silva et al., 2014). Hence, while lipids rich wastewater are attractive for biogas production, they are considered a challenging pollutant in anaerobic WWT processes (Holohan et al., 2022). For easily degradable substrates, methanogenesis is regarded as the rate-limiting step due to the slower growth rate of methanogens compared to acidogenic or acetogenic bacteria (De Vrieze et al., 2012). Moreover, the susceptibility of the methanogenic consortia to various environmental factors is one of the main drawbacks of AD (De Vrieze et al., 2012).

In addition to the existing challenges in the treatment of industrial effluents, the AD process presents long start-up periods, possible bad odours, deficiencies in pathogens and nutrients removal, and moderate to low quality of the treated effluent (Chan et al., 2009). While the primary goal of the AD process is the WWT itself, its application to concentrated effluents contributes to sustainable development via renewable energy production and pollution control, maximizing the biological WWT potential in a bio-based circular economy. However, since a post-treatment is generally required to the digestate liquid fraction and AD processes are not suitable for treating low-strength wastewaters, the need for this technology to be combined with an aerobic process for an efficient WWT stands out (Chan et al., 2009; Chuda and Ziemiński, 2021).

2.3. CONVENTIONAL ACTIVATED SLUDGE SYSTEMS

Conventional activated sludge (CAS) is the most common biological treatment system to remove soluble organic matter and nutrients from incoming effluents before discharge to receiving waters, typically yielding more sludge and carbon dioxide. CAS system is the secondary treatment in wastewater treatment plants (WWTP), which can include two other levels of treatment known as primary and tertiary (Figure 2.2). In the primary treatment, physical methods, including screening, grit removal, and sedimentation, are applied to the removal of material that will float or settle out by gravity, yielding the reduction of approximately 50 to 70% of total suspended solids (TSS), 25 to 50% of organic matter, and 65% of the oil and grease (Val del Rio, 2013). Tertiary treatment, also called advance treatment, is an extension of the secondary treatment or comprises several physicochemical treatments to further remove TSS, nutrients, and pathogens from wastewater (Metcalf and Eddy, 2003). However, advanced treatment is not always a requirement in the European Union, depending on the disposal zone (i.e., sensitive or non-sensitive areas) and the population agglomeration. According to the European Environment Agency (EEA), the Portuguese population connected to the tertiary level of treatment was only 38% in 2017, while the average in the EU was 69% (EEA, 2021).

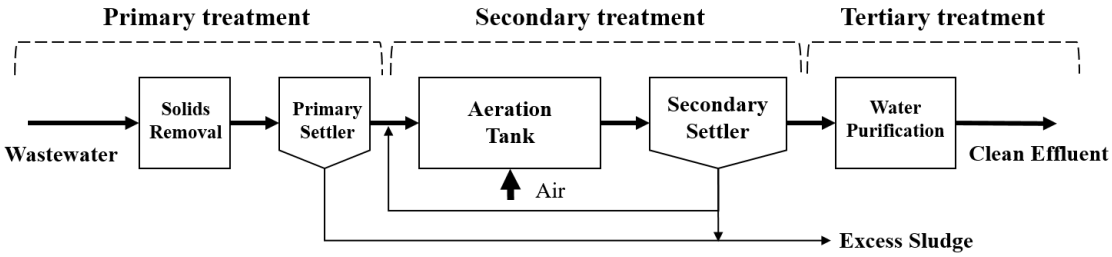


Figure 2.2 – Schematic representation of the three levels of treatment in a WWTP.

The secondary treatment is considered crucial for WWT, being responsible for eliminating more than 85% of both the TSS and organic matter contained in wastewater (Metcalf and Eddy, 2003). This biological aerobic process initiates in an aerated tank, where organic matter and nutrients are degraded by a complex microbial community known as activated sludge (AS). The AS process was discovered at the beginning of the 20th century, and the term "activated" was due to the establishment, under aerobic environments, of microorganisms able to stabilising waste, predominantly composed of bacteria yet also viruses, fungi, algae, protozoa, and metazoa (Metcalf and Eddy, 2003). Living and growing microorganisms in AS are bound together by a matrix of extracellular polymeric substances (EPS) and chemical binding forces producing a three-dimensional aggregated microbial structure named floc (Melo et al., 2022).

After the aerated tank, the clarification process occurs in a secondary settler, where the sludge is separated from the treated wastewater by sedimentation. Sludge flocculation is essential for wastewater clarification purposes and to achieve high effluent quality in WWTP; since the floccular sludge is denser than the liquid fraction, it allows the sludge to settle at the button of the clarifiers by gravity. The clarified effluent is withdrawn and part of the settled sludge is reintroduced to the aerated tank to maintain the AS concentration (Figure 2.2). However, poor settling properties are frequently observed in AS systems, resulting in low sludge concentration in the aerated tank, thus requiring large secondary settlers to handle the organic loadings, particularly in combined domestic and industrial WWT (Giesen et al., 2013). Furthermore, the AS process may result in the growth of various organisms that are not desired due to unstable operational conditions. The primary issues brought on by disturbance organisms is the bulking sludge caused by the excessive proliferation of filamentous bacteria (i.e., filamentous bulking) or the overproduction of EPS by *Zoogleal* microorganisms (i.e., non-filamentous bulking) (Guo et al., 2014). Both

filamentous and non-filamentous bulking may cause detrimental morphological changes in the flocs structure, resulting in poor settling capacities, low sludge retention and deficient treatment performance.

Despite being a well-established biological treatment process with predictable performance, the CAS system is sensitive to sudden changes in wastewater composition and environmental conditions (Cheng et al., 2011; Padrão et al., 2022; Wilén et al., 2006). The large surface areas required for the aerated tanks and secondary settlers are a common drawback of CAS systems (Giesen et al., 2013). Also, the by-product of WWT is the excess sludge production which requires proper treatment and disposal, representing 40% to 50% of the total operating costs of a WWTP (Cho et al., 2014; Yoshino et al., 2017). Hence, emerging and promising new technologies, such as aerobic granular sludge (AGS), have been developed in recent years to overcome the main drawbacks of CAS systems (van der Roest et al., 2011).

2.4. AEROBIC GRANULAR SLUDGE SYSTEMS

AGS systems is a relatively new technology developed for WWT offering the possibility to remove organic matter and nutrients in compact treatment processes (Bengtsson et al., 2018). AGS technology relies on the formation of aerobic granules in a self-immobilizing process designated as granulation (Liu and Tay, 2004). While anaerobic granules were first described in WWT studies in the ’80s, the first reported work producing aerobic granules appeared about 20 years later (Liu and Tay, 2004). Morgenroth et al. (1997) provided the foundation for obtaining aerobic granules in a sequencing batch reactor (SBR) with extremely short sedimentation and withdrawal phases, creating the conditions for further aerobic granulation process investigations in lab-scale (Beun et al., 1999; de Kreuk et al., 2005; Mosquera-Corral et al., 2005; Val Del Río et al., 2013) and pilot-scale reactors (Cetin et al., 2018; Ni et al., 2009; Pishgar et al., 2019).

The main AGS characteristics that favours efficient treatment over AS are summarized in Table 2.2. Compared to the CAS system, the AGS technology was estimated to have a 30% to 50% lower footprint and 50% to 60% fewer energy requirements (Bengtsson et al., 2019; Pronk et al., 2015). Due to the advantages presented by granular over suspended sludge, this technology has been used in studies for the treatment of domestic and industrial wastewaters (Carrera et al., 2021; Cetin et al., 2018), simultaneous nitrogen and phosphorus removal (Bassin et al., 2012a; de Kreuk et al., 2005), toxics compounds removal (Tomar et al., 2022), and xenobiotics removal (Amorim et al., 2014).

Table 2.2 – Comparison of AS and AGS characteristics for WWT. Adapted from Nancharaiah and Reddy (2018)

Characteristic	AS	AGS	Observations
Morphology	Small and irregular	Large and spherical	AGS morphology characteristics allow a faster separation from the liquid without depending on external physical forces or chemical agents.
Specific gravity	0.997-1.010	1.010-1.017	
Settling velocity	Lower settling velocities < 10 m h^{-1}	Higher settling velocities > 10 m h^{-1}	
SVI	SVI5 ≠ SVI30	SVI5 = SVI30	
Aerobic, anoxic and anaerobic microenvironments in the same structure	Minimum possibilities for anaerobic zones	Distinct microenvironments i.e. aerobic, anaerobic and anoxic zones prevails in mm size granules	Co-existing microenvironments in the same granular structure allow both oxidative and reductive biological conversion.
EPS content	Low	High	EPS are important in aggregation, stability and function of granules, providing higher tolerance to toxics
Tolerance to toxic compounds	Low	High	
Performance with shock and fluctuating organic loading	Poor	Good	

AS – Activated Sludge; AGS – Aerobic Granular Sludge; SVI – Sludge Volume Index; EPS – Extracellular Polymeric Substances.

2.4.1. Aerobic granules

Aerobic granules were defined in the 1st IWA-Workshop Aerobic Granular Sludge in Munich (2004) to distinguish from floccular sludge with good settling properties (de Kreuk et al., 2007). Thus, aerobic granules were defined as:

"*Granules making up aerobic granular activated sludge are to be understood as aggregates of microbial origin, which do not coagulate under reduced hydrodynamic shear, and which settle significantly faster than activated sludge flocs*".

Briefly, aerobic granules are formed in a self-immobilizing process without requiring carrier material, containing active microorganisms similar to those present in AS and/or biofilms, and cannot consist only of components of microbial origin (e.g. EPS). Furthermore, aerobic granules settle as individual units when the reactor is not mixed and do not coagulate, as is often the case of floccular sludge. The settling property of AS is characterized by sludge volume index (SVI), typically over a period of 30 min (SVI_{30}), whereas the terminal settling in AGS is often reached after 5 min (SVI_5); thus, a good indication of the granules formation is given by the ratio between SVI_5 and SVI_{30} values (Schwarzenbeck et al., 2005). The

minimum size of aerobic granules was set to 200 µm based on previous observations, although this value can be variable as long as all the above properties are fulfilled (de Kreuk et al., 2007).

2.4.2. Granulation process

Granulation process is a vital point in AGS technology. Aerobic granules have been typically produced in a SBR using AS as inoculum (Zhang et al., 2019). SBR operation cycle typically consists of four distinct phases: 1) influent filling; 2) reaction; 3) settling; and 4) effluent withdrawal (Figure 2.3).

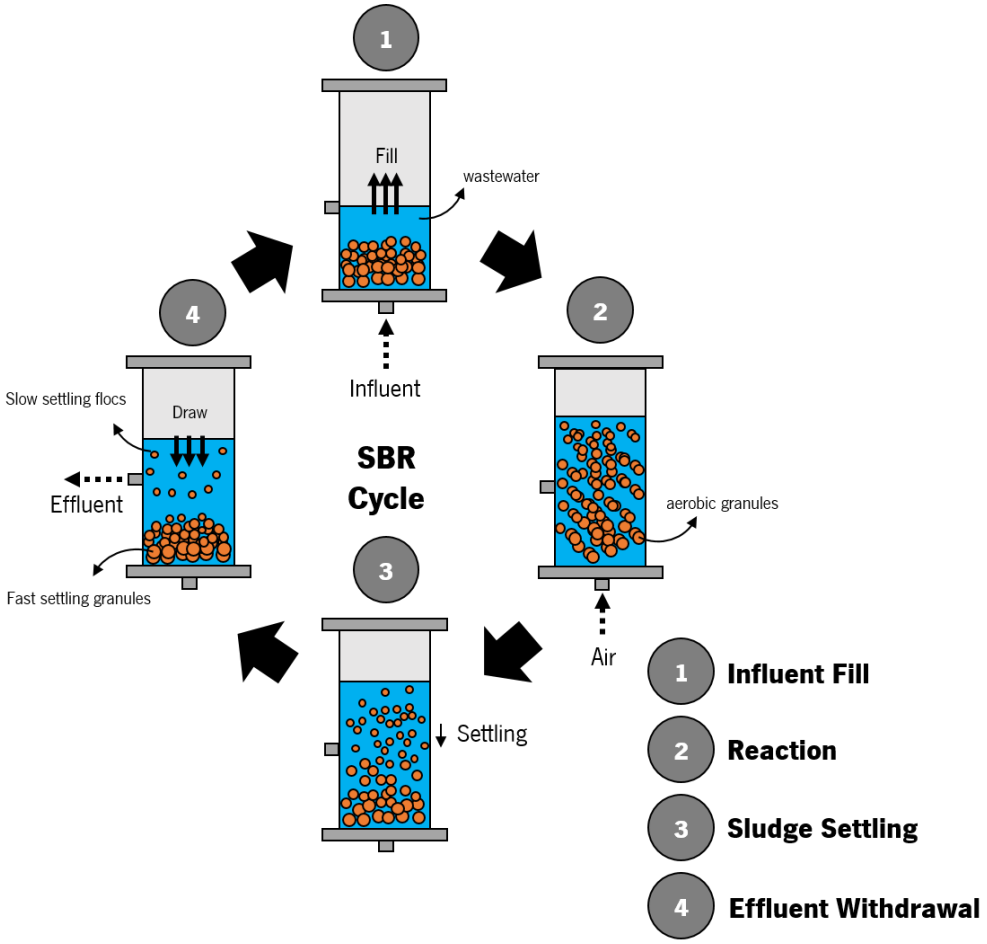


Figure 2.3 – Typical cycle in a SBR for aerobic granules formation.

SBR cycle starts with the influent entering the reactor, followed by the reaction phase, where the air is supplied through the bottom of the reactor. The sludge settling begins when the air supply ends, allowing

the retention of the settled sludge inside the reactor. The extent of the settling phase is typically short, resulting in the removal of sludge with poor settling ability during the effluent withdrawal phase.

While different environmental and operational conditions have been studied to increase our understanding of the granulation process, its underlying mechanisms are still not completely elucidated (Sarma et al., 2017; Wilén et al., 2018; Zhang et al., 2019). A granulation hypothesis has been proposed to occur in four steps (Liu and Tay, 2002): (1) physical movements initiate cell-to-cell contact, (2) cells aggregation occurs due to physical, chemical and biochemical attractive forces, (3) aggregate maturation initiates owing to EPS production, in which the cellular cluster can develop, and (4) formation of a three-dimensional aggregate in which a microbial community is structured and shaped by the hydrodynamic shear force.

2.4.3. Factors affecting aerobic granulation

The aerobic granulation process has been the subject of intensive research, namely to identify the main driving forces to achieve successful granulation. Among the factors commonly described as important for aerobic granulation in SBR are: hydrodynamic shear force (Tay et al., 2001), settling time (Qin et al., 2004a) and the feast and famine regime (Liu and Tay, 2008).

Hydrodynamic shear force

Hydrodynamic shear force is an important factor affecting aerobic granulation in SBR (Nancharaiah and Reddy, 2018). Superficial up-flow air velocity is typically used to define the shear force in SBR, corresponding to the aeration rate over the cross-sectional surface area of the reactor (Nancharaiah and Reddy, 2018; Sturm and Irvine, 2008).

Beun et al. (1999) found that granulation was favoured under high shear force, obtaining stable and smooth granules at a superficial up-flow air velocity of 4.1 cm s^{-1}. The detachment of the filamentous bacteria from the granule's surface was attributed to the shear force created by aeration. However, a superficial up-flow air velocity threshold of 1.2 cm s^{-1} was found above which compact and stable granules could be formed in SBR (Tay et al., 2001). A positive effect on EPS production, cell hydrophobicity and microbial activity was attributed to high shear, which resulted in the development of more compact and denser granules.

Granular sludge disintegration under slow superficial up-flow air velocities was confirmed by (Sturm and Irvine, 2008). While the loss of granules stability could be associated with the low shear forces, these authors concluded that dissolved oxygen (DO) is more critical in granules formation and stability since low aeration rates may limit the oxygen supply to the microbial community. Granules disintegration in SBR was found after reducing oxygen saturation levels from 100% to 40%, and stable granulation was unfeasible during the reactor start-up under low DO concentration (Mosquera-Corral et al., 2005). Thus, high shear force induced by aeration not only contributes to the formation of compact granules and suppression of filamentous bacteria overgrowth but also to the supply of sufficient oxygen to increase the stability of AGS.

Studies have shown the possibility of achieving stable aerobic granules at superficial up-flow air velocity lower than 1.2 cm s^{-1} when a low organic loading rate (OLR) is applied (Devlin et al., 2017; Henriet et al., 2016; Zhang et al., 2011). Still, morphological instability was observed when granules became larger, which led to deteriorating settling properties (Zhang et al., 2011). Large granules disintegration due to the outgrowth filaments and hollow structure was attributed to substrate limitation. While high shear was not required to obtain stable granules under low OLR, successful granulation will depend on other factors to out-compete with fast-growing aerobic microorganisms (Devlin et al., 2017).

Settling time

Another key factor for granules formation is the time allowed for the sludge to settle during the settling phase, i.e., the settling time, which is regarded as the most effective selective pressure in SBR (Beun et al., 2000; Liu et al., 2005a). The settling time is used to control the minimal imposed settling velocity of the aggregates in SBR, which will also depend on the settling height, i.e., the distance from the liquid surface to the discharge port (Liu et al., 2005a). The volume exchange ratio (i.e., the amount of working volume exchanged at the end of each SBR cycle) and the reactor geometry as the height to diameter (H/D) ratio (Kong et al., 2009) influence the settling height, thus impacting the minimal imposed sludge settling velocity in SBR. Beun et al. (2002) suggested that the SBR should have a high H/D ratio to improve the selection of granules over flocs by the difference in settling velocity, allowing to retain aggregates with settling velocities superior to 10 m h^{-1} under a short settling time (i.e., 3 min). Nevertheless, AGS has been successfully produced in SBR with considerably lower H/D ratios (Henriet et al., 2016; Liu et al., 2010; Rocktäschel et al., 2013; Schwarzenbeck et al., 2005; Val Del Río et al., 2013; Xavier et al., 2021).

For successful aerobic granulation in SBR, the minimal imposed sludge settling velocity must be set to values higher than the settling velocity of flocs. Thus, granular sludge with a settling velocity higher than the minimal imposed sludge settling velocity is retained, while floccular sludge with lower settling velocities is progressively washout. If flocs are not efficiently withdrawn from the SBR, the coexistence of granular and floccular sludge may occur (Qin et al., 2004a, 2004b), which can lead to the granulation process failure since flocs may easily outcompete aerobic granules due to its faster growth rate (Liu et al., 2005a; Yang et al., 2004). Aerobic granules can be formed at a minimal imposed sludge settling velocity above 1 m h^{-1} and become prevailing over floccular sludge at a settling velocity of 4 m h^{-1} (Liu et al., 2005b). Thus, a short settling time is standard during the aerobic granulation process in SBR.

Feast and famine regime

The microbial community is exposed to different environmental conditions during an SBR cycle. Among these environmental changes are the feast and famine periods, described as the presence and absence of organic matter in the medium (Beun et al., 2002). Generally, the microbial community responds to feast and famine periods by storing substrate as polyhydroxyalkanoates (PHAs) during the feast period and consuming them during the famine period (van Loosdrecht et al., 1997). The extent of the feast and famine periods in SBR will depend on the OLR and the duration of the aeration phase.

A recent study showed that the feast period was beneficial to the density of the granules, whereas the famine period was associated with increased microbial aggregation and adhesion (Li et al., 2022). While aerobic granules can be obtained by alternating feast and famine conditions (Liu and Tay, 2007), the duration of each period greatly influences aerobic granulation (Li et al., 2022). Short famine periods have been demonstrated to accelerate granules formation, whereas long-term stability is favoured over extended famine periods (Liu et al., 2016; Liu and Tay, 2008). However, excessive famine periods could lead to EPS consumption for endogenous respiration, which could negatively impact the AGS stability (Corsino et al., 2015). A famine period between 60% to 72% of the total aeration time was proposed to be in the optimal range to maintain good AGS density and settling properties (López-Palau et al., 2012). Recently, a feast and famine ratio of 1:3 allowed the control of EPS content at a suitable level to maintain long-term AGS stability (Iorhemen et al., 2020).

2.4.4. Microbial groups for nutrient removal in aerobic granules

Aerobic granules are a complex biofilm composed of mixed microbial populations surrounded by a three dimensional matrix of EPS which provides support for bacterial growth, interspecies proximity, cell-to-cell communication and protection against harsh environments (Franca et al., 2018). The microbial community in mature granules is distributed in a layered structure, which may vary depending on the environmental conditions and wastewater composition during granulation (Winkler et al., 2018). Aerobic, anoxic and anaerobic environments are generated due to oxygen and substrate gradients within the granules, allowing the establishment of different functional microbial groups to remove organic matter, nitrogen and phosphorus in a single granule (Figure 2.4) (Rosa-Masegosa et al., 2021; Wilén et al., 2018; Winkler et al., 2018). The granule core is composed of minerals, mainly hydroxyapatite, which has been described as originating via biologically induced precipitations of phosphorus and calcium carbonate (Mañas et al., 2011; Pishgar et al., 2020). Biologically induced precipitation may contribute to aerobic granulation in a recent mechanism proposed by Pishgar et al. (2020).

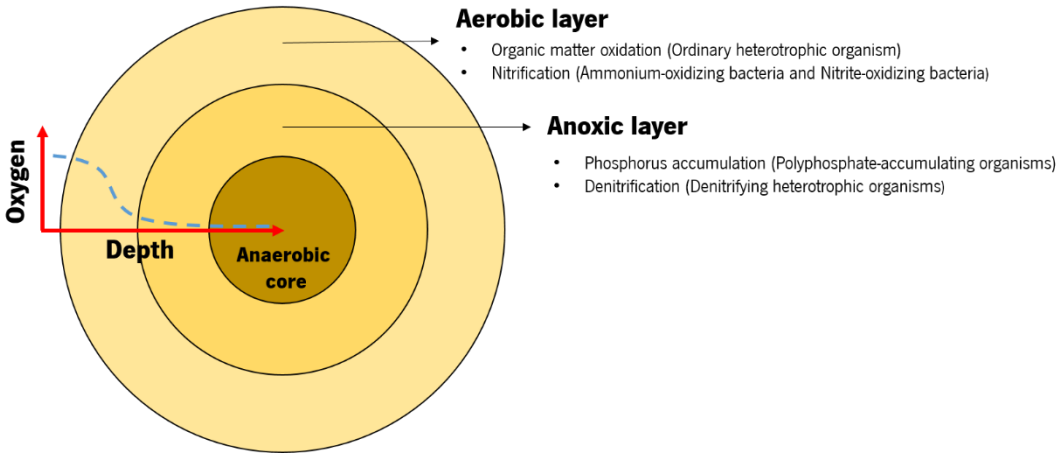


Figure 2.4 – Representation of the different aerobic, anoxic and anaerobic environments for organic matter, nitrogen and phosphorus removal in aerobic granules. Adapted from Wilén et al. (2018), and Winkler et al. (2013).

Biological nitrification is a two-step process accomplished by two autotrophic microbial groups: ammonium-oxidizing bacteria (AOB) that oxidize ammonium to nitrite and nitrite-oxidizing bacteria (NOB) that oxidize nitrite to nitrate. In AGS, both microbial groups can co-exist in the granule due to different affinities to oxygen in which AOB are typically located in the outer layers, while NOB is located more profound in the granule (Winkler et al., 2012). Simultaneous nitrification and denitrification can occur in aerobic granules due to the oxygen limitation in the inner layers of the granules (Mosquera-Corral et al., 2005), allowing the reduction of nitrite and nitrate to nitrogen gas by denitrifying heterotrophic organisms. Simultaneous nitrification and denitrification are essential to achieve efficient nitrogen removal in AGS systems. However, denitrification can be limited when oxygen concentration penetrates deeper into the granule, thus governing the size of the anoxic and aerobic zones (de Kreuk et al., 2005). While low oxygen concentration favours denitrification, it can also favour AOB prevalence over NOB among the nitrifiers (Chen et al., 2022).

The selection of slow-growing bacteria has been shown to increase the stability of aerobic granules (de Kreuk and van Loosdrecht, 2004; Liu et al., 2004). Extended anaerobic feeding has shown to favour granulation by selecting slow-growing heterotrophs polyphosphate-accumulating organism (PAO) and glycogen-accumulating organism (GAO) (de Kreuk and van Loosdrecht, 2004). Both PAO and GAO are located in the inner anoxic layer of the granules. Under anaerobic feeding, PAO and GAO convert readily biodegradable organic matter into intracellular storage biopolymers, limiting the growth of fast-growing ordinary heterotroph organisms (OHO) and contributing to the stability of granules structure (Haaksman et al., 2020). Nevertheless, for efficient phosphorus removal, PAO must outcompete GAO for substrate since PAO can store phosphorus intracellularly as polyphosphate (Poly-P) during aeration, while GAO does not contribute to phosphorus removal (Bassin et al., 2012b). AGS systems enriched with PAO over GAO have been obtained by selective granules removal (Bassin et al., 2012b; Henriet et al., 2016), mixed carbon sources (He et al., 2020), alternating anaerobic/aerobic/anoxic SBR operating mode (Wang et al., 2021), decreasing nitrogen concentration (Zou et al., 2015), decreasing superficial up-flow air velocity, and aeration time (He et al., 2018, 2017).

2.4.5. Monitoring AGS

Aerobic granulation is the gradual development from floccular sludge to compact aggregates and finally to mature granules (Liu and Tay, 2004). Considering the minimum size of granules (i.e., 200 μm), it has been proposed that a sludge volume percentage with a size below 200 μm (SVP-SB200) can be used to

determine the sludge fraction dominance during the granulation process, meaning that a granule-dominant reactor is achieved when SVP-SB200 reaches values below 50% (Liu et al., 2010). On the other hand, the evaluation of the mean size of mature granules has been commonly used to assess granules' stability (de Kreuk and van Loosdrecht, 2004). It has been suggested that granules equilibrate to a stable critical size-range due to breakage/attrition of weak larger granules and growth of smaller granules (Verawaty et al., 2013). The granules' mean size in AGS systems will depend on the wastewater strength, i.e. the concentration of organic matter and nutrients present in wastewaters (Carrera et al., 2021; Pishgar et al., 2019). However, excessive granule size may lead to the outgrowth of filamentous bacteria due to mass transfer limitations to the inner layers, which in turn weakens the granular structure, and deteriorates the AGS settling properties and the overall system performance (Figueroa et al., 2015; Moura et al., 2018). Thus, maintaining an ideal granular size range may be essential for the stability of AGS systems (Long et al., 2019). Recent studies have shown that selective granule sizes improve not only the stability of AGS (Long et al., 2019; Zhou et al., 2016) but also the nutrient removal efficiencies (Bassin et al., 2012b; Henriet et al., 2016). In this sense, diverse optimum granules' sizes have been proposed for simultaneous nitrogen and phosphorus removal (Li et al., 2019; Quoc et al., 2021a, 2021b).

The aggregate size distribution using microscopic observation coupled with image analysis software or laser particle size analysis has been commonly used to monitor the granulation progress (Guimarães et al., 2020; Liu et al., 2010; Pijuan et al., 2011). Also, more complex analyses such as scanning electron microscopy (SEM) (Pishgar et al., 2019), confocal laser scanning microscopy (CLSM) (Ni et al., 2009), and ultra-high-field nuclear magnetic resonance (UHF-NMR) (Kirkland et al., 2020), have been performed to evaluate the morphology and structure of mature granules in AGS systems. The primary microscopy methodologies used to monitor the granulation progress and granular structure in SBR are shown in Table 2.3.

Table 2.3 - Main monitoring methods during granulation studies in SBR

Reactor	Granulation period (days)	OLR (kg m^{-3} d^{-1})	Size range (mm)	Monitoring methods	Reference
Lab-scale	119	2.5 – 7.5	1.9 – 4.6	IA	(Beun et al., 1999)
Lab-scale	21	1.6	0.4 – 1.8	IA	(de Kreuk et al., 2005)
Lab-scale	30	1.6	0.6 – 1.6	IA	(Mosquera-Corral et al., 2005)
Pilot-scale	300	0.6 – 1.0	0.2 – 0.8	IA, SEM & CLSM	(Ni et al., 2009)
Lab-scale	170	2.0	0.2 – 1.1	LPSA & SEM	(Bassin et al., 2019)
Lab-scale	18 – 133	0.46 – 1.83	-	LPSA & IA	(Pijuan et al., 2011)
Pilot-scale	400	3.0	0.2 – 0.8	LPSA & IA	(Liu et al., 2010)
Pilot-scale	39 – 46	1.8 – 7.1	0.6 – 6.7	LPSA & SEM	(Pishgar et al., 2019)

IA – image analysis; SEM – Scanning electron microscopy; CLSM – Confocal laser scanning microscopy; LPSA – Laser particle size analysis

Besides the long reactor start-up periods that range from a few weeks to several months for the formation of mature granules (Liu et al., 2010; Pishgar et al., 2019; Pronk et al., 2015), the stability of the granules in long-term operation is regarded as a major issue of AGS systems (Lin et al., 2020). Granules disruption can occur under unstable operational or environmental conditions, changing the morphology of AGS from dense granular to loose floccular sludge, with deteriorating consequences to the biological activity and effluent quality (Bassin et al., 2019; Luo et al., 2014; Paulo et al., 2021; Zhang et al., 2018). The development of new methods for the characterization and evaluation of microbial aggregates in AGS systems has recently gained attention to improve process control (Ranzinger et al., 2020). Non-invasive granule characterization is essential to associate the structure and function of granules (Kirkland et al., 2020). Among these non-invasive methods, quantitative image analysis (QIA) can provide detailed morphological information, specifically when related to the dynamic changes from floccular to granular sludge and the evaluation of filamentous bacteria in AGS systems, increasing the knowledge about the rates and stability of the AGS formed under defined operating conditions (Silva et al., 2022).

2.5. QUANTITATIVE IMAGE ANALYSIS

The evaluation of images using only visual perception can be subjective and qualitative since it depends on the observer. As an alternative, using computers and software allows the extraction of quantitative information from images. QIA can be viewed as obtaining information from pixels, i.e., the minor constituent of images, removing human examination's subjectivity and extracting data that would be impossible or very difficult to obtain by other means (Amaral, 2003).

In AGS systems, image analysis methods have been mainly used to measure the mean diameter of granules obtained during aerobic granulation studies (Sguanci et al., 2019). Typically, the morphology and structure of aerobic granules are qualitatively evaluated either by simple stereomicroscope imaging (Thwaites et al., 2017) or by more complex SEM or CLSM images (Ni et al., 2009; Pishgar et al., 2019). Thus, the establishment of QIA procedure to evaluate the sludge morphological changes during aerobic granulation and the morphological and structural assessment of mature aerobic granules are still relatively unexplored.

2.5.1. Fundamentals of image analysis procedures

The general term “image analysis” refers not only to the analysis of the image itself but to the overall process, which includes previous steps of image capture and image processing. A schematic representation of the critical steps in the QIA procedure for biological process is represented in Figure 2.5.

Sample preparation and visualization

Collecting a homogenous sample representing the whole system from which it was taken is imperative for image analysis. Due to the significant differences in size, it is crucial to distinguish the different fractions composing the sludge. In AGS systems, the sludge size distribution is commonly achieved by sieving methods (Bin et al., 2011). However, AGS morphology and structure may change due to the harsh physical processes imposed by sieving methods (e.g., handling and washing). Due to the fragile nature of microbial aggregates, careful sampling, manipulation, and conservation are essential to avoid damage and preserve sample morphological integrity.

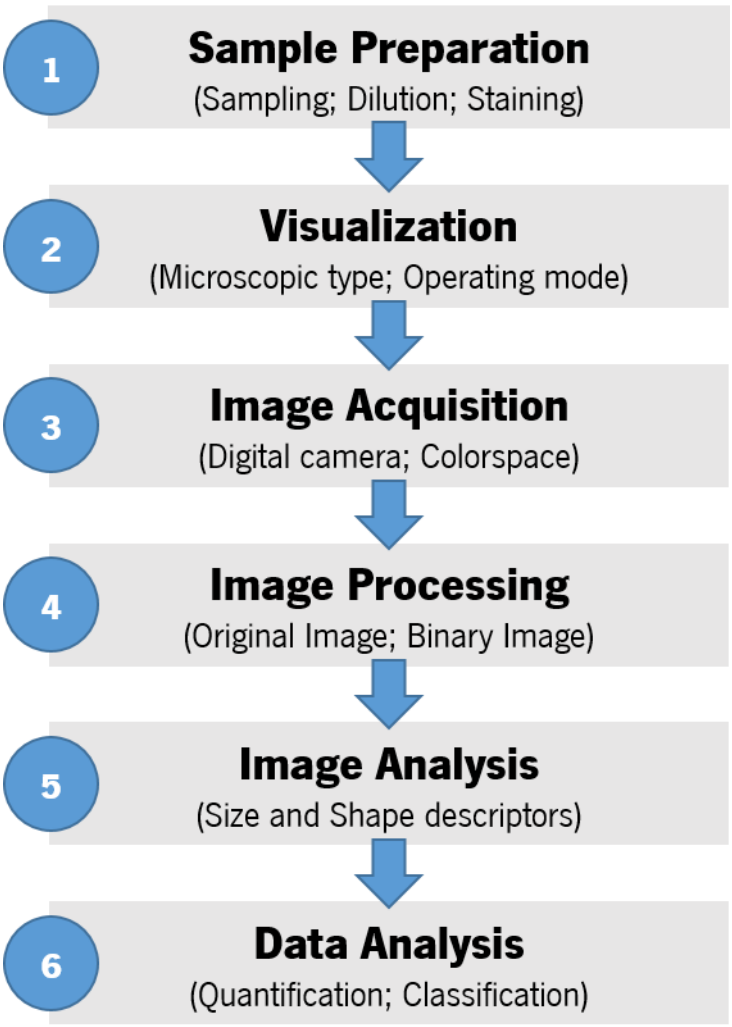


Figure 2.5 – Fundamental steps in quantitative image analysis procedures applied to biological processes. Adapted from Costa et al. (2013).

Optical microscopes are frequently used to monitor wastewater sludge samples. Selecting the most appropriate microscopy technique will depend on the physical characteristic of the object observed (e.g., size). Due to the lack of contrast of some objects, such as microbial cells or cellular constituents, several staining procedures can be used to increase contrast (Mesquita et al., 2015). Also, fluorescence dyes are commonly applied for the identification of bacterial species, distribution, viability, structure, and composition of microbial aggregates (Bassin et al., 2012b; de Kreuk et al., 2005; Ni et al., 2009; Padrão et al., 2022; Winkler et al., 2012).

The offline semi-automated system is most common in routine image analysis, consisting of sampling, preparation and visualization by an operator, with computers carrying out the quantitative task. While automatic online image analysis systems are possible (He et al., 2012; Koivuranta et al., 2015),

equipment costs and the difficulty of implementing them in full-scale WWTP are the main drawbacks. Nevertheless, with the emergence of new and more powerful digital cameras, it may be possible to overcome these problems in the near future (Costa et al., 2013).

Image acquisition

Digital cameras are constantly progressing in terms of image quality. These cameras work similarly to film cameras, yet instead of using a film to capture the light that comes from the lenses, digital cameras use a sensor to convert the light into an electrical signal. The sensor may be either a complementary metal-oxide-semiconductor (CMOS) or a charge-coupled device (CCD), which are the most common sensors used for quantitative microscopy applications (Lambert and Waters, 2014). However, CCD cameras are preferable for image analysis due to their benefit of producing low noise (Lambert and Waters, 2014). The electrical signal converted by the sensor is recorded into a digital code which a computer can process.

The number of possible values of each image element or pixel is determined by the bit depth (Figure 2.6). Eight bits monochrome images have 256 brightness values or levels ($2^8 = 256$) that range from black (0) to white (255) and are the most common in image analysis (Costa et al., 2013). Since colour is essential in fluorescence microscopy, images are converted to 24-bit, which have three channels (3 channels x 8 bit = 24 bits), namely Red, Green, and Blue (RGB), each with 256 brightness levels.

After the digital camera has captured the images, they must be stored on a computer hard drive to be further analysed. Images can be stored in several different formats, such as BMP (Bitmap), JPEG (Joint Photographic Experts Group), and TIFF (Tagged Image File Format). However, TIFF and BMP are the most used format in image analysis since they do not present any information loss. Since all the image data is kept in these formats, the generated file size is considerably larger than in other compressed formats.

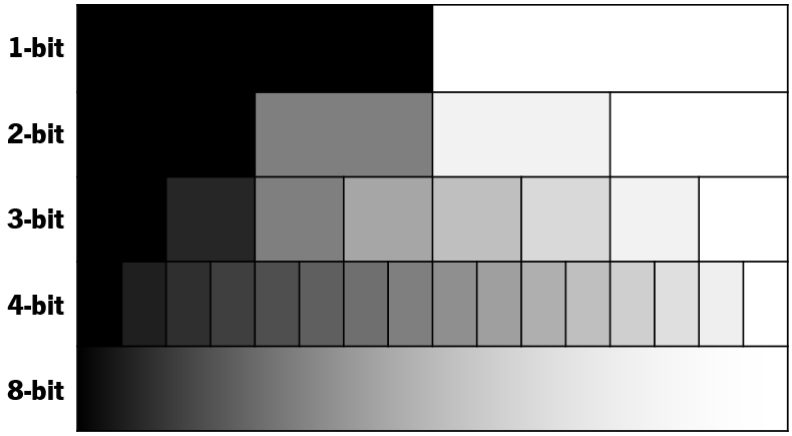


Figure 2.6 – Grey-scale signal brightness levels of a pixel at different bit depths. Adapted from Lambert and Waters (2014).

Image processing

The acquired images are processed to extract the inherent information. There are several software packages allowing extracting information from images, including ImageJ (Schneider et al., 2012), Matlab (Amaral, 2003), Visilog (Montes-H, 2005), and DAIME (Daims et al., 2006). First, the operator may define a series of processing parameters, such as background, object, and debris identification and segmentation threshold. If necessary, contrast enhancement or background correction may be performed to distinguish the image's object adequately. Original digital images are transformed into binary images in the segmentation step, where white pixels (value 1) identify the object and black pixels (value 0) identify the background (Figure 2.7). Segmentation is critical and should be automated to avoid the subjectivity of different operators (Pons and Vivier, 1999). While binary images are typically created by defining one segmentation threshold, in AS samples protruding and free filaments can be discriminated from the flocs structure by using two thresholds (Jenné et al., 2003), generating two different binary images (Figure 2.8). The final step of image processing is labelling, where a discrete number is given to all pixels that belong to an object, differing from object to object (Costa et al., 2013).

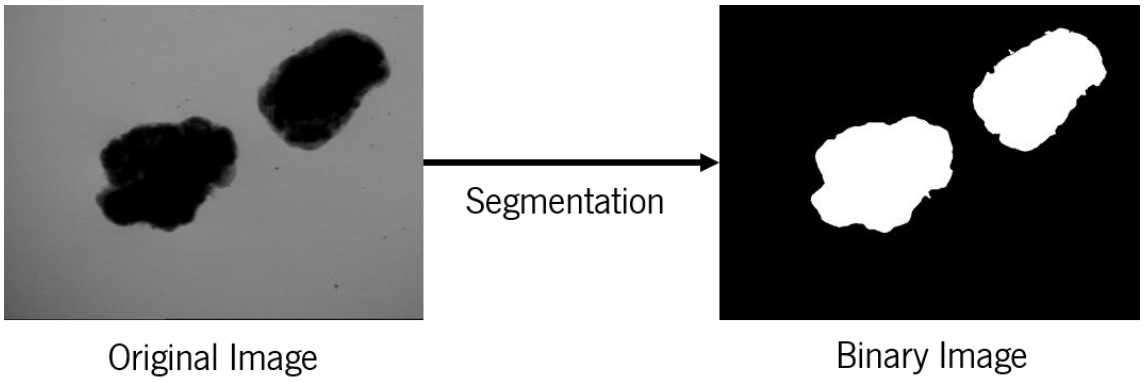


Figure 2.7 – Grey-scale image processing: the binary image generated from the original image segmentation. Images obtained during this work.

Image analysis and data analysis

Once the final image is obtained, it is possible to determine several Euclidean morphological parameters from the segmented binary image (Amaral, 2003). These parameters may be subdivided into size and shape descriptors. Size descriptors are derived by automatically counting the pixels corresponding to each object and then using that number to calculate each parameter that can be converted from pixel to metric units using a calibration factor (Amaral, 2003). The main size measurements used to characterize AS are the area, equivalent diameter, length, width, and perimeter (Jenné et al., 2006, 2003). While size descriptors are related to the size of the objects, shape descriptors are dimensionless parameters that describe their form and should be invariant regardless of their size (Pons and Vivier, 1999). Among the most common are circularity, elongation, roundness, compactness, and eccentricity (Amaral, 2003; Jenné et al., 2006; Pons and Vivier, 1999).

Aerobic and anaerobic WWT processes may generate much data concerning operating parameters and morphological data obtained from QIA. Advanced mathematical and statistical methods such as multivariate statistical analysis are crucial to integrate both data and extract the most relevant information underlying their relationships (Mesquita et al., 2013).

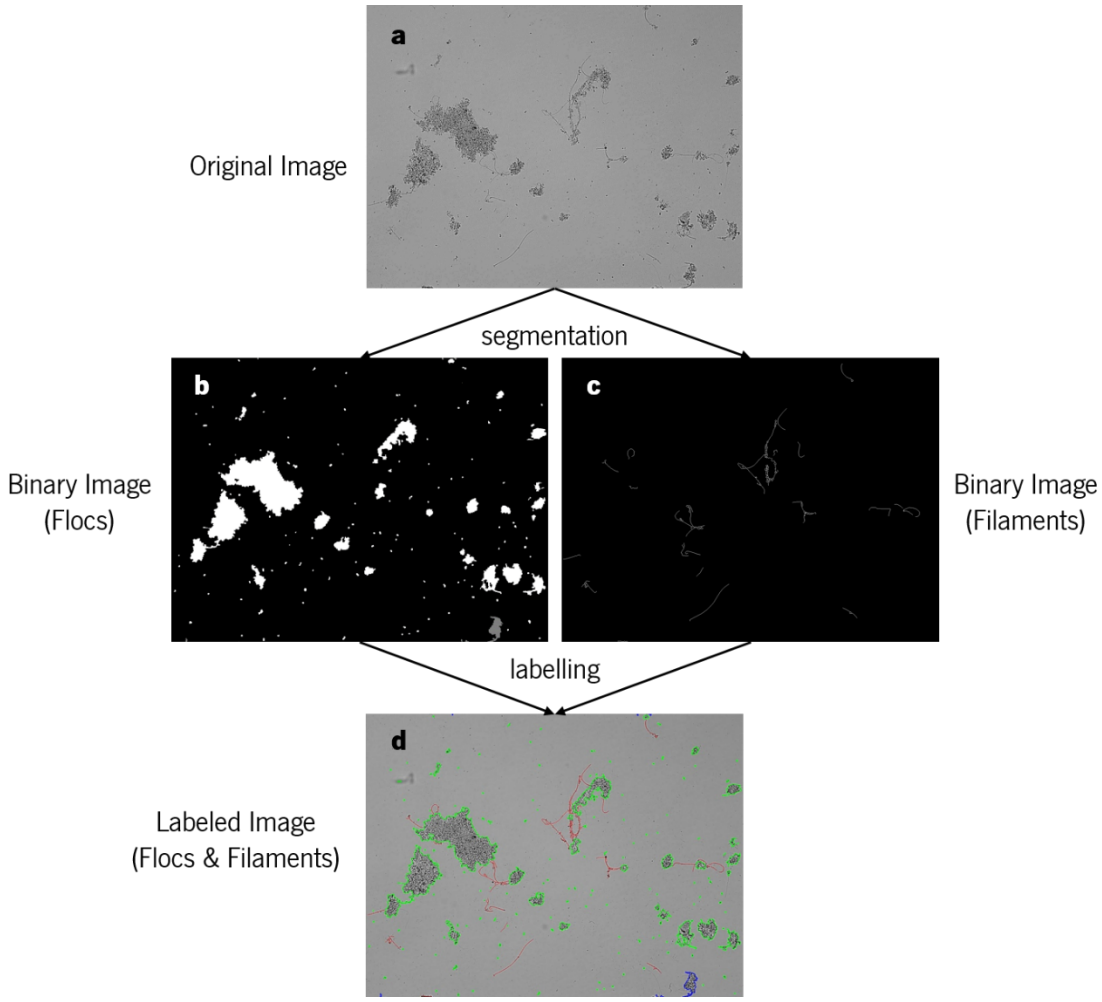


Figure 2.8 – Original image from activated sludge containing flocs and filaments (a). Distinct binary images containing flocs (b) and filaments (c). Labelled image identifying the flocs (green), filaments (red), and excluded object (blue) (d). Images obtained during this work.

2.6. CHEMOMETRIC ANALYSIS

Chemometrics is an interdisciplinary science that couples mathematics and multivariate statistics to extract information from chemical methods. The value of chemometrics in environmental science has been proven with the increased use of data processing techniques over the last two decades (Mesquita et al., 2013). Principal component analysis (PCA) and partial least squares (PLS) are the most widely used multivariate statistical analysis techniques in WWTP operation.

Principal component analysis

PCA determines linear combinations, called principal components (PCs), of a raw dataset, projecting it into a new coordinate system with the observations described by scores and variables by loadings. Being an iterative process, each resulting PC captures the maximum variation not explained by the former PCs to visualize latent structures and phenomena in the data. A dimensional reduction is also achieved given that the resulting PCs are orthogonal and, hence, uncorrelated. PCA has been widely used to interpret large data set generated in AS system (Jenné et al., 2006) or anaerobic systems (Costa et al., 2010). In AGS systems, PCA has been used to evaluate and identify relevant operational parameters and microbial communities affecting aerobic granulation (Bassin et al., 2019; Cui et al., 2021; Dockx et al., 2021).

Partial Least Squares

PLS is an iterative algorithm that extracts linear combinations of the essential features of a raw X dataset while modelling the Y data dependence on the work set to perform a multivariate calibration of the Y variable from the X dataset (Teppola et al., 1997; Wold et al., 2001). Monitoring complex processes using the PLS approach can be helpful since it can reduce the high dimensional strongly cross-correlated data to a much smaller and interpretable set of latent variables (Teppola et al., 1997). PLS reduces the dimension of the predictors that are correlated with Y while capturing a large amount of the variation in the X dataset. Using QIA data, PLS has been successfully applied to predict the effluent quality in AS and AGS systems (Costa et al., 2022; Mesquita et al., 2016). Thus, applying chemometrics to QIA data can provide additional valuable information for process control.

2.7. REFERENCES

Alves, M.M., Pereira, M.A., Sousa, D.Z., Cavaleiro, A.J., Picavet, M., Smidt, H., Stams, A.J.M., 2009. Waste lipids to energy: How to optimize methane production from long-chain fatty acids (LCFA). Microb. Biotechnol. 2, 538–550. https://doi.org/10.1111/j.1751-7915.2009.00100.x

Amaral, A.L.P., 2003. Image analysis in biotechnological processes: applications to wastewater treatment. PhD thesis, University of Minho. http://hdl.handle.net/1822/4506.

Amorim, C.L., Maia, A.S., Mesquita, R.B.R., Rangel, A.O.S.S., van Loosdrecht, M.C.M., Tiritan, M.E., Castro, P.M.L., 2014. Performance of aerobic granular sludge in a sequencing batch bioreactor exposed to ofloxacin, norfloxacin and ciprofloxacin. Water Res. 50, 101–113. https://doi.org/10.1016/j.watres.2013.10.043

Balasuriya, B.T.G., Ghose, A., Gheewala, S.H., Prapaspongsa, T., 2022. Assessment of eutrophication potential from fertiliser application in agricultural systems in Thailand. Sci. Total Environ. 833, 154993. https://doi.org/10.1016/j.scitotenv.2022.154993

Bassin, J.P., Kleerebezem, R., Dezotti, M., van Loosdrecht, M.C.M., 2012a. Simultaneous nitrogen and phosphate removal in aerobic granular sludge reactors operated at different temperatures. Water Res. 46, 3805–3816. https://doi.org/10.1016/j.watres.2012.04.015

Bassin, J.P., Tavares, D.C., Borges, R.C., Dezotti, M., 2019. Development of aerobic granular sludge under tropical climate conditions: The key role of inoculum adaptation under reduced sludge washout for stable granulation. J. Environ. Manage. 230, 168–182. https://doi.org/10.1016/j.jenvman.2018.09.072

Bassin, J.P., Winkler, M.K.H., Kleerebezem, R., Dezotti, M., van Loosdrecht, M.C.M., 2012b. Improved phosphate removal by selective sludge discharge in aerobic granular sludge reactors. Biotechnol. Bioeng. 109, 1919–1928. https://doi.org/10.1002/bit.24457

Bengtsson, S., de Blois, M., Wilén, B., Gustavsson, D., 2019. A comparison of aerobic granular sludge with conventional and compact biological treatment technologies. Environ. Technol. 40, 2769–2778. https://doi.org/10.1080/09593330.2018.1452985

Bengtsson, S., de Blois, M., Wilén, B.M., Gustavsson, D., 2018. Treatment of municipal wastewater with aerobic granular sludge. Crit. Rev. Environ. Sci. Technol. 48, 119–166. https://doi.org/10.1080/10643389.2018.1439653

Beun, J.., Hendriks, A., van Loosdrecht, M.C.., Morgenroth, E., Wilderer, P.., Heijnen, J.., 1999. Aerobic granulation in a sequencing batch reactor. Water Res. 33, 2283–2290. https://doi.org/10.1016/S0043-1354(98)00463-1

Beun, J.J., Van Loosdrecht, M.C.M., Heijnen, J.J., 2002. Aerobic granulation in a sequencing batch airlift reactor. Water Res. 36, 702–712. https://doi.org/10.1016/S0043-1354(01)00250-0

Beun, J.J., Van Loosdrecht, M.C.M., Heijnen, J.J., 2000. Aerobic granulation. Water Sci. Technol. 41, 41–48. https://doi.org/10.2166/wst.2000.0423

Bin, Z., Zhe, C., Zhigang, Q., Min, J., Zhiqiang, C., Zhaoli, C., Junwen, L., Xuan, W., Jingfeng, W., 2011. Dynamic and distribution of ammonia-oxidizing bacteria communities during sludge granulation in an anaerobic-aerobic sequencing batch reactor. Water Res. 45, 6207–6216. https://doi.org/10.1016/j.watres.2011.09.026

Carrera, P., Casero-Díaz, T., Castro-Barros, C.M., Méndez, R., Val del Río, A., Mosquera-Corral, A., 2021. Features of aerobic granular sludge formation treating fluctuating industrial saline wastewater at pilot scale. J. Environ. Manage. 296. https://doi.org/10.1016/j.jenvman.2021.113135

Cetin, E., Karakas, E., Dulekgurgen, E., Ovez, S., Kolukirik, M., Yilmaz, G., 2018. Effects of high-concentration influent suspended solids on aerobic granulation in pilot-scale sequencing batch reactors treating real domestic wastewater. Water Res. 131, 74–89. https://doi.org/10.1016/j.watres.2017.12.014

Chan, Y.J., Chong, M.F., Law, C.L., Hassell, D.G., 2009. A review on anaerobic-aerobic treatment of industrial and municipal wastewater. Chem. Eng. J. 155, 1–18. https://doi.org/10.1016/j.cej.2009.06.041

Chen, D., Li, H., Xue, X., Zhang, L., Hou, Y., Chen, H., Zhang, Y., Song, Y., Zhao, S., Guo, J., 2022. Enhanced simultaneous partial nitrification and denitrification performance of aerobic granular sludge via tapered aeration in sequencing batch reactor for treating low strength and low COD/TN ratio municipal wastewater. Environ. Res. 209, 112743. https://doi.org/10.1016/j.envres.2022.112743

Cheng, C.I., Chao, Y.M., Lin, M.C., Lin, C.H., 2011. Influence of temperature on process performance of activated sludge in coking wastewater treatment plant. Water Pract. Technol. 6. https://doi.org/10.2166/WPT.2011.018

Cho, S.K., Ju, H.J., Lee, J.G., Kim, S.H., 2014. Alkaline-mechanical pretreatment process for enhanced anaerobic digestion of thickened waste activated sludge with a novel crushing device: Performance evaluation and economic analysis. Bioresour. Technol. 165, 183–190.

https://doi.org/10.1016/j.biortech.2014.03.138

Chuda, A., Ziemiński, K., 2021. Challenges in treatment of digestate liquid fraction from biogas plant. Performance of nitrogen removal and microbial activity in activated sludge process. Energies 14. https://doi.org/10.3390/en14217321

Corsino, S.F., Campo, R., Di Bella, G., Torregrossa, M., Viviani, G., 2015. Cultivation of granular sludge with hypersaline oily wastewater. Int. Biodeterior. Biodegrad. 105, 192–202. https://doi.org/10.1016/j.ibiod.2015.09.009

Costa, J.C., Alves, M.M., Ferreira, E.C., 2010. A chemometric tool to monitor high-rate anaerobic granular sludge reactors during load and toxic disturbances. Biochem. Eng. J. 53, 38–43. https://doi.org/10.1016/j.bej.2008.12.006

Costa, J.C., Gonçalves, P.R., Nobre, A., Alves, M.M., 2012. Biomethanation potential of macroalgae *Ulva* spp. and *Gracilaria* spp. and in co-digestion with waste activated sludge. Bioresour. Technol. 114, 320–326. https://doi.org/10.1016/j.biortech.2012.03.011

Costa, J.C., Mesquita, D.P., Amaral, A.L., Alves, M.M., Ferreira, E.C., 2013. Quantitative image analysis for the characterization of microbial aggregates in biological wastewater treatment: a review. Environ. Sci. Pollut. Res. 20, 5887–5912. https://doi.org/10.1007/s11356-013-1824-5

Costa, J.G., Paulo, A.M.S., Amorim, C.L., Amaral, A.L., Castro, P.M.L., Ferreira, E.C., Mesquita, D.P., 2022. Quantitative image analysis as a robust tool to assess effluent quality from an aerobic granular sludge system treating industrial wastewater. Chemosphere 291. https://doi.org/10.1016/j.chemosphere.2021.132773

Cui, F., Kim, Minkyung, Park, C., Kim, D., Mo, K., Kim, Moonil, 2021. Application of principal component analysis (PCA) to the assessment of parameter correlations in the partial-nitrification process using aerobic granular sludge. J. Environ. Manage. 288, 112408. https://doi.org/10.1016/j.jenvman.2021.112408

Daims, H., Lücker, S., Wagner, M., 2006. Daime, a Novel Image Analysis Program for Microbial Ecology and Biofilm Research. Environ. Microbiol. 8, 200–213. https://doi.org/10.1111/j.1462-2920.2005.00880.x

de Kreuk, M.K., Heijnen, J.J., Van Loosdrecht, M.C.M., 2005. Simultaneous COD, nitrogen, and phosphate removal by aerobic granular sludge. Biotechnol. Bioeng. 90, 761–769. https://doi.org/10.1002/bit.20470

de Kreuk, M.K., Kishida, N., van Loosdrecht, M.C.M., 2007. Aerobic granular sludge - State of the art. Water Sci. Technol. 55, 75–81. https://doi.org/10.2166/wst.2007.244

de Kreuk, M.K., van Loosdrecht, M.C.M., 2004. Selection of slow growing organisms as a means for improving aerobic granular sludge stability. Water Sci. Technol. 49, 9–17. https://doi.org/10.2166/wst.2004.0792

De Vrieze, J., Hennebel, T., Boon, N., Verstraete, W., 2012. Methanosarcina: The rediscovered methanogen for heavy duty biomethanation. Bioresour. Technol. 112, 1–9. https://doi.org/10.1016/j.biortech.2012.02.079

Devlin, T.R., di Biase, A., Kowalski, M., Oleszkiewicz, J.A., 2017. Granulation of activated sludge under low hydrodynamic shear and different wastewater characteristics. Bioresour. Technol. 224, 229–235. https://doi.org/10.1016/j.biortech.2016.11.005

Dockx, L., Caluwé, M., De Vleeschauwer, F., Dobbeleers, T., Dries, J., 2021. Impact of the substrate composition on enhanced biological phosphorus removal during formation of aerobic granular sludge. Bioresour. Technol. 337. https://doi.org/10.1016/j.biortech.2021.125482

Donkor, K.O., Gottumukkala, L.D., Lin, R., Murphy, J.D., 2022. A perspective on the combination of alkali pre-treatment with bioaugmentation to improve biogas production from lignocellulose biomass. Bioresour.

Technol. 351, 126950. https://doi.org/10.1016/j.biortech.2022.126950

Duarte, M.S., Oliveira, J. V., Pereira, C., Carvalho, M., Mesquita, D.P., Alves, M.M., 2021. Volatile Fatty Acids (VFA) Production from Wastewaters with High Salinity—Influence of pH, Salinity and Reactor Configuration. Fermentation 7, 303. https://doi.org/10.3390/fermentation7040303

EEA., 2021. Urban wastewater treatment in Europe. Available online: https://www.eea.europa.eu/data-and-maps/indicators/urban-waste-water-treatment/urban-waste-water-treatment-assessment-5 (accessed on 30 may 2022).

Figueroa, M., Val Del Río, A., Campos, J.L., Méndez, R., Mosquera-Corral, A., 2015. Filamentous bacteria existence in aerobic granular reactors. Bioprocess Biosyst. Eng. 38, 841–851. https://doi.org/10.1007/s00449-014-1327-x

Franca, R.D.G., Pinheiro, H.M., van Loosdrecht, M.C.M., Lourenço, N.D., 2018. Stability of aerobic granules during long-term bioreactor operation. Biotechnol. Adv. 36, 228–246. https://doi.org/10.1016/j.biotechadv.2017.11.005

Giesen, A., de Bruin, L.M.M., Niermans, R.P., van der Roest, H.F., 2013. Advancements in the application of aerobic granular biomass technology for sustainable treatment of wastewater. Water Pract. Technol. 8, 47–54. https://doi.org/10.2166/wpt.2013.007

Guimarães, L.B., Wagner, J., Akaboci, T.R.V., Daudt, G.C., Nielsen, P.H., van Loosdrecht, M.C.M., Weissbrodt, D.G., da Costa, R.H.R., 2020. Elucidating performance failures in use of granular sludge for nutrient removal from domestic wastewater in a warm coastal climate region. Environ. Technol. (United Kingdom) 41, 1896–1911. https://doi.org/10.1080/09593330.2018.1551938

Guo, J., Peng, Y., Wang, S., Yang, X., Yuan, Z., 2014. Filamentous and non-filamentous bulking of activated sludge encountered under nutrients limitation or deficiency conditions. Chem. Eng. J. 255, 453–461. https://doi.org/10.1016/j.cej.2014.06.075

Haaksman, V.A., Mirghorayshi, M., van Loosdrecht, M.C.M., Pronk, M., 2020. Impact of aerobic availability of readily biodegradable COD on morphological stability of aerobic granular sludge. Water Res. 187, 116402. https://doi.org/10.1016/j.watres.2020.116402

He, Q., Chen, L., Zhang, S., Wang, L., Liang, J., Xia, W., Wang, H., Zhou, J., 2018. Simultaneous nitrification, denitrification and phosphorus removal in aerobic granular sequencing batch reactors with high aeration intensity: Impact of aeration time. Bioresour. Technol. 263, 214–222. https://doi.org/10.1016/j.biortech.2018.05.007

He, Q., Song, J., Zhang, W., Gao, S., Wang, H., Yu, J., 2020. Enhanced simultaneous nitrification, denitrification and phosphorus removal through mixed carbon source by aerobic granular sludge. J. Hazard. Mater. 382, 121043. https://doi.org/10.1016/j.jhazmat.2019.121043

He, Q., Zhang, W., Zhang, S., Wang, H., 2017. Enanced nitrogen removal in an aerobic granular sequencing batch reactor performing simultaneous nitrification, endogenous denitrification and phosphorus removal with low superficial gas velocity. Chem. Eng. J. 326, 1223–1231. https://doi.org/10.1016/j.cej.2017.06.071

He, W., Nan, J., Li, H., Li, S., 2012. Characteristic analysis on temporal evolution of floc size and structure in low-shear flow. Water Res. 46, 509–520. https://doi.org/10.1016/j.watres.2011.11.040

Henriet, O., Meunier, C., Henry, P., Mahillon, J., 2016. Improving phosphorus removal in aerobic granular sludge processes through selective microbial management. Bioresour. Technol. 211, 298–306. https://doi.org/10.1016/j.biortech.2016.03.099

Holohan, B.C., Duarte, M.S., Szabo-Corbacho, M.A., Cavaleiro, A.J., Salvador, A.F., Pereira, M.A., Ziels, R.M., Frijters, C.T.M.J., Pacheco-Ruiz, S., Carballa, M., Sousa, D.Z., Stams, A.J.M., O'Flaherty, V., van Lier, J.B.,

Alves, M.M., 2022. Principles, Advances, and Perspectives of Anaerobic Digestion of Lipids. Environ. Sci. Technol. 56, 4749–4775. https://doi.org/10.1021/acs.est.1c08722

Iorhemen, O.T., Zaghloul, M.S., Hamza, R.A., Tay, J.H., 2020. Long-term aerobic granular sludge stability through anaerobic slow feeding, fixed feast-famine period ratio, and fixed SRT. J. Environ. Chem. Eng. 8, 103681. https://doi.org/10.1016/j.jece.2020.103681

Jenné, R., Banadda, E.N., Gins, G., Deurinck, J., Smets, I.Y., Geeraerd, A.H., Van Impe, J.F., 2006. Use of image analysis for sludge characterisation: studying the relation between floc shape and sludge settleability. Water Sci. Technol. 54, 167–174. https://doi.org/10.2166/wst.2006.384

Jenné, R., Banadda, E.N., Philips, N., Van Impe, J.F., 2003. Image Analysis as a Monitoring Tool for Activated Sludge Properties in Lab-Scale Installations. J. Environ. Sci. Heal. Part A 38, 2009–2018. https://doi.org/10.1081/ESE-120023328

Kirkland, C.M., Krug, J.R., Vergeldt, F.J., van den Berg, L., Velders, A.H., Seymour, J.D., Codd, S.L., van As, H., de Kreuk, M.K., 2020. Characterizing the structure of aerobic granular sludge using ultra-high field magnetic resonance. Water Sci. Technol. 82, 627–639. https://doi.org/10.2166/wst.2020.341

Koivuranta, E., Stoor, T., Hattuniemi, J., Niinimäki, J., 2015. On-line optical monitoring of activated sludge floc morphology. J. Water Process Eng. 5, 28–34. https://doi.org/10.1016/j.jwpe.2014.12.009

Kong, Y., Liu, Y.Q., Tay, J.H., Wong, F.S., Zhu, J., 2009. Aerobic granulation in sequencing batch reactors with different reactor height/diameter ratios. Enzyme Microb. Technol. 45, 379–383. https://doi.org/10.1016/j.enzmictec.2009.06.014

Lambert, T.J., Waters, J.C., 2014. Assessing camera performance for quantitative microscopy, 1st ed, Methods in Cell Biology. Elsevier Inc. https://doi.org/10.1016/B978-0-12-420138-5.00003-3

Lemaire, R., Webb, R.I., Yuan, Z., 2008. Micro-scale observations of the structure of aerobic microbial granules used for the treatment of nutrient-rich industrial wastewater. ISME J. 2, 528–541. https://doi.org/10.1038/ismej.2008.12

Li, Z., Meng, Q., Wan, C., Zhang, C., Tan, X., Liu, X., 2022. Aggregation performance and adhesion behavior of microbes in response to feast/famine condition: Rapid granulation of aerobic granular sludge. Environ. Res. 208, 112780. https://doi.org/10.1016/j.envres.2022.112780

Li, Z.H., Zhu, Y.M., Zhang, Y.L., Zhang, Y.R., He, C.B., Yang, C.J., 2019. Characterization of aerobic granular sludge of different sizes for nitrogen and phosphorus removal. Environ. Technol. (United Kingdom) 40, 3622–3631. https://doi.org/10.1080/09593330.2018.1483971

Lin, H., Ma, R., Hu, Y., Lin, J., Sun, S., Jiang, J., Li, T., Liao, Q., Luo, J., 2020. Reviewing bottlenecks in aerobic granular sludge technology : Slow granulation and low granular stability. Environ. Pollut. 263, 114638. https://doi.org/10.1016/j.envpol.2020.114638

Liu, X., Sun, S., Ma, B., Zhang, C., Wan, C., Lee, D.J., 2016. Understanding of aerobic granulation enhanced by starvation in the perspective of quorum sensing. Appl. Microbiol. Biotechnol. 100, 3747–3755. https://doi.org/10.1007/s00253-015-7246-1

Liu, Y., Tay, J.-H., 2002. The essential role of hydrodynamic shear force in the formation of biofilm and granular sludge. Water Res. 36, 1653–1665. https://doi.org/10.1016/S0043-1354(01)00379-7

Liu, Y., Tay, J.H., 2004. State of the art of biogranulation technology for wastewater treatment. Biotechnol. Adv. 22, 533–563. https://doi.org/10.1016/j.biotechadv.2004.05.001

Liu, Y., Wang, Z.W., Qin, L., Liu, Y.Q., Tay, J.H., 2005a. Selection pressure-driven aerobic granulation in a sequencing batch reactor. Appl. Microbiol. Biotechnol. 67, 26–32. https://doi.org/10.1007/s00253-004-1820-2

Liu, Y., Wang, Z.W., Tay, J.H., 2005b. A unified theory for upscaling aerobic granular sludge sequencing batch reactors. Biotechnol. Adv. 23, 335–344. https://doi.org/10.1016/j.biotechadv.2005.04.001

Liu, Y., Yang, S.F., Tay, J.H., 2004. Improved stability of aerobic granules by selecting slow-growing nitrifying bacteria. J. Biotechnol. 108, 161–169. https://doi.org/10.1016/j.jbiotec.2003.11.008

Liu, Y.Q., Moy, B., Kong, Y.H., Tay, J.H., 2010. Formation, physical characteristics and microbial community structure of aerobic granules in a pilot-scale sequencing batch reactor for real wastewater treatment. Enzyme Microb. Technol. 46, 520–525. https://doi.org/10.1016/j.enzmictec.2010.02.001

Liu, Y.Q., Tay, J.H., 2008. Influence of starvation time on formation and stability of aerobic granules in sequencing batch reactors. Bioresour. Technol. 99, 980–985. https://doi.org/10.1016/j.biortech.2007.03.011

Liu, Y.Q., Tay, J.H., 2007. Characteristics and stability of aerobic granules cultivated with different starvation time. Appl. Microbiol. Biotechnol. 75, 205–210. https://doi.org/10.1007/s00253-006-0797-4

Long, B., Xuan, X., Yang, C., Zhang, L., Cheng, Y., Wang, J., 2019. Stability of aerobic granular sludge in a pilot scale sequencing batch reactor enhanced by granular particle size control. Chemosphere 225, 460–469. https://doi.org/10.1016/j.chemosphere.2019.03.048

López-Palau, S., Pinto, A., Basset, N., Dosta, J., Mata-Álvarez, J., 2012. ORP slope and feast-famine strategy as the basis of the control of a granular sequencing batch reactor treating winery wastewater. Biochem. Eng. J. 68, 190–198. https://doi.org/10.1016/j.bej.2012.08.002

Luo, J., Hao, T., Wei, L., Mackey, H.R., Lin, Z., Chen, G.H., 2014. Impact of influent COD/N ratio on disintegration of aerobic granular sludge. Water Res. 62, 127–135. https://doi.org/10.1016/j.watres.2014.05.037

Mañas, A., Biscans, B., Spérandio, M., 2011. Biologically induced phosphorus precipitation in aerobic granular sludge process. Water Res. 45, 3776–3786. https://doi.org/10.1016/j.watres.2011.04.031

Melo, A., Quintelas, C., Ferreira, E.C., Mesquita, D.P., 2022. The Role of Extracellular Polymeric Substances in Micropollutant Removal. Front. Chem. Eng. 4, 1–13. https://doi.org/10.3389/fceng.2022.778469

Mesquita, D.P., Amaral, A.L., Ferreira, E.C., 2016. Estimation of effluent quality parameters from an activated sludge system using quantitative image analysis. Chem. Eng. J. 285, 349–357. https://doi.org/10.1016/j.cej.2015.09.110

Mesquita, D.P., Amaral, A.L., Ferreira, E.C., 2013. Activated sludge characterization through microscopy: A review on quantitative image analysis and chemometric techniques. Anal. Chim. Acta 802, 14–28. https://doi.org/10.1016/j.aca.2013.09.016

Mesquita, D.P., Amaral, A.L., Leal, C., Oehmen, A., Reis, M.A.M., Ferreira, E.C., 2015. Analytica Chimica Acta Polyhydroxyalkanoate granules quanti fi cation in mixed microbial cultures using image analysis : Sudan Black B versus Nile Blue A staining. Anal. Chim. Acta 865, 8–15. https://doi.org/10.1016/j.aca.2015.01.018

Metcalf and Eddy, 2003. Wastewater Engineering: Treatment and Reuse, 4th ed, McGraw-Hill. Boston.

Montes-H, G., 2005. Swelling-shrinkage measurements of bentonite using coupled environmental scanning electron microscopy and digital image analysis. J. Colloid Interface Sci. 284, 271–277. https://doi.org/10.1016/j.jcis.2004.09.025

Morgenroth, E., Sherden, T., Van Loosdrecht, M.C.M., Heijnen, J.J., Wilderer, P.A., 1997. Aerobic granular sludge in a sequencing batch reactor. Water Res. 31, 3191–3194. https://doi.org/10.1016/S0043-1354(97)00216-9

Mosquera-Corral, A., De Kreuk, M.K., Heijnen, J.J., Van Loosdrecht, M.C.M., 2005. Effects of oxygen

concentration on N-removal in an aerobic granular sludge reactor. Water Res. 39, 2676–2686. https://doi.org/10.1016/j.watres.2005.04.065

Moura, L.L., Duarte, K.L.S., Santiago, E.P., Mahler, C.F., Bassin, J.P., 2018. Strategies to re-establish stable granulation after filamentous outgrowth: Insights from lab-scale experiments. Process Saf. Environ. Prot. 117, 606–615. https://doi.org/10.1016/j.psep.2018.06.005

Nancharaiah, Y. V., Reddy, G.K.K., 2018. Aerobic granular sludge technology: Mechanisms of granulation and biotechnological applications. Bioresour. Technol. 247, 1128–1143. https://doi.org/10.1016/j.biortech.2017.09.131

Ni, B.J., Xie, W.M., Liu, S.G., Yu, H.Q., Wang, Y.Z., Wang, G., Dai, X.L., 2009. Granulation of activated sludge in a pilot-scale sequencing batch reactor for the treatment of low-strength municipal wastewater. Water Res. 43, 751–761. https://doi.org/10.1016/j.watres.2008.11.009

Padrão, J., Ferreira, V., Mesquita, D.P., Cortez, S., Dias, N., Duarte, M.S., Tortella, G., Fernandes, I., Mota, M., Nicolau, A., 2022. Negative impacts of cleaning agent DEPTAL MCL® on activated sludge wastewater treatment system. Sci. Total Environ. 838, 155957. https://doi.org/10.1016/j.scitotenv.2022.155957

Paulo, A.M.S., Amorim, C.L., Costa, J., Mesquita, D.P., Ferreira, E.C., Castro, P.M.L., 2021. Long-term stability of a non-adapted aerobic granular sludge process treating fish canning wastewater associated to EPS producers in the core microbiome. Sci. Total Environ. 756. https://doi.org/10.1016/j.scitotenv.2020.144007

Pereira, M.A., 2003. Anaerobic biodegradation of long chain fatty acids: biomethanisation of biomass-associated LCFA as a challenge for the anaerobic treatment of effluents with high lipid/LCFA content. PhD thesis, University of Minho. http://hdl.handle.net/1822/4650.

Pijuan, M., Werner, U., Yuan, Z., 2011. Reducing the startup time of aerobic granular sludge reactors through seeding floccular sludge with crushed aerobic granules. Water Res. 45, 5075–5083. https://doi.org/10.1016/j.watres.2011.07.009

Pishgar, R., Dominic, J.A., Sheng, Z., Tay, J.H., 2019. Influence of operation mode and wastewater strength on aerobic granulation at pilot scale: Startup period, granular sludge characteristics, and effluent quality. Water Res. 160, 81–96. https://doi.org/10.1016/j.watres.2019.05.026

Pishgar, R., Lee, J., Dominic, J.A., Hosseini, S., Tay, J.H., Chu, A., 2020. Augmentation of Biogranules for Enhanced Performance of Full-Scale Lagoon-Based Municipal Wastewater Treatment Plants. Appl. Biochem. Biotechnol. 191, 426–443. https://doi.org/10.1007/s12010-020-03256-3

Pons, M.N., Vivier, H., 1999. Biomass Quantification by Image Analysis, in: Bioanalysis and Biosensors for Bioprocess Monitoring - Adv. Biochem. Engin./Biotechnol. Springer, Berlin, pp. 133–184.

Preethi, Banu J, R., Varjani, S., P, S., Tyagi, V.K., Gunasekaran, M., 2022. Breakthrough in hydrolysis of waste biomass by physico-chemical pretreatment processes for efficient anaerobic digestion. Chemosphere 294, 133617. https://doi.org/10.1016/j.chemosphere.2022.133617

Pronk, M., de Kreuk, M.K., de Bruin, B., Kamminga, P., Kleerebezem, R., van Loosdrecht, M.C.M., 2015. Full scale performance of the aerobic granular sludge process for sewage treatment. Water Res. 84, 207–217. https://doi.org/10.1016/j.watres.2015.07.011

Qin, L., Liu, Y., Tay, J.H., 2004a. Effect of settling time on aerobic granulation in sequencing batch reactor. Biochem. Eng. J. 21, 47–52. https://doi.org/10.1016/j.bej.2004.03.005

Qin, L., Tay, J.H., Liu, Y., 2004b. Selection pressure is a driving force of aerobic granulation in sequencing batch reactors. Process Biochem. 39, 579–584. https://doi.org/10.1016/S0032-9592(03)00125-0

Quoc, B.N., Armenta, M., Carter, J.A., Bucher, R., Sukapanpotharam, P., Bryson, S.J., Stahl, D.A., Stensel, H.D.,

Winkler, M.K.H., 2021a. An investigation into the optimal granular sludge size for simultaneous nitrogen and phosphate removal. Water Res. 198, 117119. https://doi.org/10.1016/j.watres.2021.117119

Quoc, B.N., Wei, S., Armenta, M., Bucher, R., Sukapanpotharam, P., Stahl, D.A., Stensel, H.D., Winkler, M.K.H., 2021b. Aerobic granular sludge: Impact of size distribution on nitrification capacity. Water Res. 188, 116445. https://doi.org/10.1016/j.watres.2020.116445

Ranzinger, F., Matern, M., Layer, M., Guthausen, G., Wagner, M., Derlon, N., Horn, H., 2020. Transport and retention of artificial and real wastewater particles inside a bed of settled aerobic granular sludge assessed applying magnetic resonance imaging. Water Res. X 7, 100050. https://doi.org/10.1016/j.wroa.2020.100050

Rocktäschel, T., Klarmann, C., Helmreich, B., Ochoa, J., Boisson, P., Sørensen, K.H., Horn, H., 2013. Comparison of two different anaerobic feeding strategies to establish a stable aerobic granulated sludge bed. Water Res. 47, 6423–6431. https://doi.org/10.1016/j.watres.2013.08.014

Rosa-Masegosa, A., Muñoz-Palazon, B., Gonzalez-Martinez, A., Fenice, M., Gorrasi, S., Gonzalez-Lopez, J., 2021. New advances in aerobic granular sludge technology using continuous flow reactors: Engineering and microbiological aspects. Water (Switzerland) 13, 1–20. https://doi.org/10.3390/w13131792

Sarma, S.J., Tay, J.H., Chu, A., 2017. Finding Knowledge Gaps in Aerobic Granulation Technology. Trends Biotechnol. 35, 66–78. https://doi.org/10.1016/j.tibtech.2016.07.003

Schink, B., 1997. Energetics of syntrophic cooperation in methanogenic degradation. Microbiol. Mol. Biol. Rev. 61, 262–280. https://doi.org/1092-2172/97/$04.0010

Schneider, C.A., Rasband, W.S., Eliceiri, K.W., 2012. NIH Image to ImageJ: 25 years of image analysis. Nat. Methods 9, 671–675. https://doi.org/10.1038/nmeth.2089

Schwarzenbeck, N., Borges, J.M., Wilderer, P.A., 2005. Treatment of dairy effluents in an aerobic granular sludge sequencing batch reactor. Appl. Microbiol. Biotechnol. 66, 711–718. https://doi.org/10.1007/s00253-004-1748-6

Sguanci, S., Lubello, C., Caffaz, S., Lotti, T., 2019. Long-term stability of aerobic granular sludge for the treatment of very low-strength real domestic wastewater. J. Clean. Prod. 222, 882–890. https://doi.org/10.1016/j.jclepro.2019.03.061

Silva, S.A., Cavaleiro, A.J., Pereira, M.A., Stams, A.J.M., Alves, M.M., Sousa, D.Z., 2014. Long-term acclimation of anaerobic sludges for high-rate methanogenesis from LCFA. Biomass and Bioenergy 67, 297–303. https://doi.org/10.1016/j.biombioe.2014.05.012

Silva, S.A., Val del Río, A., Amaral, A.L., Ferreira, E.C., Alves, M.M., Mesquita, D.P., 2022. Monitoring morphological changes from activated sludge to aerobic granular sludge under distinct organic loading rates and increasing minimal imposed sludge settling velocities through quantitative image analysis. Chemosphere 286, 131637. https://doi.org/10.1016/j.chemosphere.2021.131637

Sturm, B.S.M., Irvine, R.L., 2008. Dissolved oxygen as a key parameter to aerobic granule formation. Water Sci. Technol. 58, 781–787. https://doi.org/10.2166/wst.2008.393

Tay, J.H., Liu, Q.S., Liu, Y., 2001. The effects of shear force on the formation, structure and metabolism of aerobic granules. Appl. Microbiol. Biotechnol. 57, 227–233. https://doi.org/10.1007/s002530100766

Teppola, P., Mujunen, S.P., Minkkinen, P., 1997. Partial least squares modeling of an activated sludge plant: A case study. Chemom. Intell. Lab. Syst. 38, 197–208. https://doi.org/10.1016/S0169-7439(97)00055-5

Thwaites, B.J., Reeve, P., Dinesh, N., Short, M.D., van den Akker, B., 2017. Comparison of an anaerobic feed and split anaerobic–aerobic feed on granular sludge development, performance and ecology. Chemosphere 172, 408–417. https://doi.org/10.1016/j.chemosphere.2016.12.133

Tomar, S.K., Kumar, R., Chakraborty, S., 2022. Simultaneous biodegradation of pyridine, indole, and ammonium along with phenol and thiocyanate by aerobic granular sludge. J. Hazard. Mater. 422, 126861. https://doi.org/10.1016/j.jhazmat.2021.126861

Val del Rio, A., 2013. Aerobic granular biomass systems: a challenge for a better wastewater treatment and sludge management. Universidade de Santiago de Compostela http://hdl.handle.net/10347/7286.

Val Del Río, A., Figueroa, M., Mosquera-Corral, A., Campos, J.L., Méndez, R., 2013. Stability of aerobic granular biomass treating the effluent from a seafood industry. Int. J. Environ. Res. 7, 265–276. https://doi.org/10.22059/ijer.2013.606

van der Roest, H.F., de Bruin, L.M.M., Gademan, G., Coelho, F., 2011. Towards sustainable waste water treatment with Dutch Nereda® technology. Water Pract. Technol. 6, 3–6. https://doi.org/10.2166/wpt.2011.059

van Lier, J.B., van der Zee, F.P., Frijters, C.T.M.J., Ersahin, M.E., 2015. Celebrating 40 years anaerobic sludge bed reactors for industrial wastewater treatment. Rev. Environ. Sci. Bio/Technology 14, 681–702. https://doi.org/10.1007/s11157-015-9375-5

van Loosdrecht, M.C.M., Pot, M.A., Heijnen, J.J., 1997. Importance of bacterial storage polymers in bioprocesses. Water Sci. Technol. 35, 41–47. https://doi.org/10.1016/S0273-1223(96)00877-3

Verawaty, M., Tait, S., Pijuan, M., Yuan, Z., Bond, P.L., 2013. Breakage and growth towards a stable aerobic granule size during the treatment of wastewater. Water Res. 47, 5338–5349. https://doi.org/10.1016/j.watres.2013.06.012

Wang, R., Yang, C., Hu, H., Yang, Q., Du, B., 2021. The impact of the varying nutrient concentrations on the enhanced biological phosphorus removal performance and functional phosphorus-accumulating and denitrifying genes in an anaerobic–aerobic–anoxic sequencing batch reactor. Environ. Technol. Innov. 21. https://doi.org/10.1016/j.eti.2020.101256

Wilén, B.M., Liébana, R., Persson, F., Modin, O., Hermansson, M., 2018. The mechanisms of granulation of activated sludge in wastewater treatment, its optimization, and impact on effluent quality. Appl. Microbiol. Biotechnol. 102, 5005–5020. https://doi.org/10.1007/s00253-018-8990-9

Wilén, B.M., Lumley, D., Mattsson, A., Mino, T., 2006. Rain events and their effect on effluent quality studied at a full scale activated sludge treatment plant. Water Sci. Technol. 54, 201–208. https://doi.org/10.2166/wst.2006.721

Winkler, M.K.H., Bassin, J.P., Kleerebezem, R., Sorokin, D.Y., Van Loosdrecht, M.C.M., 2012. Unravelling the reasons for disproportion in the ratio of AOB and NOB in aerobic granular sludge. Appl. Microbiol. Biotechnol. 94, 1657–1666. https://doi.org/10.1007/s00253-012-4126-9

Winkler, M.K.H., Kleerebezem, R., De Bruin, L.M.M., Verheijen, P.J.T., Abbas, B., Habermacher, J., Van Loosdrecht, M.C.M., 2013. Microbial diversity differences within aerobic granular sludge and activated sludge flocs. Appl. Microbiol. Biotechnol. 97, 7447–7458. https://doi.org/10.1007/s00253-012-4472-7

Winkler, M.K.H., Meunier, C., Henriet, O., Mahillon, J., Suárez-Ojeda, M.E., Del Moro, G., De Sanctis, M., Di Iaconi, C., Weissbrodt, D.G., 2018. An integrative review of granular sludge for the biological removal of nutrients and recalcitrant organic matter from wastewater. Chem. Eng. J. 336, 489–502. https://doi.org/10.1016/j.cej.2017.12.026

Wold, S., Sjöström, M., Eriksson, L., 2001. PLS-regression: A basic tool of chemometrics. Chemom. Intell. Lab. Syst. 58, 109–130. https://doi.org/10.1016/S0169-7439(01)00155-1

Xavier, J.A., Guimarães, L.B., Magnus, B.S., Leite, W.R., Vilar, V.J.P., da Costa, R.H.R., 2021. How volumetric exchange ratio and carbon availability contribute to enhance granular sludge stability in a fill/draw mode SBR treating domestic wastewater? J. Water Process Eng. 40.

https://doi.org/10.1016/j.jwpe.2021.101917

Yang, S.F., Liu, Q.S., Tay, J.H., Liu, Y., 2004. Growth kinetics of aerobic granules developed in sequencing batch reactors. Lett. Appl. Microbiol. 38, 106–112. https://doi.org/10.1111/j.1472-765X.2003.01452.x

Yoshino, H., Suenaga, T., Fujii, T., Hori, T., Terada, A., Hosomi, M., 2017. Efficacy of a high-pressure jet device for excess sludge reduction in a conventional activated sludge process: Pilot-scale demonstration. Chem. Eng. J. 326, 78–86. https://doi.org/10.1016/j.cej.2017.05.084

Yuan, H., Zhu, N., 2016. Progress in inhibition mechanisms and process control of intermediates and by-products in sewage sludge anaerobic digestion. Renew. Sustain. Energy Rev. 58, 429–438. https://doi.org/10.1016/j.rser.2015.12.261

Zhang, H., Dong, F., Jiang, T., Wei, Y., Wang, T., Yang, F., 2011. Aerobic granulation with low strength wastewater at low aeration rate in A/O/A SBR reactor. Enzyme Microb. Technol. 49, 215–222. https://doi.org/10.1016/j.enzmictec.2011.05.006

Zhang, Y., Dong, X., Nuramkhaan, M., Lei, Z., Shimizu, K., Zhang, Z., Adachi, Y., Lee, D.J., Tay, J.H., 2019. Rapid granulation of aerobic granular sludge: A mini review on operation strategies and comparative analysis. Bioresour. Technol. Reports 7, 100206. https://doi.org/10.1016/j.biteb.2019.100206

Zhang, Z., Yu, Z., Dong, J., Wang, Z., Ma, K., Xu, X., Alvarezc, P.J.J., Zhu, L., 2018. Stability of aerobic granular sludge under condition of low influent C/N ratio: Correlation of sludge property and functional microorganism. Bioresour. Technol. 270, 391–399. https://doi.org/10.1016/j.biortech.2018.09.045

Zhou, J. heng, Zhang, Z. ming, Zhao, H., Yu, H. tian, Alvarez, P.J.J., Xu, X. yang, Zhu, L., 2016. Optimizing granules size distribution for aerobic granular sludge stability: Effect of a novel funnel-shaped internals on hydraulic shear stress. Bioresour. Technol. 216, 562–570. https://doi.org/10.1016/j.biortech.2016.05.079

Zou, J., Li, Y., Zhang, L., Wang, R., Sun, J., 2015. Understanding the impact of influent nitrogen concentration on granule size and microbial community in a granule-based enhanced biological phosphorus removal system. Bioresour. Technol. 177, 209–216. https://doi.org/10.1016/j.biortech.2014.11.093

CHAPTER 3

Monitoring morphological changes from activated sludge to aerobic granular sludge under distinct organic loading rates and increasing minimal imposed sludge settling velocities through quantitative image analysis

Quantitative image analysis (QIA) was used for monitoring the morphology of activated sludge (AS) during a granulation process and, thus, to define and quantify, unequivocally, structural changes in microbial aggregates correlated with the sludge properties and granulation rates. Two sequencing batch reactors fed with acetate at organic loading rates of 1.1 ± 0.6 kg_{COD} m^{-3} d^{-1} (R1) and 2.0 ± 0.2 kg_{COD} m^{-3} d^{-1} (R2) and three minimal imposed sludge settling velocities (0.27 m h^{-1}, 0.53 m h^{-1}, and 5.3 m h^{-1}) induced distinct granulation processes and rates. QIA results evidenced the turning point from flocculation to granulation processes by revealing the differences in the aggregates' stratification patterns and quantifying the morphology of aggregates with an equivalent diameter (Deq) of 200 μm ≤ Deq ≤ 650 μm. Multivariate statistical analysis of the QIA data allowed to distinguish the granulation status in both systems by clustering the observations according to the sludge aggregation and granules maturation status and successfully predicted the sludge volume index measured at 5 min (SVI_5) and 30 min (SVI_{30}). These results evidence the possibility of defining the granulation rate unequivocally and anticipating the sludge settling properties at the early stages of the process using QIA data. Hence, QIA could be used to predict episodes of granules disruption and hindered settling ability in aerobic granulation sludge processes.

This chapter is based on the following scientific article:

Silva, S.A., Val del Río, A., Amaral, A.L., Ferreira, E.C., Alves, M.M., Mesquita, D.P. (2022) Monitoring morphological changes from activated sludge to aerobic granular sludge under distinct organic loading rates and increasing minimal imposed sludge settling velocities through quantitative image analysis. Chemosphere 286. https://doi.org/10.1016/j.chemosphere.2021.131637

3.1. INTRODUCTION

The aerobic granular sludge (AGS) is a breakthrough technology with tremendous potential to become the new standard for aerobic treatment of wastewater due to its compact design and lower footprint. Synthetic media and real wastewaters have been used to produce granules from AS in sequencing batch reactors (SBR) (Carrera et al., 2019; Devlin et al., 2017; Li et al., 2008; Liu et al., 2017; Morgenroth et al., 1997; Sguanci et al., 2019). The process of granules formation, i.e. granulation, is generally described as a stepwise process triggered by certain environmental conditions (Liu and Tay, 2002; Wilén et al., 2018). In lab-scale SBR, granulation can occur within a few weeks; however it may vary depending on the type of substrate (Pronk et al., 2015a), operating conditions (Rollemberg et al., 2019), and the presence of recalcitrant compounds (Jiang et al., 2021).

Nevertheless, the long start-up periods needed to obtain mature granules, and their stability, are still concerns of the AGS technology, which is particularly observed in scale-up studies. For instance, Liu et al. (2010) reported that the predominance of granules was only achieved after 400 days in a pilot-scale SBR used to treat a mixture of domestic and industrial wastewater. Also, Pronk et al. (2015b) reported that a start-up period of 5 months was necessary to achieve stable granules in a full-scale AGS plant treating domestic wastewater. Wagner et al. (2015) reported that the granulation process was slower in the presence of particulate organic matter than with readily biodegradable soluble substrate and that a substantial flocs fraction always remained in the system. More recently, Xavier et al. (2021) achieved a granular fraction of over 80% in less than three months in a pilot-scale reactor fed with low strength domestic wastewater. However, the granular fraction could not be maintained throughout the reactor operation. Although complete conversion from conventional activated sludge (CAS) to AGS is often reported in lab-scale studies, the coexistence of floccular and granular fractions in pilot- and full-scale AGS systems is observed even after the granulation start-up period (Liu et al., 2010; Pronk et al., 2015b; Xavier et al., 2021). This floccular sludge is particularly critical for the clarification process.

The qualitative characterization, by visual inspection, of granular sludge transitioning from CAS to granules is rather subjective and pales in importance to the ratio SVI_{30}/SVI_5 of the sludge volume index measured at 5 min (SVI_5) and 30 min (SVI_{30}). This parameter is commonly used to monitor SBR granulation status (Liu and Tay, 2007), though similar SVI_{30} and SVI_5 values can occur in a floc dominated sludge (Liu et al., 2010) compared to a granular dominated sludge, making the SVI on its own unfit to monitor the granulation status. Several authors defined the percentage of aggregates larger than 200 μm in equivalent diameter (Deq) as an indicator of the granules percentage in aerobic reactors, given that de Kreuk et al.

(2007) defined this size as the minimal size of granules. Detailed morphological information, specifically related to the aggregated biomass dynamic changes and filamentous bacteria, is useful during sludge granulation in SBR start-up periods, being relevant to increasing knowledge about the rates and stability of the AGS formed under defined operating conditions.

QIA is a powerful monitoring tool to quantify morphological changes of sludge aggregates in both aerobic (Mesquita et al., 2011a) and anaerobic treatment processes (Amaral et al., 2004; Araya-Kroff et al., 2004). In these studies, it was possible to assess disturbances in CAS systems and quantify morphological changes during anaerobic granulation and deterioration in an expanded granular sludge blanket reactor (EGSB) reactor using QIA. Recently, the effect of pharmaceutically active compounds on mature aerobic granules was assessed through QIA (Leal et al., 2021a; Leal et al., 2021b). In aerobic granulation studies, Beun et al. (2002) determined the diameter, aspect ratio and shape factor of granules formed using QIA and reported that the aspect ratio and shape factor stabilized prior to the average diameter. Also, the granules formation process in an SBR treating soybean processing wastewater was described by QIA (Su and Yu, 2005). These authors suggested that the decrease of the granule's roundness and aspect ratio evidenced that the flocs evolved gradually to dense, regular and round aggregates induced by the detachment of loosely adhered microorganisms under high shear forces (Su and Yu, 2005). However, only a few parameters were used to describe the granulation process in these works, and quantitative information about the flocs and filaments was limited or non-existent. It has been suggested that filamentous bacteria could generate structural support to initiate granules formation (Zhang et al., 2011). The possibility of measuring the length of free and protruding filamentous bacteria is a powerful feature of QIA in this context. Filamentous growth on an anaerobic sludge bed has already been quantified during detergent shock loads, acting as an early warning indicator of sludge washout in anaerobic digesters (Costa et al., 2007).

Coupling operational data, from biological treatment systems, with the large amount of data provided by QIA in sludge characterization, requires multivariable statistical techniques to extract the most relevant information and properly monitor these systems. Multivariable statistical techniques, such as principal component analysis (PCA) and partial least squares (PLS), have been successfully applied to predict the effect of toxic loads in anaerobic granular sludge (Costa et al., 2009) and to predict the effluent quality in CAS systems (Mesquita et al., 2016). Recently, SVI_{30} of mature aerobic granules could be predicted using a multivariable statistical technique with QIA data (Leal et al., 2020). Furthermore, timely detection of

potential problems in biological wastewater treatment is the main advantage of QIA procedures over standard monitoring techniques (Costa et al., 2013).

This study aims to identify the morphological parameters sensitive to the sludge granulation status and sludge settling properties, using QIA techniques and multivariate statistical analysis, during two granulation processes from activated to granular sludge under different organic loading rates (OLR) and increasing minimal imposed sludge settling velocities (MISSV).

3.2. MATERIAL AND METHODS

3.2.1. Reactors set-up and experimental conditions

Two lab-scale SBR (R1 and R2) with a working volume of 1 L were used in this experiment and operated in parallel with two different OLR. The reactors dimensions were 9 cm in diameter and 18.5 cm in height. The hydraulic retention time was 12 h, with an exchange ratio of 50%. Both SBR were operated in cycles of 6 h, integrating 4 different phases, i.e. anaerobic feed, aeration, settling, and effluent removal. Oxygen was supplied at the bottom of the reactors, resulting in a superficial air velocity of 2 cm s^{-1}, providing complete mixing during the aeration phase and dissolved oxygen saturation in the famine period. The reactors were operated in 3 distinct stages, with increasing MISSV of 0.27 m h^{-1} (stage I), 0.53 m h^{-1} (stage II), and 5.3 m h^{-1} (stage III). Detailed information is shown in Table 3.1. The MISSV was calculated using the following equation (Liu et al., 2005):

$$MISSV = \frac{L}{t_s}$$

where L is the distance (m) to the discharge port and t_s is the settling time (h).

Table 3.1 – Time of each phase during the SBR cycle, throughout the entire operation, and MISSV in the different operation stage

Phase	Units	Stage I (day 0 – 27)	Stage II (day 28 – 38)	Stage III (day 39 – 69)
Anaerobic feed	min	120	120	120
Aerobic reaction		210	220	229
Settling		20	10	1
Effluent removal		10	10	10
MISSV	m h^{-1}	0.27	0.53	5.3

Activated sludge from the municipal wastewater treatment plant of Frossos (Braga, Portugal) was used as inoculum. Both reactors were fed with sodium acetate as sole carbon source, with an OLR of 1.1 ± 0.6 kg_{COD} m^{-3} d^{-1} and 2.0 ± 0.2 kg_{COD} m^{-3} d^{-1} applied in R1 and R2, respectively. Beyond carbon source, 10 mL and 20 mL of a macronutrients stock solution was added (per L^{-1}) to R1 and R2, respectively, with the following composition: $MgSO_4.7H_2O$ (9 g L^{-1}), KCl (4 g L^{-1}), $CaCl_2.2H_2O$ (3 g L^{-1}), NH_4Cl (20 g L^{-1}), K_2HPO_4 (64 g L^{-1}), and KH_2PO_4 (15 g L^{-1}). A volume of 1.5 mL (per L^{-1}) of a concentrated trace solution was added to both reactors with the following composition: $FeCl_3.6H_2O$ 6 g L^{-1}; H_3BO_3 0.6 g L^{-1}; $CuSO_4.5H_2O$ 0.12 g L^{-1}; KI 0.72 g L^{-1}; $MnCl_2.4H_2O$ 0.48 g L^{-1}; $Na_2MoO_2.2H_2O$ 0.24 g L^{-1}; $ZnSO_4.7H_2O$ 0.48 g L^{-1}; $CoCl_2.6H_2O$ 0.6 g L^{-1}, and EDTA 40 g L^{-1}.

3.2.2. Analytical methods

Mixed liquor volatile suspended solids (MLVSS), effluent volatile suspended solids ($VSS_{effluent}$), and sludge volume index at 5 min (SVI_5) and 30 min (SVI_{30}) were determined according to the Standard Methods (APHA, 2005). Chemical oxygen demand (COD) of both influent and effluent was determined using a COD-cuvette test kit (Hach-Lange GmbH, Dusseldorf, Germany) and DR2800™ spectrophotometer (Hach-Lange, GmbH). The COD concentration available for the aeration period ($COD_{aeration}$) was determined at the transition between anaerobic feeding and aeration phases.

3.2.3. Quantitative image analysis

3.2.3.1. Image acquisition

Alongside the determination of the operational parameters, a sample volume of 10 mL was collected for sludge observation at the beginning of the aeration phase, when a complete mixture of the sludge was obtained. Aggregates and filaments images were acquired in bright-field with a 100x magnification using an Olympus BX-51 microscope (Olympus, Shinjuku, Japan) and an Olympus DP71 camera (Olympus, Shinjuku, Japan). For that purpose, a 10 µL sample was placed in a slide by means of a micropipette with a sectioned tip to allow the passage of aggregates, and a cover slip (20 x 20 mm) was positioned on top. This procedure was performed in triplicate for each sample. In order to have representative information about the sludge's morphology, a total of 150 images were acquired per sample (3 x 50 images screened per slide). Images were acquired with cellSens software (Olympus, Shinjuku, Japan), in 1360 x 1024 pixels and 8-bit format.

Granules images were acquired using an Olympus SZ-40 stereomicroscope (Olympus, Shinjuku, Japan), with a 15x magnification. Prior to image acquisition, the sludge samples were diluted and granules were let to settle. Floccular sludge in supernatant was discarded and the settled granules were resuspended to its initial volume. For image acquisition, a fixed volume was placed in a Petri dish and all the aggregates present in that volume were captured. This procedure was performed in duplicate. Images were recorded with a CCD AVC D5CE Sony video camera (Sony, Tokyo, Japan) and Image Pro Plus software (Media Cybernetics, MD, USA), in 768 x 576 pixels and 8-bit format.

Typical images acquired at the end of each stage are provided in Figure 3.1.

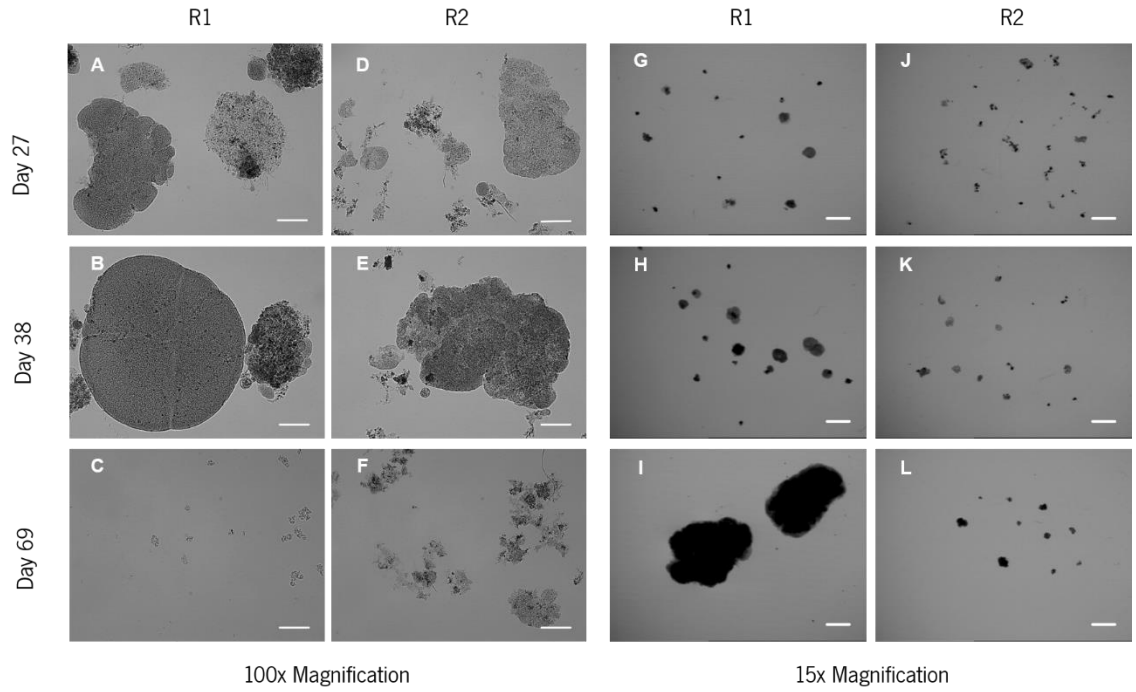


Figure 3.1 – Aggregates observed in bright-field microscopy at 100x magnification in R1 (A-C) and R2 (D-F) at the end of stage I (day 27), stage II (day 38) and stage III (day 69). Granules observed in stereomicroscopy at 15x magnification in R1 (G-I) and R2 (J-L) at the end of stage I (day 27), stage II (day 38) and stage III (day 69). Scale corresponds to 100 µm and 1000 µm for 100x and 15x magnification, respectively.

3.2.3.2. Image processing and analysis

All aggregates and filaments image processing, including pre-treatment, segmentation and debris elimination steps, was performed as described in Mesquita et al. (2016). Binary images were created with the recognised aggregates and free and protruding filamentous bacteria, allowing the subsequent morphological parameters determination (Figure 3.2). All aggregates with Deq < 200 µm were considered flocs, and aggregates with Deq ≥ 200 µm were considered granules (de Kreuk et al., 2007), based on the aggregates area (Area), from which the Deq was calculated:

$$Deq = 2F_{cal}\sqrt{\frac{Area}{\pi}}$$

where F_{cal} is the calibration factor (μm $pixel^{-1}$).

Bright-field microscopy allowed to monitor aggregates with Deq below 650 μm (Figure 3.2a,b) since larger aggregates were cut-off by the boundaries (Figure 3.2c,d). For that reason, aggregates with Deq above 650 μm were quantified by stereomicroscopy (Figure 3.2e,f).

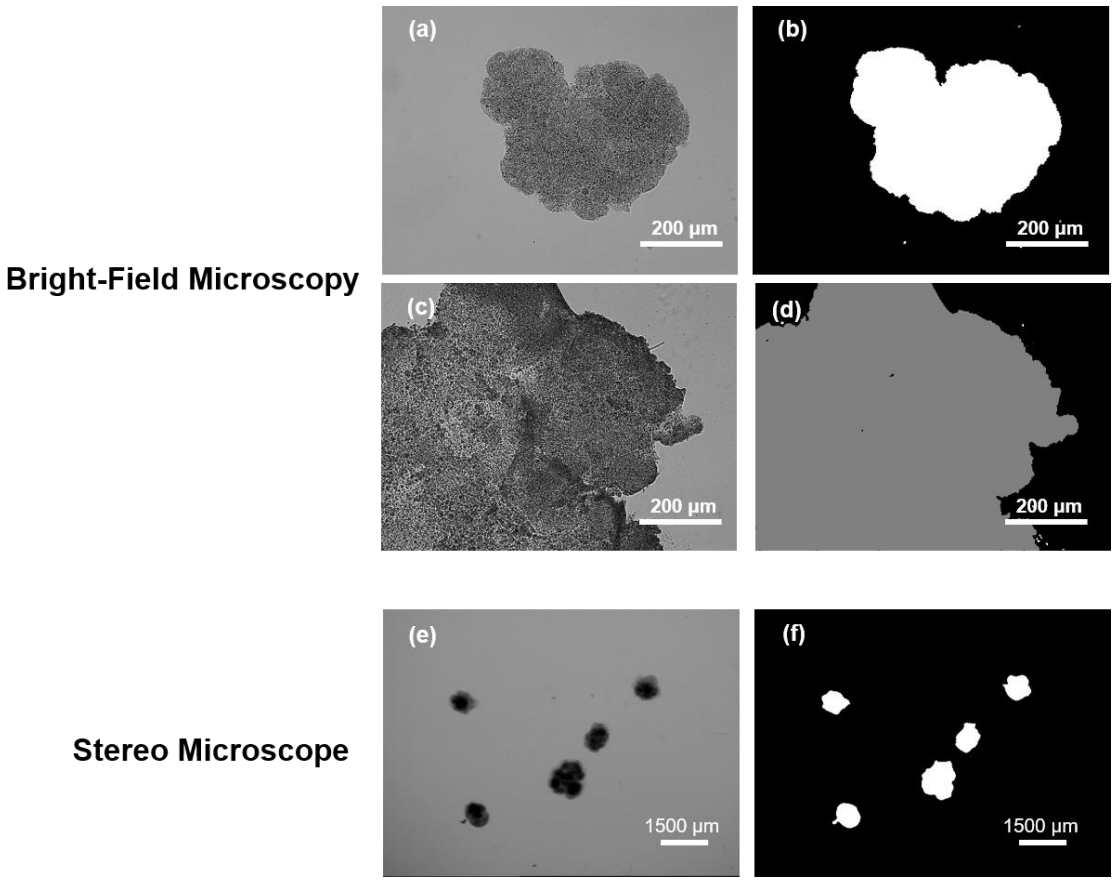


Figure 3.2 – Original grey scale images acquired through bright-field microscopy with a 100x amplification (a, c) and stereomicroscopy with a 15x amplification (e) and respective final binary images (b, d, f).

The sum of all the recognized aggregates area per unit of volume was used to determine the specific area ($Area_{spec}$) for each Deq size range, calculated as follows:

$$Area_{spec} = \frac{\sum Area}{Volume}$$

The sum of all free and protruding filaments length (TL) per unit of volume was calculated as follows:

$$TL = \frac{\sum Length}{Volume}$$

where Length is the filament length (mm). In the case of aggregates and filaments quantified by bright field microscopy, the volume considered was the volume of each image V_{image}, calculated as follows:

$$H = \frac{V_{sample}}{A_{cover\ slip}}$$

$$V_{image} = H \times A_{image}$$

where, H is the distance between the slide and the cover slip (mm), V_{sample} is the sample volume placed in the slide (mm^3), $A_{cover\ slip}$ is the area of the cover slip (mm^2), and the A_{image} is the area of the image (mm^2) determined using the F_{cal}.

A total of 69 parameters were determined to characterize the aggregates morphology and filaments content during the granulation process (Annexe Table A1). The morphology of the aggregates within a Deq size range was characterized by several shape descriptors, with the solidity, eccentricity and convexity studied in detail. The aggregates solidity (Sol) was determined as follows:

$$Sol = \frac{Area}{Area_C}$$

where $Area_C$ is the convex envelope area (Amaral, 2003). The aggregates eccentricity (Ecc) was determined as follows:

$$Ecc = \frac{(4\pi)^2 (M_{2x}-M_{2y})^2+4M_{2xy}^2}{Area^2}$$

where M_{2xy} is the second horizontal (x) and vertical (y) orders moment (Amaral, 2003).

The aggregates convexity (Conv) was calculated as follows:

$$\text{Conv} = \frac{\text{Perimeter}_C}{\text{Perimeter}}$$

where Perimeter_C is the convex envelope perimeter (Amaral, 2003). More information about the calculation of these parameters can be found in Amaral (2003). The image processing and analysis routines were performed in Matlab™ 8.5 (the MathWorks Inc, USA).

3.2.4. Multivariate statistical analysis

Principal component analysis (PCA) aims to determine hidden and complex relationships between parameters that compose an X dataset. PCA was performed using the morphological data determined by QIA (Annexe Table A1). A total of 66 parameters and 40 observations composed the X dataset matrix. Prior to PCA, each variable was scaled as described in Costa et al. (2009). The mathematical principles of PCA can be found in Rosen (2001).

Partial least squares (PLS) regression was performed as described in Mesquita et al. (2016) to predict sludge settling ability (Y), namely SVI_5 and SVI_{30}, using 69 parameters and 40 observations that composed the X dataset matrix. PLS models were performed independently for each reactor and then combined as the ensemble PLS model (Amaral et al., 2013; Mesquita et al., 2016). Therefore, the overall dataset was divided into two datasets of 69 parameters and 20 observations corresponding to each reactor operation. Each dataset was randomly divided into a training set (67% of observations) and a validation set (33% of the observations) to calibrate and validate the model, respectively. To reduce the number of X predictors, a first PLS was performed for each target Y, allowing to determine the variable importance in projection (VIP) of each predictor of the X dataset. To avoid overfitting, the number of predictors for the second PLS model was equal to $n/2$, with n being the number of observations of the training dataset. Also, whenever two VIP variables exhibited a correlation coefficient above 0.7, the one presenting the lowest VIP value was excluded. Thus, the second PLS was performed using only 6 variables presenting the highest VIP values (Table 3.2). The PLS models root mean square error of prediction (RMSEP) and residual predictive deviation (RPD) were used as the basis of the prediction's accuracy. PCA and PLS were performed in Matlab™ 8.5 (the MathWorks Inc, USA).

Table 3.2 – Variables selected for the second PLS with the highest VIP value for each reactor

	R1		R2	
Target Y	**Predictors X**	**VIP**	**Predictors X**	**VIP**
SVI_5	TL/Vol	2.38	$Deq_{200\text{-}650\mu m}$	1.90
	$Deq_{>650\mu m}$	2.27	$Deq_{>650\mu m}$	1.86
	$LrgC_{<100\mu m}$	1.49	$Area_{>650\mu m}$/Vol	1.65
	$Deq_{200\text{-}650\mu m}$	1.44	$Nb_{200\text{-}650\mu m}$/Vol	1.58
	$TNb_{<650\mu m}$/Vol	1.34	$RelArea_{200\text{-}650\mu m}$	1.54
	$Area_{>200\mu m}$/Vol	1.25	$RelArea_{<100\mu m}$	1.46
SVI_{30}	TL/Vol	2.55	$Deq_{200\text{-}650\mu m}$	2.11
	$Deq_{>650\mu m}$	2.46	$Deq_{>650\mu m}$	1.62
	$TNb_{<650\mu m}$/Vol	1.55	$Nb_{200\text{-}650\mu m}$/Vol	1.52
	$LrgC_{<100\mu m}$	1.47	$RelArea_{200\text{-}650\mu m}$	1.51
	$Deq_{200\text{-}650\mu m}$	1.43	$\%Area_{100\text{-}200\mu m}$	1.40
	$LrgC_{100\text{-}200\mu m}$	1.21	$LrgC_{<100\mu m}$	1.36

3.3. RESULTS

3.3.1. Sludge properties: Solids concentration, settling properties and COD depletion

In R1, after an initial washout of 66% of the inoculated MLVSS, the MLVSS increased steadily during stage I from day 6 to day 27 (Figure 3.3a). In R2, 36% more MLVSS accumulated during stage I, reaching a stable value of 4 g L^{-1} on day 15. Decreasing the settling time in stage II and stage III induced the selection of aggregates with a MISSV of 0.53 m h^{-1} and 5.3 m h^{-1}, respectively (Table 3.1), with a concomitant change in the MLVSS that oscillated between 2.1 – 3.3 g L^{-1} in R1 and 3.5 – 4.7 g L^{-1} in R2 during stage II, and a severe, yet transient reduction of about 50% in the MLVSS concentration in both reactors in stage III (Figure 3.3a).

The $VSS_{effluent}$ gradually decreased in both reactors and remained rather stable from day 11 until the end of stage II in R1 though more unstable in R2 (Figure 3.3b). Larger fluctuations in $VSS_{effluent}$ in R2 were persistent in stage III, increasing drastically up to 0.45 g L^{-1}, whereas stable values around 0.05 g L^{-1} were observed in R1, after a slight transient increase just after the change of the settling time (Figure 3.3b).

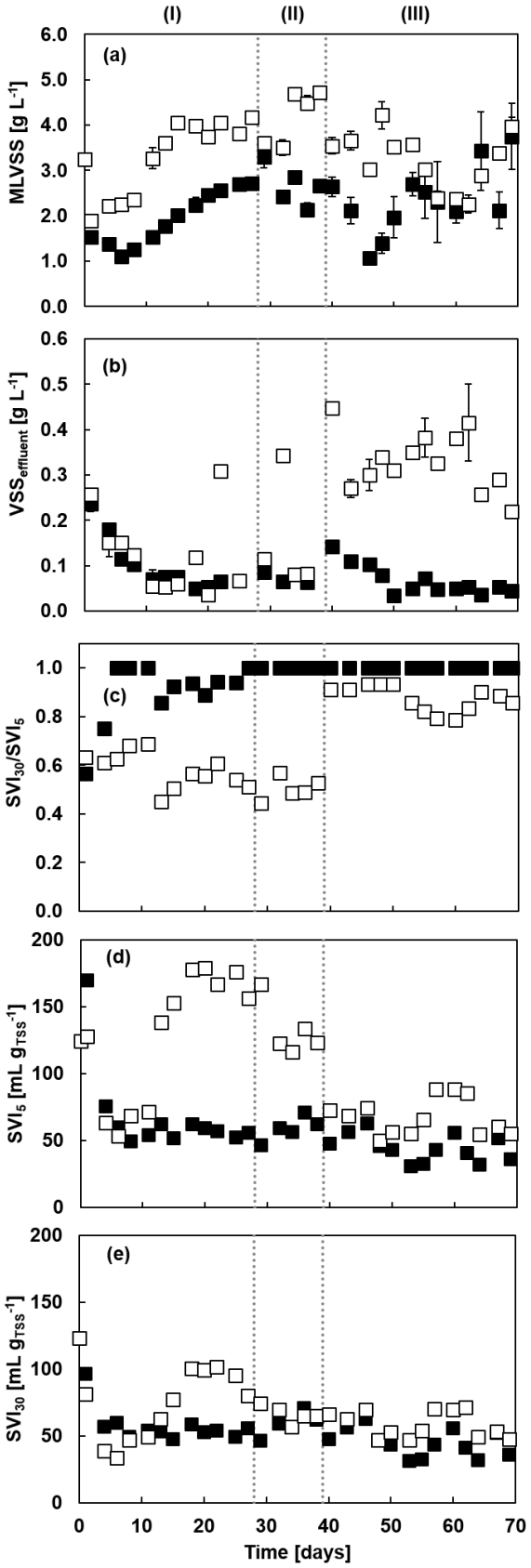


Figure 3.3 – Sludge profiles of MLVSS (a), $VSS_{effluent}$ (b), SVI_{30}/SVI_5 ratio (c), SVI_5 (d), and SVI_{30} (e) in R1 (■) and R2 (□). Operational stages I, II and III.

The SVI_{30}/SVI_5 rapidly increased in R1 and reached a value of one in the first 6 days of operation, and despite the transient SVI_{30}/SVI_5 decrease observed in stage I, the excellent sludge settling characteristics remained unchanged also after reducing the settling time in stages II and III (Figure 3.3c). In R2, the SVI_{30}/SVI_5 oscillated between 0.5 and 0.7 during stages I and II (Figure 3.3c), and albeit the SVI_{30} decreased to values similar to R1 in stage II, SVI_5 was still considerably higher (Figure 3.3d). After reducing the settling time in stage III, SVI_5 approached SVI_{30} (Figure 3.3e), indicating that the sludge settling ability considerably improved, with the SVI_{30}/SVI_5 reaching values above 0.9, yet with an oscillatory tendency (Figure 3.3c).

Both reactors exhibited good COD removal efficiencies throughout all stages (Figure 3.4a). The amount of substrate available during the aerobic phase ($COD_{aeration}$) decreased from stage I to stage II in both reactors, indicating an efficient substrate consumption during the anaerobic feeding phase (Figure 3.4b). In stage III, when the MISSV was increased to 5.3 m h^{-1}, an increase in $COD_{aeration}$ was observed in both reactors, though more significant in R2, likely due to the severe washout observed in this reactor in stage III (Figure 3.4b).

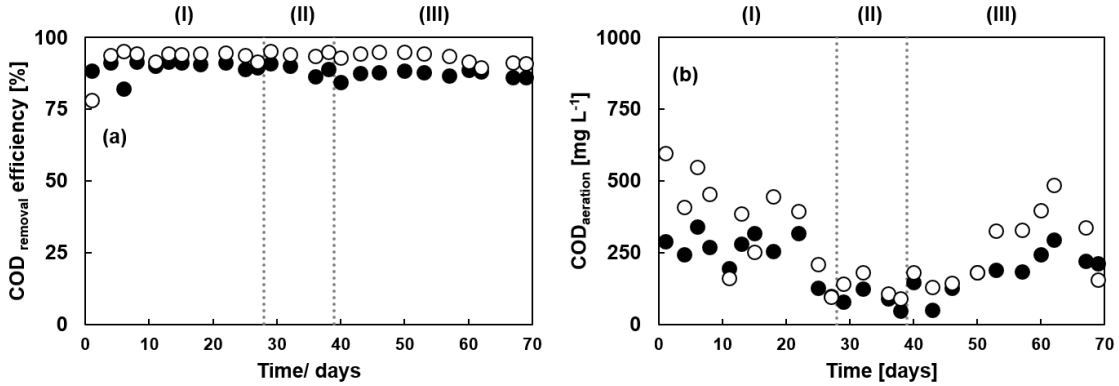


Figure 3.4 – COD removal efficiencies (a) and $COD_{aeration}$ (b) in R1 (●) and R2 (○), during the operational stages I, II and III.

3.3.2. QIA as monitoring tool for sludge morphological changes in granulation

3.3.2.1. Aggregates distribution and filamentous content

The formation and distribution of aggregates revealed differences in the dynamic behaviour between flocs (Deq < 200 µm), granules (Deq ≥ 200 µm), and filamentous bacteria in both reactors (Figure 3.5). After 8 days of operation in R1, the $Area_{spec}$ of aggregates with Deq < 200 µm decreased drastically in circa 50% and remained rather stable during stage I (Figure 3.5a). In R2, the $Area_{spec}$ of these aggregates gradually increased during stage I and was 1.8x higher at day 27 than in the inoculum (Figure 3.5b). The formation of small granules, i.e., with 200 µm ≤ Deq ≤ 650 µm, started after 4 days of operation in both reactors, yet a higher granulation rate was observed in R1 than in R2 (Figure 3.5a,b). Larger granules with Deq > 650 µm were formed at the lowest MISSV (0.27 m h^{-1}; stage I), but only in R1 and after day 15 (Figure 3.5a). In R1, from day 38 to 50, the increase of the MISSV to 5.3 m h^{-1} (stage III) induced a significant increase of the $Area_{spec}$ of granules with Deq > 650 µm, more pronounced from day 46 onwards, revealing the maturation of granules in R1 (Figure 3.5a). This was simultaneous with the decrease in the $Area_{spec}$ of granules with 200 µm ≤ Deq ≤ 650 µm from 2.6 ± 0.3 mm^2 μL^{-1} to 0.4 ± 0.2 mm^2 μL^{-1} in the same period (Figure 3.5a). Conversely in R2, the $Area_{spec}$ of granules with 200 µm ≤ Deq ≤ 650 µm continued its increasing trend during stage II and part of stage III (Figure 3.5b), and granules with Deq > 650 µm started to accumulate in the same period, but well below the values observed in R1 (Figure 3.5a,b). Simultaneously, the $Area_{spec}$ of flocs decreased about 60% with the increase in the MISSV. Yet from day 46, concomitant with the biomass washout, the flocs $Area_{spec}$ started to fluctuate and increase, opposite to the granules counterpart, revealing the instability of the granulation process in R2 in that period (Figure 3.5b).

Most filamentous bacteria present in the inoculum were washed-out in the first 8 days of operation (Figure 3.5c). The filament length (TL/Vol), of both protruding and free filaments, was higher in R1 than in R2 during most of stage I. Throughout stage II and III, the TL/Vol continued to increase in R2, reaching a maximum of 33 ± 3 mm μL^{-1} at day 62, which was 15x higher than the filaments length quantified in R1 (Figure 3.5c).

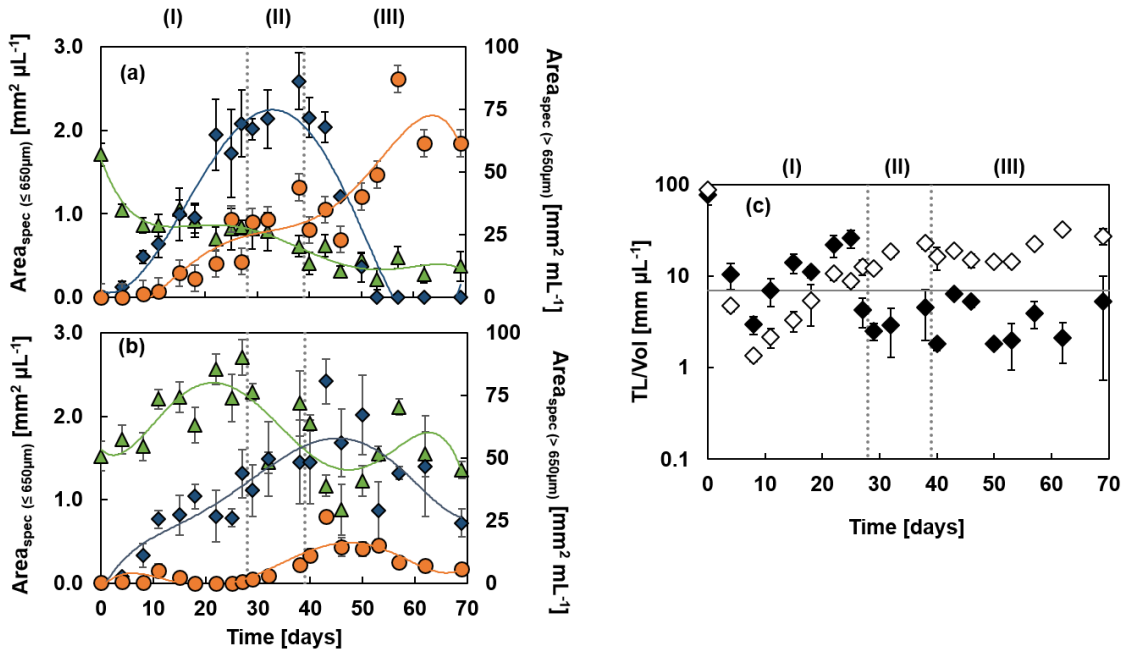


Figure 3.5 – The specific area of aggregates in the different size range: Deq < 200 µm (▲); 200 µm ≤ Deq ≤ 650 µm (◆) and Deq > 650 µm (●) in R1 (a) and R2 (b). Filaments length (c) in R1 (◆) and R2 (◇) with filaments content threshold of 7 mm µL^{-1} (——), according to Mesquita (2010). Operational stages I, II, III.

3.3.2.2. Morphology characterization of granules with 200 µm ≤ Deq ≤ 650 µm

The morphology of the small granules, i.e., with 200 µm ≤ Deq ≤ 650 µm revealed major differences between the two reactors, related with the distinct granulation rates. Initially, the granules exhibited a low solidity elongated structure (high eccentricity values) and somewhat irregular boundaries (low convexity values) as presented in Figure 3.6. In R1, the granules became progressively more compact (increasing solidity values), circular (decreasing eccentricity values) and smooth (increasing convexity values) throughout the reactor operation (Figure 3.6). In R2, the structure of the granules remained rather stable throughout stage I, and structural changes were only observed after decreasing the settling time in stage II and III, particularly in terms of solidity and convexity which increased until day 46 (Figure 3.6a,c). From that day onwards, the granules loss of structural integrity in R2 was evidenced by the gradual decrease in both solidity and convexity and increase in eccentricity (Figure 3.6).

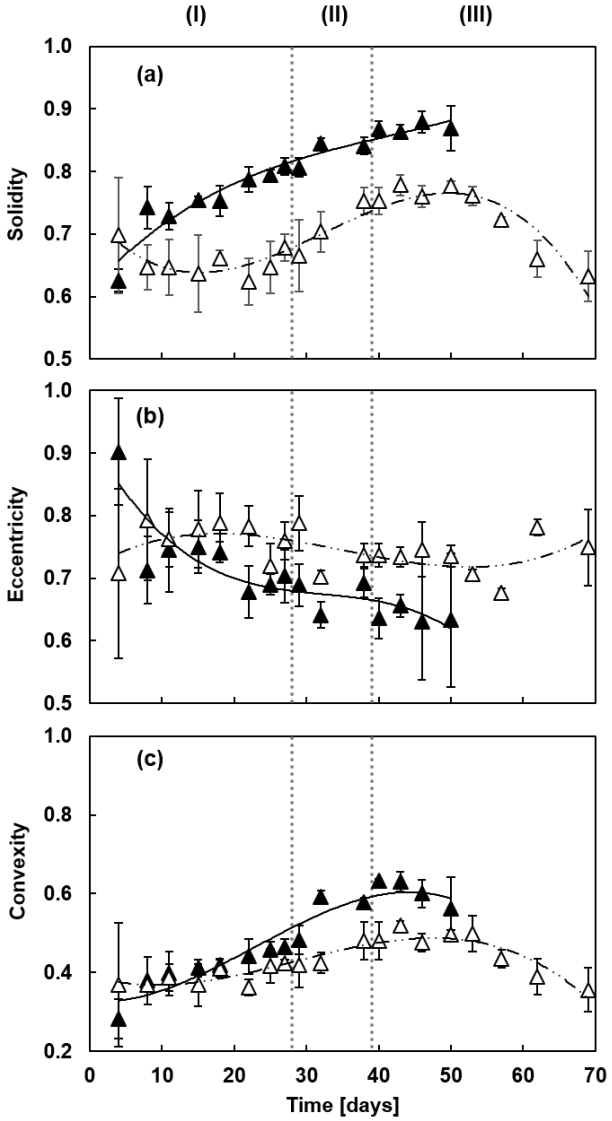


Figure 3.6 – The solidity (a), eccentricity (b), and convexity (c) of aggregates with 200 μm ≤ Deq ≤ 650 μm present in R1 (▲) and R2 (△), during the operational stages I, II and III.

3.3.3. Multivariate statistical analysis

3.3.3.1. PLS

A PLS analysis was performed to predict SVI_5 and SVI_{30} using exclusively QIA data (Figure 3.7). The regression analysis between the predicted and observed (measured) values presented good prediction abilities with correlation coefficients (R^2) of 0.9637 and 0.842 for SVI_5 and SVI_{30}, respectively (Figure 3.7). The RMSEP of both models was low for both SVI_5 (7.6 mL g_{TSS}^{-1}) and SVI_{30} (5.2 mL g_{TSS}^{-1}), representing 5.2% and 5.6% of the values range observed for SVI_5 and SVI_{30}, respectively (Figure 3.7). The RPD values for

both PLS models were 5.57 and 4.12 for SVI_5 and SVI_{30}, respectively, above the value 3 considered to be the threshold for a satisfactory prediction (Cozzolino et al., 2004). The assessment of SVI_5 and SVI_{30}, depended on a relatively similar set of variables, both for R1 and for R2 (Table 3.2). Indeed, 5 out of the 6 main morphological parameters employed for both SVI predictions in R1 were the same, encompassed within the filamentous bacteria, overall aggregates, granules size, and flocs morphology. On the other hand, 4 out of the 6 main morphological parameters employed for the SVI predictions in R2 were also similar, comprised within the overall aggregates, granules size, and flocs morphology.

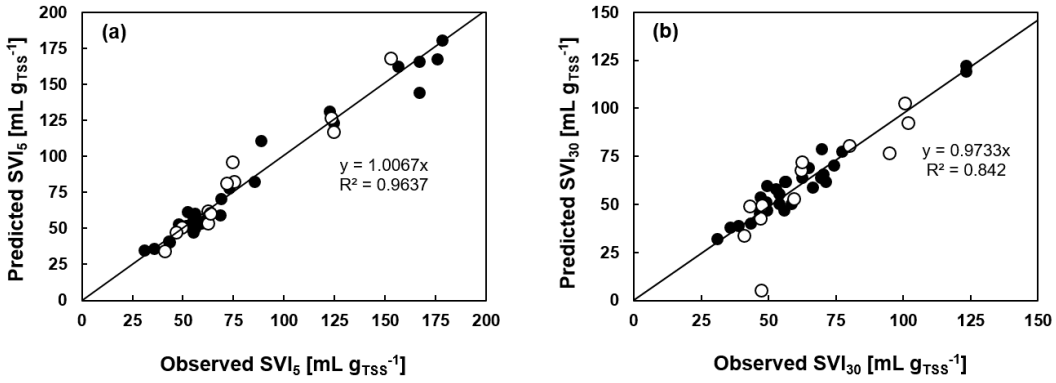


Figure 3.7 – Correlation between observed and predicted SVI_5 (a) and SVI_{30} (b). Calibration (●) and validation (○) data set.

3.3.3.2. PCA

A PCA was performed due to the large amount of data generated by QIA determining, for each principal component (PC), the scores containing information on how the samples points are related to each other, and the loadings establishing the influence of each variable on the PC (Figure 3.8). The two most relevant PC (PC1 and PC2) given by PCA, explained 68.7% of the dataset variance and were used in this analysis. In Figure 3.8a it is possible to observe 4 main clusters, corresponding to the morphological changes of the seed AS throughout the reactors operation. The first cluster (C1), located at the top left quadrant with high scores in PC2, incorporates the initial inoculum for both reactors (day 0), and the second (C2), third (C3) and fourth (C4) clusters encompass the remaining sludge observations of R1 and R2 (Figure 3.8a).

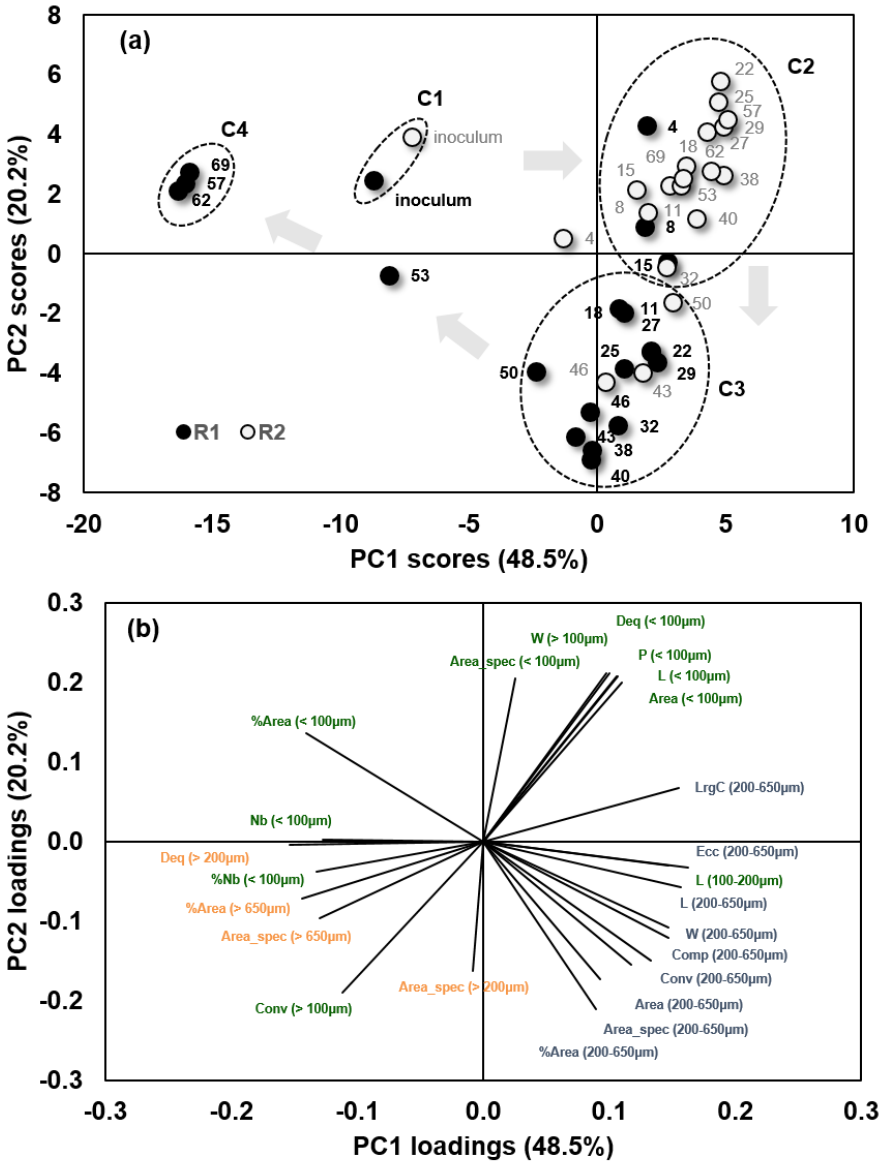


Figure 3.8 – PCA scores plot of the QIA dataset for PC1 vs PC2 (a) of R1 (●) and R2 (○). Variables loadings plot of the PC1 and PC2 (b).

PC1 allowed to clearly distinguish C1 from C4 and both from C2 and C3 clusters, whereas PC2 allowed to distinguish the C2 and C3 clusters. The C2 cluster was situated in the top right corner (high PC1 and PC2 values) which, according to Figure 3.8b, is positively influenced by the parameters related mainly with the morphology and prevalence of the aggregates below 200 µm (and between 200 µm and 650 µm at some extent). Thus, it can be implied that the C2 cluster was related with the first development of the inoculum toward the obtainment of a granular structure (Figure 3.8a,b). On the other hand, the C3 cluster differed from the C2 cluster by shifting mostly along the PC2 axis (Figure 3.8a) towards negative

PC2 values. The parameters that negatively influenced PC2 were mostly related with the morphology and prevalence of granules with 200 μm ≤ Deq ≤ 650 μm. A transient shift toward the C3 cluster could be observed in R2 (days 43, 46 and 50), corresponding to an increase amount of these granules. However, such trend did not endure, with the subsequent points again being allocated to the C2 cluster (in accordance with the biomass washout and instability in R2). On the other hand, most R1 observations fell within the C3 cluster, though, from day 50 onwards moved back (negatively) in the PC1 axis, influenced by the granules maturation process. Indeed, the 3 final observations (days 57, 62 and 69) formed the C4 cluster located in the top left quadrant (Figure 3.8a), which can find a parallel to the fact that PC1 is negatively influenced by the parameters related with the morphology and prevalence of the larger granules (Deq > 650 μm).

3.4. DISCUSSION

Faster granulation is often reported in AGS systems treating wastewater at high OLR, however, the resulting granules are usually unstable and granule disruption is often observed (Liu and Tay, 2015; Val Del Río et al., 2013). Stable granules are usually obtained at low OLR (≤ 2.0 kgCOD m^{-3} d^{-1}), commonly found in CAS systems (Franca et al., 2018). One major disadvantage is the extended period of time required for granulation, monitored by the dynamic sludge settling behaviour (Pronk et al., 2015b), even though the treatment requirements in full-scale AGS systems can be achieved prior to the completion of the granulation process.

The gradual decrease of the settling time, which determines the MISSV, is commonly applied to select fast settling granules over slow settling flocs, influencing the granulation rate. However, establishing a turning point based on sludge properties and qualitative observations, is extremely ambiguous, since granulation is a transient process of gradual morphological changes from flocs to granules (Liu et al., 2010). Both floccular and granular sludge are expected to coexist even after the granulation is completed, hence, monitoring the sludge morphology of flocs and granules, as well as the filamentous bacteria proliferation could help understanding the sludge tendency to granulate at an early stage of the process and monitor the process stability overtime. More importantly, collecting precise and quantitative morphological information about how the granulation process occurs in different operating conditions is relevant to the academic and technical communities in predicting granulation rates and granule stability. In accordance, a QIA technique was used in this study to monitor and quantify the sludge morphological differences and evolution in both reactors during the granulation process.

The performed sludge monitoring allowed to infer the start of the granulation process in R1 during stage I, were it reached a stable MLVSS concentration and good settling properties. On the other hand, in R2, good settling properties were attained only after the increase of the MISSV to 5.3 m h^{-1} in stage III, thus suggesting a slower granulation process. QIA data evidenced that the operating conditions applied to R1 and R2 were effective to promote the formation and accumulation of granules. In both reactors the granulation started at the MISSV of 0.27 m h^{-1}, with the formation and accumulation of small granules with 200 μm ≤ Deq ≤ 650 μm after 4 days (Figure 3.5a,b). Nevertheless, the granulation process was evidently slower in R2 which had a higher organic load applied. Previous works have shown that high OLR (up to 12 kg_{COD} m^{-3} d^{-1}) can be used as a strategy to speed up the granulation start-up process when combined with strong hydraulic selective pressures (Liu and Tay, 2015). Thus, while the MISSV of 0.27 m h^{-1} promoted microbial aggregation in R2 at an early stage of the operation, only after the increase of the MISSV to 0.53 m h^{-1} and later to 5.3 m h^{-1} the formation of larger granules (Deq > 650 μm) was induced (though still to a lower degree than in RI), evidencing that a higher selective pressure was required to stimulate the granulation process. However, the granulation in R2 was rather unstable and transitory leading to biomass and granules washout at the end of the operation. In R1, a strong increase of granules with Deq > 650 μm was observed after the increase of the MISSV to 5.3 m h^{-1}, leading to mature granules, particularly from day 46 onwards (Figure 3.5a). This was possibly due to the increase in the food-to-microorganisms ratio (F/M), since high F/M influences the formation of larger granules (Li et al., 2011).

Throughout the granulation process in R1, the SVI_5 equalled SVI_{30}, considered an indication of full granulation (Liu and Tay, 2007), just after 6 days when granules were far from being predominant in terms of $Area_{spec}$ (Figure 3.5a). However, studies performed in pilot-scale have shown SVI_{30}/SVI_5 values above 0.9 for AGS while still dominated by flocs (Liu et al., 2010). And, although in this study the SVI_{30}/SVI_5 ratio did not reveal the degree of granulation in the reactors, the decrease of both SVI_5 and SVI_{30} in R1 was consistent with the decrease of the flocs $Area_{spec}$. On the other hand, the floccular sludge decrease was not so prominent in R2, with the inefficient withdrawal of the slow settling aggregates sustaining the gradual increase of SVI_5 and SVI_{30} throughout stage I and potentially delayed the granulation process in this reactor (Beun et al., 1999). The reason behind the prevalence of flocs in R2 seems to be related with sludge aggregation and disruption phenomena, as shown by the distinct morphology of the granules with 200 μm ≤ Deq ≤ 650 μm in both reactors.

The use of granules morphological parameters, such as aspect ratio and shape factor, for monitoring the granulation process has already been employed by Beun et al. (2002). These parameters increased in

the first 10 days of the operation, remaining stable throughout the remaining timespan even after transitory disruption. In our work, while the evolution in the granules morphology in R1 evidenced a progressively stronger structure throughout the granulation process, the R2 granules lower solidity and convexity, and higher eccentricity, reflected disturbances in the granulation process and may have been indirectly related to the higher presence of flocs. Furthermore, the structural changes evidenced by the shape descriptors from day 29 to day 46 in R2 suggest a stronger microbial aggregation, leading to the formation and accumulation of larger granules (Deq > 650 μm) in the same period. Conversely, after 46 days, the shape descriptors revealed a progressive granules disruption and washout correlated with the flocs increase and higher suspended solids in the effluent ($VSS_{effluent}$).

According to Mesquita (2010), a filamentous bacteria content threshold of 7 mm μL^{-1} was found below which filaments are irrelevant to the sludge settling ability. In R1, the decrease in SVI_{30}/SVI_5 value observed from day 11 to 25 in stage I was concomitant with the increase of protruding and free filamentous bacteria content above 7 mm μL^{-1} in the same period (Figure 3.3c, Figure 3.5c). Indeed, after day 25, the protruding and free filamentous bacteria content remained below 7 mm μL^{-1} reflecting the constant SVI_{30}/SVI_5 ratio. In R2, the free and protruding filaments content rose above 7 mm μL^{-1} at the end of stage I and remained higher throughout stage II and III, affecting the settling ability of the sludge. Also, the increase of filaments content during stage III is in accordance with the instability of the granules structure in this period.

Several works have reported a clear relation between QIA data and sludge settling ability in CAS systems (Amaral et al., 2013; Amaral and Ferreira, 2005; Grijspeerdt and Verstraete, 1997), though this relation was yet to be proven during a granulation process. In accordance, the current study allowed to advance in this assumption, with the PLS analysis performed with QIA data achieving a high correlation regression (R^2 0.964) between the predicted and observed SVI_5. Even though a good correlation regression (R^2 0.842) between the predicted and observed SVI_{30} was also found, it was evidently lower than for SVI_5, evidencing a deeper complex relation between the sludge morphological changes during granulation and the sludge settling behaviour. For both R1 and R2, the main parameters found most adequate to predict the sludge settling ability encompassed the aggregates, granules size and flocs morphology (Table 3.2). It is known that the aggregates play a defining role in the sludge (both granular and floccular) settling ability (Amaral et al., 2013; Leal et al., 2020). However, a noticeable difference between the sludge settling ability prediction in the two reactors was the fact that, a clear dependency on the filamentous bacteria was found in R1. It may be assumed that high settling ability is obtained for sludge presenting good granular

properties (i.e. R1), and the growth of filamentous bacteria lead to changes in the settling properties, thus assuming larger importance in prediction models. On the other hand, for sludge presenting poor granular properties (i.e. R2), the SVI is mainly dependent on the aggregates size, morphology and lesser with the growth of filamentous bacteria. To construct a generalized PLS model able to be applied in all granulation processes is very complex and involves gathering a vast number of observations in distinct conditions. However, care should be taken not to force a single unified and less adapted solution that would not be as accurate for that particular system and let each PLS model address the specificities of the system studied. Therefore, given the complexity and diversity of AGS systems, the PLS flexibility on determining the most significant parameters for each system, can be considered an advantage.

PCA has been already used to identify several AS disturbances through the combination of morphological and physiological data (Mesquita et al., 2011b). More recently, PCA was used to identify the variables associated with the hindered settling velocity of AS in the presence of ferric chloride precipitates (Asensi et al., 2019). Here, the use of PCA in the QIA data allowed to study the evolution of the different phases of the granulation process in both reactors.

Several hypothesis exist regarding the mechanism behind granules formation, such as floccular aggregation (Verawaty et al., 2012), microbial outgrowth from a single microcolony (Barr et al., 2010), or by newly germinated fungal spores (Sarma and Tay, 2018). However, there is no consensus due to the lack of supporting and clear evidences (Sarma and Tay, 2018; Wilén et al., 2018). In this study, the use of PCA with the QIA data allowed to clearly distinguish 4 main clusters associated with the different phases of the granulation process. Cluster C2 (most R2 observations) was formed in the initial stages of the granulation process, and the distinction to the inoculum cluster was mainly due to the morphology and prevalence of the aggregates below 200 μm, evidencing the initial flocs aggregation into larger structures. It seems reasonable to assume that, in this step, variations in the aggregates size and morphology are expected to occur. The distinction between clusters C2 and C3 (most R1 observations) reflected these changes, driven by the evolution towards a granular sludge, as reflected by the relation of the morphology and prevalence of the granules with 200 μm ≤ Deq ≤ 650 μm. The granulation process is assumed to continue by a maturation step, in which, the growth of the immobilized biomass, EPS production and hydrodynamic shear shapes the form of the granules (Sarma et al., 2017). This seemed to be the case with the final data points of R1 which formed the cluster C4, mainly influenced by the size and predominance of larger granules with Deq > 650 μm which reflects the granules maturation. Therefore, the distinct granulation status of both systems could be established overtime from the use of a PCA with

the QIA data. This allowed to follow the granulation process, enlightening the differences between the two operating strategies and, thus, being able to anticipate process instability.

3.5. CONCLUSION

The granulation rate heavily depended on the substrate concentration alongside the MISSV. In R1 (1.1 ± 0.6 kg_{COD} m^{-3} d^{-1}) a good granulation ability could be obtained right from the MISSV. On the other hand, only at higher MISSV (and mainly at 5.3 m h^{-1}) granulation leading to larger granules (Deq > 650 µm) was observed in R2 (2.0 ± 0.2 kg_{COD} m^{-3} d^{-1}), yet at a lower extension than in R1. Larger granules accounted for 96.1% and 9.4% in term of $Area_{spec}$ of the granular fraction in R1 and R2, respectively. The morphological differences (solidity, eccentricity and convexity) of the small granules (200 µm ≤ Deq ≤ 650 µm) reflected the degree of sludge aggregation and could be used as indicators in the effort to anticipate process instability. Good settling properties were achieved with both OLR, with SVI_5 below 40 mL g_{TSS}^{-1} and 60 mL g_{TSS}^{-1} in R1 and R2, respectively. The sludge morphological data was successfully used to predict the sludge settling properties (SVI_5 and SVI_{30}) by PLS regression, with a correlation coefficient of 0.964 and 0.842 for SVI_5 and SVI_{30}, respectively. Finally, the distinct granulation status of both systems overtime could be established from the use of a PCA with the QIA data, allowing to follow the granulation process, which, in conjunction with the use of the PLS models allows for a timely detection of potential problems.

3.6. REFERENCES

Amaral, A.L., Ferreira, E.C., 2005. Activated sludge monitoring of a wastewater treatment plant using image analysis and partial least squares regression. Anal. Chim. Acta 544, 246–253. https://doi.org/10.1016/j.aca.2004.12.061

Amaral, A.L., Mesquita, D.P., Ferreira, E.C., 2013. Automatic identification of activated sludge disturbances and assessment of operational parameters. Chemosphere 91, 705–710. https://doi.org/10.1016/j.chemosphere.2012.12.066

Amaral, A.L., Pereira, M.A., Da Motta, M., Pons, M.N., Mota, M., Ferreira, E.C., Alves, M.M., 2004. Development of image analysis techniques as a tool to detect and quantify morphological changes in anaerobic sludge: II. Application to a granule deterioration process triggered by contact with oleic acid. Biotechnol. Bioeng. 87, 194–199. https://doi.org/10.1002/bit.20129

Amaral, A.L.P., 2003. Image analysis in biotechnological processes: applications to wastewater treatment. PhD thesis, University of Minho. http://hdl.handle.net/1822/4506

APHA, 2005. Standard Methods for the Examination of Water & Wastewater 21st Edition. Am. Public Heal. Assoc. Am. Water Work. A ssociation, Water Environ. Fed.

Araya-Kroff, P., Amaral, A.L., Neves, L., Ferreira, E.C., Pons, M.N., Mota, M., Alves, M.M., 2004. Development of image analysis techniques as a tool to detect and quantify morphological changes in anaerobic sludge: I. Application to a granulation process. Biotechnol. Bioeng. 87, 184–193. https://doi.org/10.1002/bit.20207

Asensi, E., Zambrano, D., Alemany, E., Aguado, D., 2019. Effect of the addition of precipitated ferric chloride on the morphology and settling characteristics of activated sludge flocs. Sep. Purif. Technol. 227, 115711. https://doi.org/10.1016/j.seppur.2019.115711

Barr, J.J., Cook, A.E., Bond, P.L., 2010. Granule formation mechanisms within an aerobic wastewater system for phosphorus removal. Appl. Environ. Microbiol. 76, 7588–7597. https://doi.org/10.1128/AEM.00864-10

Beun, J.., Hendriks, A., van Loosdrecht, M.C.., Morgenroth, E., Wilderer, P.., Heijnen, J.., 1999. Aerobic granulation in a sequencing batch reactor. Water Res. 33, 2283–2290. https://doi.org/10.1016/S0043-1354(98)00463-1

Beun, J.J., Van Loosdrecht, M.C.M., Heijnen, J.J., 2002. Aerobic granulation in a sequencing batch airlift reactor. Water Res. 36, 702–712. https://doi.org/10.1016/S0043-1354(01)00250-0

Carrera, P., Mosquera-Corral, A., Méndez, R., Campos, J.L., Val del Rio, A., 2019. Pulsed aeration enhances aerobic granular biomass properties. Biochem. Eng. J. 149, 107244. https://doi.org/10.1016/j.bej.2019.107244

Costa, J.C., Abreu, A.A., Ferreira, E.C., Alves, M.M., 2007. Quantitative image analysis as a diagnostic tool for monitoring structural changes of anaerobic granular sludge during detergent shock loads. Biotechnol. Bioeng. 98, 60–68. https://doi.org/10.1002/bit.21381

Costa, J.C., Alves, M.M., Ferreira, E.C., 2009. Principal component analysis and quantitative image analysis to predict effects of toxics in anaerobic granular sludge. Bioresour. Technol. 100, 1180–1185. https://doi.org/10.1016/j.biortech.2008.09.018

Costa, J.C., Mesquita, D.P., Amaral, A.L., Alves, M.M., Ferreira, E.C., 2013. Quantitative image analysis for the characterization of microbial aggregates in biological wastewater treatment: a review. Environ. Sci. Pollut. Res. 20, 5887–5912. https://doi.org/10.1007/s11356-013-1824-5

Cozzolino, D., Kwiatkowski, M.J., Parker, M., Cynkar, W.U., Dambergs, R.G., Gishen, M., Herderich, M.J., 2004. Prediction of phenolic compounds in red wine fermentations by visible and near infrared spectroscopy. Anal. Chim. Acta 513, 73–80. https://doi.org/10.1016/j.aca.2003.08.066

de Kreuk, M.K., Kishida, N., van Loosdrecht, M.C.M., 2007. Aerobic granular sludge - State of the art. Water Sci. Technol. 55, 75–81. https://doi.org/10.2166/wst.2007.244

Devlin, T.R., di Biase, A., Kowalski, M., Oleszkiewicz, J.A., 2017. Granulation of activated sludge under low hydrodynamic shear and different wastewater characteristics. Bioresour. Technol. 224, 229–235. https://doi.org/10.1016/j.biortech.2016.11.005

Franca, R.D.G., Pinheiro, H.M., van Loosdrecht, M.C.M., Lourenço, N.D., 2018. Stability of aerobic granules during long-term bioreactor operation. Biotechnol. Adv. 36, 228–246. https://doi.org/10.1016/j.biotechadv.2017.11.005

Grijspeerdt, K., Verstraete, W., 1997. Image analysis to estimate the settleability and concentration of activated sludge. Water Res. 31, 1126–1134. https://doi.org/10.1016/S0043-1354(96)00350-8

Jiang, Y., Shi, X., Ng, H.Y., 2021. Aerobic granular sludge systems for treating hypersaline pharmaceutical wastewater: Start-up, long-term performances and metabolic function. J. Hazard. Mater. 412, 125229. https://doi.org/10.1016/j.jhazmat.2021.125229

Leal, C., Val del Río, A., Ferreira, E.C., Mesquita, D., Amaral, A.L., 2021b. Validation of a quantitative image

analysis methodology for the assessment of the morphology and structure of aerobic granular sludge in the presence of pharmaceutically active compounds. Environ. Technol. Innov. 23, 101639. https://doi.org/10.1016/j.eti.2021.101639

Leal, C., Val del Río, A., Mesquita, D.P., Amaral, A.L., Castro, P.M.L., Ferreira, E.C., 2020. Sludge volume index and suspended solids estimation of mature aerobic granular sludge by quantitative image analysis and chemometric tools. Sep. Purif. Technol. 234, 116049. https://doi.org/10.1016/j.seppur.2019.116049

Leal, C.S., Lopes, M., Val del Río, A., Quintelas, C., Castro, P.M.L., Ferreira, E.C., Amaral, A.L., Mesquita, D.P., 2021a. Assessment of an aerobic granular sludge system in the presence of pharmaceutically active compounds by quantitative image analysis and chemometric techniques. J. Environ. Manage. 289, 112474. https://doi.org/10.1016/j.jenvman.2021.112474

Li, A.J., Li, X.Y., Yu, H.Q., 2011. Effect of the food-to-microorganism (F/M) ratio on the formation and size of aerobic sludge granules. Process Biochem. 46, 2269–2276. https://doi.org/10.1016/j.procbio.2011.09.007

Li, A.J., Yang, S.F., Li, X.Y., Gu, J.D., 2008. Microbial population dynamics during aerobic sludge granulation at different organic loading rates. Water Res. 42, 3552–3560. https://doi.org/10.1016/j.watres.2008.05.005

Liu, J., Li, J., Wang, X., Zhang, Q., Littleton, H., 2017. Rapid aerobic granulation in an SBR treating piggery wastewater by seeding sludge from a municipal WWTP. J. Environ. Sci. (China) 51, 332–341. https://doi.org/10.1016/j.jes.2016.06.012

Liu, Y., Tay, J.-H., 2002. The essential role of hydrodynamic shear force in the formation of biofilm and granular sludge. Water Res. 36, 1653–1665. https://doi.org/10.1016/S0043-1354(01)00379-7

Liu, Y., Wang, Z.W., Tay, J.H., 2005. A unified theory for upscaling aerobic granular sludge sequencing batch reactors. Biotechnol. Adv. 23, 335–344. https://doi.org/10.1016/j.biotechadv.2005.04.001

Liu, Y.Q., Moy, B., Kong, Y.H., Tay, J.H., 2010. Formation, physical characteristics and microbial community structure of aerobic granules in a pilot-scale sequencing batch reactor for real wastewater treatment. Enzyme Microb. Technol. 46, 520–525. https://doi.org/10.1016/j.enzmictec.2010.02.001

Liu, Y.Q., Tay, J.H., 2015. Fast formation of aerobic granules by combining strong hydraulic selection pressure with overstressed organic loading rate. Water Res. 80, 256–266. https://doi.org/10.1016/j.watres.2015.05.015

Liu, Y.Q., Tay, J.H., 2007. Characteristics and stability of aerobic granules cultivated with different starvation time. Appl. Microbiol. Biotechnol. 75, 205–210. https://doi.org/10.1007/s00253-006-0797-4

Mesquita, D., 2010. Image analysis and chemometric tools to characterize aggregated and filamentous bacteria in activated sludge process. PhD thesis, University of Minho. http://hdl.handle.net/1822/12470

Mesquita, D.P., Amaral, A.L., Ferreira, E.C., 2016. Estimation of effluent quality parameters from an activated sludge system using quantitative image analysis. Chem. Eng. J. 285, 349–357. https://doi.org/10.1016/j.cej.2015.09.110

Mesquita, D.P., Amaral, A.L., Ferreira, E.C., 2011a. Identifying different types of bulking in an activated sludge system through quantitative image analysis. Chemosphere 85, 643–652. https://doi.org/10.1016/j.chemosphere.2011.07.012

Mesquita, D.P., Amaral, A.L., Ferreira, E.C., 2011b. Characterization of activated sludge abnormalities by image analysis and chemometric techniques. Anal. Chim. Acta 705, 235–242. https://doi.org/10.1016/j.aca.2011.05.050

Morgenroth, E., Sherden, T., Van Loosdrecht, M.C.M., Heijnen, J.J., Wilderer, P.A., 1997. Aerobic granular

sludge in a sequencing batch reactor. Water Res. 31, 3191–3194. https://doi.org/10.1016/S0043-1354(97)00216-9

Pronk, M., Abbas, B., Al-zuhairy, S.H.K., Kraan, R., Kleerebezem, R., van Loosdrecht, M.C.M., 2015a. Effect and behaviour of different substrates in relation to the formation of aerobic granular sludge. Appl. Microbiol. Biotechnol. 99, 5257–5268. https://doi.org/10.1007/s00253-014-6358-3

Pronk, M., de Kreuk, M.K., de Bruin, B., Kamminga, P., Kleerebezem, R., van Loosdrecht, M.C.M., 2015b. Full scale performance of the aerobic granular sludge process for sewage treatment. Water Res. 84, 207–217. https://doi.org/10.1016/j.watres.2015.07.011

Rollemberg, S.L. de S., Barros, A.R.M., de Lima, J.P.M., Santos, A.F., Firmino, P.I.M., dos Santos, A.B., 2019. Influence of sequencing batch reactor configuration on aerobic granules growth: Engineering and microbiological aspects. J. Clean. Prod. 238. https://doi.org/10.1016/j.jclepro.2019.117906

Rosen, C., 2001. A chemometric approch to process monitoring and control with application to wastewater treatment operation, PhD thesis, Lund University.

Sarma, S.J., Tay, J.H., 2018. Aerobic granulation for future wastewater treatment technology: Challenges ahead. Environ. Sci. Water Res. Technol. 4, 9–15. https://doi.org/10.1039/c7ew00148g

Sarma, S.J., Tay, J.H., Chu, A., 2017. Finding Knowledge Gaps in Aerobic Granulation Technology. Trends Biotechnol. 35, 66–78. https://doi.org/10.1016/j.tibtech.2016.07.003

Sguanci, S., Lubello, C., Caffaz, S., Lotti, T., 2019. Long-term stability of aerobic granular sludge for the treatment of very low-strength real domestic wastewater. J. Clean. Prod. 222, 882–890. https://doi.org/10.1016/j.jclepro.2019.03.061

Su, K.Z., Yu, H.Q., 2005. Formation and characterization of aerobic granules in a sequencing batch reactor treating soybean-processing wastewater. Environ. Sci. Technol. 39, 2818–2827. https://doi.org/10.1021/es048950y

Val Del Río, A., Figueroa, M., Mosquera-Corral, A., Campos, J.L., Méndez, R., 2013. Stability of aerobic granular biomass treating the effluent from a seafood industry. Int. J. Environ. Res. 7, 265–276. https://doi.org/10.22059/ijer.2013.606

Verawaty, M., Pijuan, M., Yuan, Z., Bond, P.L., 2012. Determining the mechanisms for aerobic granulation from mixed seed of floccular and crushed granules in activated sludge wastewater treatment. Water Res. 46, 761–771. https://doi.org/10.1016/j.watres.2011.11.054

Wagner, J., Weissbrodt, D.G., Manguin, V., Ribeiro da Costa, R.H., Morgenroth, E., Derlon, N., 2015. Effect of particulate organic substrate on aerobic granulation and operating conditions of sequencing batch reactors. Water Res. 85, 158–166. https://doi.org/10.1016/j.watres.2015.08.030

Wilén, B.M., Liébana, R., Persson, F., Modin, O., Hermansson, M., 2018. The mechanisms of granulation of activated sludge in wastewater treatment, its optimization, and impact on effluent quality. Appl. Microbiol. Biotechnol. 102, 5005–5020. https://doi.org/10.1007/s00253-018-8990-9

Xavier, J.A., Guimarães, L.B., Magnus, B.S., Leite, W.R., Vilar, V.J.P., da Costa, R.H.R., 2021. How volumetric exchange ratio and carbon availability contribute to enhance granular sludge stability in a fill/draw mode SBR treating domestic wastewater? J. Water Process Eng. 40. https://doi.org/10.1016/j.jwpe.2021.101917

Zhang, B., Ji, M., Qiu, Z., Liu, H., Wang, J., Li, J., 2011. Microbial population dynamics during sludge granulation in an anaerobic-aerobic biological phosphorus removal system. Bioresour. Technol. 102, 2474–2480. https://doi.org/10.1016/j.biortech.2010.11.017

CHAPTER 4

Characterization of aerobic granular sludge formation under washout dynamics through quantitative image analysis: The influence of COD/N

Aerobic granulation from activated sludge was studied in three sequencing batch reactors (SBR) operated under washout dynamics and chemical oxygen demand (COD)-to-nitrogen ratio (COD/N) of 10 (R1), 5 (R2), and 2 (R3). The structural changes in microbial aggregates (i.e., flocs, filaments, and granules) were assessed through quantitative image analysis (QIA) and correlated with the reactor's performance. Aerobic granular sludge (AGS) was successfully achieved in R1 and R3 but was unsuccessful in R2. The sludge washout negatively affected nutrient removal efficiencies, though it favoured granulation in all reactors. The polyphosphate accumulating organisms (PAO) activity was more affected by the gradual decrease in settling time than ammonium-oxidizing bacteria (AOB) and nitrite-oxidizing bacteria (NOB) activity. In R1, the AOB activity recovered rapidly after sludge washout, whereas the recovery of NOB was only observed subsequently to the prevalence of larger granules. The increase in phosphate removal efficiency was concomitant to the increase in the granular fraction volume and number of large granules. The result showed that the poor ammonium removal efficiencies during the granulation in R2 and R3 favoured the development of viscous bulking and filamentous bacteria. The subsequent reduction in viscosity and formation of compact and regular granules after reaching efficient ammonium removal in R3 indicated that granulation was favoured by the establishment of nitrifying bacteria (i.e., AOB). The QIA data evidenced a complex relationship between nutrient removal and sludge morphology during the granulation process. The effluent's ammonium, phosphate, nitrite, and nitrate concentration was successfully estimated with partial least square (PLS) using morphological data from flocs, filaments, and granules obtained from QIA. The good predictions achieved for all target variables with parameters belonging to the floccular and granular fractions indicated the potential of QIA to monitor and control the granulation process.

4.1. INTRODUCTION

Aerobic granular sludge (AGS) technology has the potential to become the new standard for aerobic wastewater treatment due to several advantages over activated sludge, which is still the most common biological treatment process in wastewater treatment plants (Franca et al., 2018). In AGS systems, the anoxic and aerobic microorganisms are retained in the form of granules, allowing the removal of organic matter and nutrients (i.e., nitrogen and phosphorus) simultaneously in a single reactor which contributes to its smaller footprint and lowers the energy requirements (Bengtsson et al., 2019; Pronk et al., 2015). Due to the layered granular structure and high extracellular polymeric substance content, AGS present higher resilience to toxic compounds and variance in wastewater composition (Adav et al., 2008). Research has shown the ability of AGS to treat recalcitrant industrial effluents, such as textile, pharmaceutical, petrochemical and saline wastewaters (Cai et al., 2021). However, long granulation periods and granules instability have been pointed to as the critical issues of AGS technology preventing its large-scale application (Lin et al., 2020).

The aerobic granulation process consists of a gradual development from seed sludge to compact aggregates, further to initial granules and mature granular sludge (Liu and Tay, 2004). Among the various operational parameters that can affect the granulation process, short settling times have been pointed out as fundamental to enhance aerobic granulation by removing slow settling aggregates (Beun et al., 2000; Qin et al., 2004). However, biological nutrient removal decrease during the granulation period due to the washout of slow-growing microorganisms, such as nitrifying bacteria (i.e., ammonium-oxidizing bacteria (AOB) and nitrite-oxidizing bacteria (NOB)) and polyphosphate accumulating organisms (PAO), induced by shorts settling time (Weissbrodt et al., 2012). The formation of unstable granular sludge with filamentous proliferation was recently reported in a sequencing batch reactor (SBR) owing to poor nutrient removal abilities from the seed sludge (Bassin et al., 2019). Nevertheless, dense and stable granules were successfully formed after an adaptation period of 40 days under reduced washout conditions, favouring the development of nitrifying bacteria (Bassin et al., 2019). Hence, the granular stability was attributed to the development of the nitrifying activity. Also, the selection of slow-growing microorganisms, such as PAO, has been shown to favour the achievement of stable granules (de Kreuk et al., 2005). Thus, the absence of nutrient removal capacity during the granulation process may impact granules morphology and stability.

Chemical oxygen demand (COD)-to-nitrogen ratio (COD/N) could be an essential operational parameter in the formation and the stability of AGS. During granulation from activated sludge, previous result has

shown that under decreasing COD/N ratio nitrifying activity increases while the heterotrophic activity decreases, resulting in compact and small size granules (Wu et al., 2012; Yang et al., 2005). In other works using mature granules, the decrease in the COD/N ratio from 4 to 1 resulted in the disintegration of AGS and the reduction in the nitrification rate attributed to microbial changes due to sludge washout (Luo et al., 2014). In contrast, stable and compact granules (650 μm) were maintained after gradual decrease in the COD/N ratio from 15 to 5 (Zhang et al., 2018).

Detailed sludge morphological information of the dynamic changes (i.e., from floccular to granular sludge) and filamentous bacteria observed during granulation is relevant, increasing the knowledge about the rates and stability of the AGS formed under defined operating conditions. Relevant sludge morphological information has been successfully extracted through QIA coupled with multivariate statistical methods, which allowed the estimation of sludge volume index, density and effluent quality in AGS systems (Costa et al., 2022; Leal et al., 2022; Silva et al., 2022). In this work, the biological nutrient removal capabilities and the sludge morphological changes during granulation was evaluated in SBR operated under different COD/N ratios and washout dynamics.

4.2. MATERIAL AND METHODS

4.2.1. Reactors setup and operating conditions

Three identical lab-scale SBR with a working volume of 1 L were operated in parallel. The reactors had a height to diameter ratio (H/D) of 2. SBR were operated using synchronized timers to control influent/effluent pumps and the air valve. Airflow was controlled using a gas flowmeter (Cole Parmer, United States), providing complete mixing and dissolved oxygen (DO) during aeration. The SBR were operated at room temperature, and pH was not controlled but monitored. The reactors were operated in cycles of 6 h under variable volume and at a volume exchange ratio (VER) of 50% to achieve an identical hydraulic retention time (HRT) of 12 h. SBR cycles encompassed four distinct phases: static anaerobic feed, aeration, settling, and effluent withdrawal (Table 4.1). The reactors were operated under decreasing settling times, selecting for aggregates with increasing minimal imposed sludge settling velocities (MISSV) (Table 4.2).

Table 4.1 – The reactor's operating condition

Parameter	Unit	R1	R2	R3
Cycle time	h	6	6	6
Cycle phases				
Anaerobic	min	120	120	120
Aerobic	min	180 – 234	180 – 234	180 – 234
Settling	min	55 – 1	55 – 1	55 – 1
Effluent withdrawal	min	5	5	5
MISSV	m h^{-1}	0.1 – 5.3	0.1 – 5.3	0.1 – 5.3
HRT	h	12	12	12
pH	-	8.0 ± 0.3	8.5 ± 0.3	8.4 ± 0.3
Temperature	°C	19.7 ± 1.1	19.7 ± 1.0	19.8 ± 1.0

Table 4.2 – The settling time and MISSV during SBR operation

Operational days	Settling time (min)	MISSV (m h^{-1})
0 - 6	55	0.1
6 - 13	20	0.27
13 - 20	10	0.53
20 - 25	1	5.3
25 - 79	20	0.27
79 - 92	10	0.53
92 - 158	1	5.3

Activated sludge from the municipal wastewater treatment plant of Frossos Braga – Portugal, was used as inoculum at a concentration of 4 g L^{-1} mixed liquor volatile suspended solids (MLVSS). In order to monitor granulation under distinct nitrogen concentrations, three SBR (R1, R2, and R3) were fed with a synthetic medium containing 1.04 g L^{-1} $C_2H_3NaO_2 \cdot 3H_2O$ (as carbon source), 0.112 g L^{-1} K_2HPO_4 (as $P\text{-}PO_4^{3-}$ source), and NH_4Cl (as $N\text{-}NH_4^+$ source) concentrations of 0.19 g L^{-1} (R1), 0.38 g L^{-1} (R2) and 0.96 g L^{-1} (R3), resulting in a COD/N of 10, 5 and 2, respectively (Table 4.3). Sodium bicarbonate ($NaHCO_3$) to ammonium chloride ratio was set at 3 in each reactor to maintain alkalinity during biological nitrification. Synthetic medium was prepared with tap water supplemented with $MgSO_4.7H_2O$ (0.09 g L^{-1}), $CaCl_2.2H_2O$ (0.03 g L^{-1}), and 0.75 mL (per L^{-1}) of a trace solution containing: $FeCl_3.6H_2O$ (6 g L^{-1}); H_3BO_3 (0.6 g L^{-1}); $CuSO_4.5H_2O$ (0.12 g L^{-1}); KI (0.72 g L^{-1}); $MnCl_2.4H_2O$ (0.48 g L^{-1}); $Na_2MoO_2.2H_2O$ (0.24 g L^{-1}); $ZnSO_4.7H_2O$ (0.48 g L^{-1}); $CoCl_2.6H_2O$ (0.6 g L^{-1}), and EDTA (40 g L^{-1}).

Table 4.3 – The main component concentration in the synthetic feed

Component	Unit	R1	R2	R3
Chemical oxygen demand (COD)	mg L^{-1}	477 ± 58	471 ± 72	479 ± 55
Ammonium nitrogen (N-NH_4^+)	mg L^{-1}	48 ± 6	93 ± 8	230 ± 20
Phosphate (P-PO_4^{3-})	mg L^{-1}	20 ± 1	19 ± 1	20 ± 2
COD/N	-	10	5	2

4.2.2. Analytical methods

Mixed liquor volatile suspended solids (MLVSS) were determined according to the Standard Methods (APHA, 2005). COD, ammonium nitrogen (N-NH_4^+), phosphate (P-PO_4^{3-}), nitrite (N-NO_2^-), and nitrate (N-NO_3^-) concentrations were determined spectrophotometrically using a cuvette test kit (Hach-Lange GmbH, Dusseldorf, Germany) and DR2800TM spectrophotometer (Hach-Lange, GmbH). COD, ammonium and phosphate removal efficiencies were calculated using the following equation:

$$\text{Removal efficiency (\%)} = \left(\frac{C_{in}-C_{eff}}{C_{in}}\right)X100$$

where, C_{in} and C_{eff} are the influent and effluent concentration, respectively.

4.2.3. Quantitative image analysis

4.2.3.1. Sludge sampling, image acquisition, processing and analysis

A sample volume of 10 mL was collected at the beginning of the aeration phase when the complete mixture was attained. A sedimentation separation technique was applied to separate the granular and floccular biomass fractions, considering the different settling times of each fraction. All aggregates with an equivalent diameter (Deq) < 200 μm were considered flocs, and aggregates with Deq ≥ 200 μm were considered granules (de Kreuk et al., 2007).

For flocs and filaments characterization, a 10 μL sample was placed on a slide employing a micropipette with a sectioned tip to allow the passage of flocs and filaments, and a coverslip (20 x 20 mm) was positioned on top. This procedure was performed in triplicate, resulting in 150 images being acquired per sample. Regarding granules characterization, a sample volume was placed in a Petri dish, and all the granules present in that volume were captured. The sample volume was adjusted to avoid significant increments of the time spent for granules characterization. The minimum and the maximum number of

granules captured for each reactor are shown in Table 4.4. Images of flocs and filaments were acquired through bright-field using an Olympus BX-51 microscope (Olympus, Shinjuku, Japan) with 100x magnification, coupled to an Olympus DP71 camera (Olympus, Shinjuku, Japan), and cellSens software (Olympus, Shinjuku, Japan) in 1360 x 1024 pixels and 8-bit format. Images of granules were acquired with an Olympus SZ-40 stereomicroscope (Olympus, Shinjuku, Japan) with 15x magnification, coupled to a CCD AVC D5CE Sony video camera (Sony, Tokyo, Japan), and Image Pro Plus software (Media Cybernetics, MD, USA) in 768 x 576 pixels and 8-bit format.

Table 4.4 – Minimum and maximum number of granules captured in each reactor

Number of granules	**R1**	**R2**	**R3**
Minimum	406	105	169
Maximum	2060	490	688
Average ± standard deviation	805 ± 476	350 ± 122	369 ± 160

Binary images were created using the images from flocs and filaments fraction and granules from the granular fraction, allowing the determination of the morphological parameters (Annexe Table A1). In accordance to their Deq, the floccular and granular fractions were divided into 2 and 3 classes, respectively. Hence, flocs classes (Fc) were Fc1 (Deq < 100 μm) and Fc2 (100 μm < Deq < 200 μm), whereas the granules classes (Gc) were Gc1 (200 μm ≤ Deq ≤ 600 μm), Gc2 (600 μm < Deq < 1000 μm), and Gc3 (Deq ≥ 1000 μm). The Deq of each aggregates was determined by the Area parameter as described in Chapter 3. The total area of flocs (TA_{Flocs}/Vol) per unit of volume, expressed in (mm^2 μL^{-1}), was calculate using the equation:

$$TA_{Flocs}/Vol = \frac{\sum Area}{Volume}$$

where Area is the area of each floc and volume is the volume of each image (V_{image}) calculated as described in Chapter 3. The ratio between total filament length (see Chapter 3) and TA_{Flocs} was calculated as:

$$TL/TA_{Flocs} = \frac{TL}{TA_{Flocs}}$$

In the case of granular fraction quantified by stereomicroscopy, the TA of granules ($TA_{Granules}/Vol$) present in the sample, expressed in ($mm^2\ mL^{-1}$) was calculate using the equation:

$$TA_{Granules}/Vol = \frac{\sum A}{Vol}$$

where A is the area of each granule and Vol is the volume of sample analysed (mL^{-1}). The specific area and volume of granules per unit of volume for each granule size class was calculated using the following equations:

$$Area/Vol = \frac{\sum_{i=1}^{n} A}{Vol}$$

$$Volume/Vol = \frac{\sum_{i=1}^{n} V}{Vol}$$

where A is the area and V is the volume of each *i* granule belonging to *n* size class, and Vol is the volume of sample analysed (mL^{-1}). Image processing and analysis were performed in MatlabTM 8.5 (the MathWorks Inc, USA) using two programmes developed in Amaral (2003), and adapted thereafter (Leal et al., 2021). Detailed information about image processing and analysis, including pre-treatment, segmentation, and debris elimination steps is described in Leal et al. (2021).

4.2.4. Multivariate statistical analysis

Partial least squares (PLS) regression is a statistical method that models a large dataset of independent variables (X) to predict a dependent variable (Y). In this work, PLS regression was performed to predict the effluent concentrations of $P\text{-}PO_4^{3-}$,$N\text{-}NH_4^+$, $N\text{-}NO_2^-$, and $N\text{-}NO_3^-$ (Y dataset), using morphological information obtained through QIA (X dataset) (Annexe Table A1). For each dependent variable Y, the overall dataset was composed of 22 observations and 127 parameters (X dataset). The observations were randomly divided into training set (67% of observations) and validation set (33% of the observations) to calibrate and validate the model, respectively. This division was repeated 2500 times from the original dataset, and the correlation coefficient (R^2) between the predicted and observed Y variable was determined. To avoid overfitting, the number of predictors X was equal to n/2, with n being the number of observations of the training dataset. To select the best predictors X, a first PLS was performed for each target Y, allowing to determine the variable importance in projection (VIP) of each predictor of the X dataset. Whenever two VIP variables exhibited a correlation coefficient ≥ 0.7, the one presenting the

lowest VIP value was excluded and the next variable was selected. Thus, the final PLS was performed using the 7 variables presenting the highest VIP values (Table 4.5). PLS models root mean square errors (RMSEP) and residual predictive deviation (RPD) were used as the basis of the predictions accuracy. PLS were performed in MatlabTM 8.5 (the MathWorks Inc, USA).

Table 4.5 – Set of independent variables (X) and respective VIP used in the PLS models for prediction of each target variable (Y)

Dependent variable (matrix Y)	Independent variables (matrix X)	VIP
P-PO_4^{3-}	Ext_{Fc1}	1.53
	$\%Area_{Gc1}$	1.24
	$\%Nb_{Gc3}$	1.22
	TL/TSS	0.80
	L_{Fc2}	0.70
	TL/TA_{Flocs}	0.56
	W_{Fc2}	0.42
N-NH_4^+	Vol_{Gc3}	1.80
	Rob_{Fc1}	1.57
	TL/TSS	0.67
	Nb_{Gc3}/Vol	0.57
	Nb_{Gc1}/Vol	0.51
	Vol_{Gc2}/Vol	0.38
	TA_{Flocs}/Vol	0.37
N-NO_2^-	Vol_{Gc1}/Vol	1.67
	$Round_{Fc2}$	1.22
	Deq_{Fc2}	0.94
	TA_{Flocs}/Vol	0.90
	$Excc_{Fc2}$	0.88
	$\%Nb_{Gc3}$	0.40
	$Excc_{Fc1}$	0.33
N-NO_3^-	$\%Area_{Gc1}$	1.64
	Nb_{Fc1}/Vol	1.25
	W_{Fc2}	1.16
	$\%Nb_{Gc3}$	0.81
	Nb_{Flocs}/Vol	0.67
	Ext_{Fc1}	0.41
	$Area_{Flocs}$	0.35

Fc1 – Deq < 100 µm; Fc2 – 100 µm < Deq < 200 µm; Flocs – Overall flocs;
Gc1 – 200 µm ≤ Deq ≤ 600 µm; Gc2 – 600 µm < Deq < 1000 µm; Gc3 – Deq ≥ 1000 µm

4.3. RESULTS

4.3.1. Sludge concentration and settling properties in SBR

Reactors R1, R2, and R3 were inoculated with 4 g L^{-1} in MLVSS of suspended sludge. At the early stage, circa 60% of MLVSS was lost in all reactors under 55 min of settling time (Figure 4.1a). Despite the gradual decrease in the settling time from 55 min to 10 min, the MLVSS increased in all reactors (Figure 4.1a). Under 1 min settling time, the MLVSS decreased severally, although more biomass was retained in R1. After biomass washout, the MLVSS increased in all reactors, with the highest concentration observed in R3 (i.e., 10.2 ± 3 g L^{-1}) and the least in R2 (i.e., 2.2 ± 0.01 g L^{-1}) at the end of the operation (Figure 4.1a).

The highest biomass concentration in the effluent was observed in R1 from day 16 to day 25, reaching 0.64 ± 0.02 g L^{-1}, which was 1.8 and 1.6 times more than in R2 and R3, respectively (Figure 4.1b). The food-to-microorganism ratio (F/M) remained, for the most part, between 0.1 and 0.6 g_{COD} g_{VSS}^{-1} d^{-1} (Figure 4.1c). However, the lower biomass retention in R2 and R3 during the biomass washout event increased the F/M to 8.75 and 3.28 g_{COD} g_{VSS}^{-1} d^{-1}, respectively (Figure 4.1a,c). The SVI_{30}/SVI_5 ratio remained between 0.4 and 0.7 during the first 25 days (Figure 4.1d). In R1, the SVI_{30}/SVI_5 remained above 0.9 after the biomass washout, while in R2 and R3, a progressive decrease to 0.6 was observed. The SVI_{30}/SVI_5 increased in all reactors with the subsequent decrease in settling time on days 79 and 92, oscillating between 0.8 and 1 (Figure 4.1d).

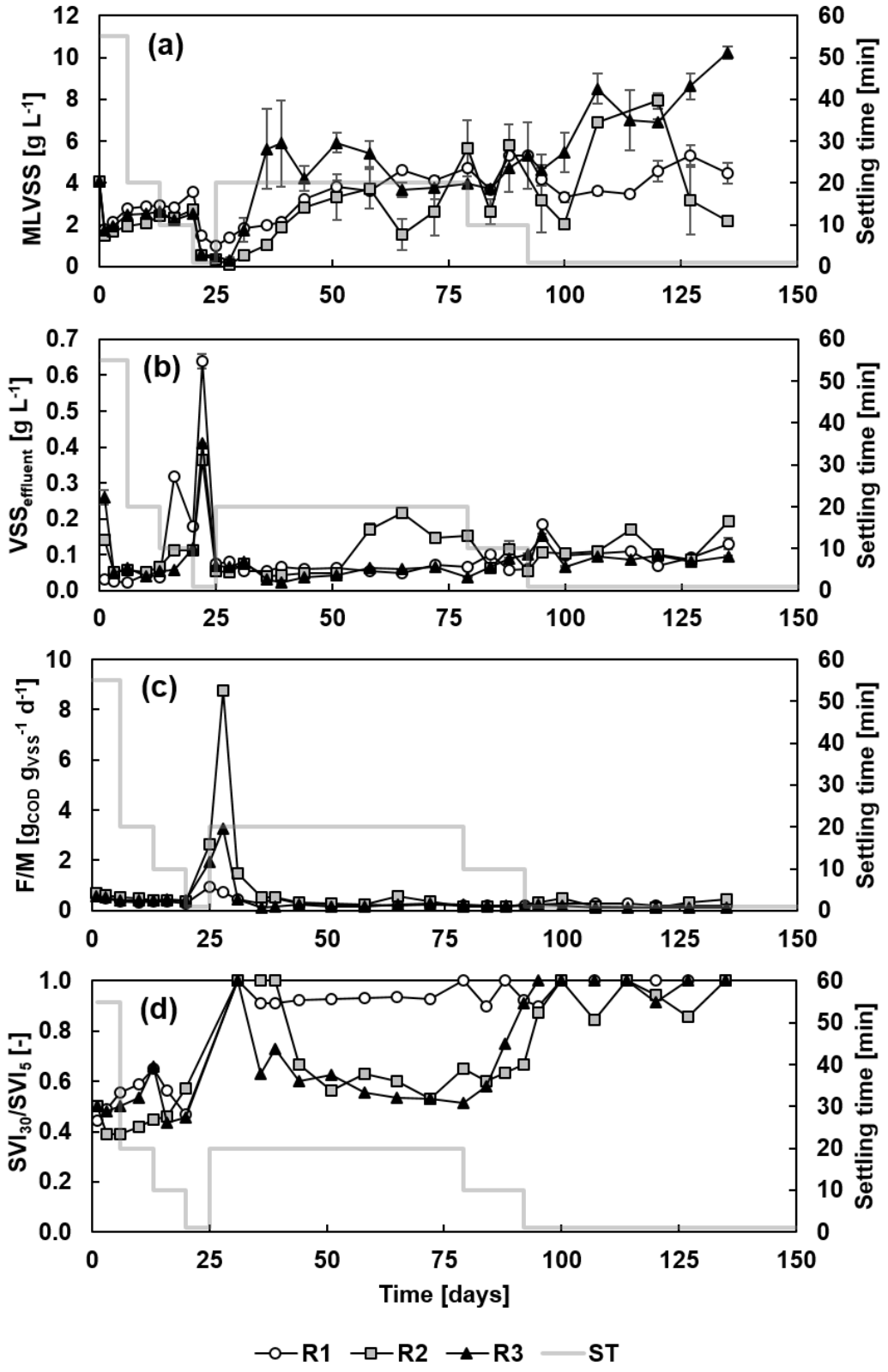


Figure 4.1 – MLVSS (a), $VSS_{effluent}$ (b), F/M ratio (c), and SVI_{30}/SVI_5 (d) profiles in R1 (—○—), R2 (—□—), and R3 (—▲—). The settling time (ST) (——) applied throughout the reactors' operation.

4.3.2. COD and nutrients removal

The COD, phosphate, and ammonium removal efficiencies are shown in Figure 4.2. The COD removal efficiencies were stable throughout the operation in all reactors, reaching 95 ± 2%, 91±4%, and 92 ± 3% in R1, R2, and R3, respectively (Figure 4.2a). For the most part, ammonium nitrogen was efficiently removed in R1, yet a transient decrease in the removal efficiency (circa 50%) was observed following the biomass washout, which was gradually recovered afterward (Figure 4.2b). In R2, the ammonium removal efficiency mainly remained below 50%, while in R3, ammonium removal increased from day 79 (Figure 4.2b). Phosphate removal efficiency exhibited a decreasing trend in the first 25 days in all reactors, yet a steeper decrease was observed in R2 and R3, induced by the gradual decrease in the settling time, suggesting the loss of microbial activity due to inhibitory and sludge washout conditions (Figure 4.2c). After the subsequent increase in the settling time to 20 min, the phosphate removal efficiencies remained relatively low (i.e., < 12%). Nevertheless, phosphate removal gradually increased from day 100 in R1, following a transitory instability period (from day 79 to 95). In contrast, phosphate removal efficiencies in R2 and R3 varied between 2% - 15% and 3% – 13%, respectively, throughout the operation (Figure 4.2c).

In R1, nitrate accumulated up to 20 mg L^{-1} during the first 20 days, decreasing drastically under a 1 min settling time (Figure 4.3a). Partial nitrification was observed after biomass washout, with nitrite concentration reaching 16 mg L^{-1} on day 51, concomitant with ammonium removal (Figure 4.3b). Nitrate concentration increased sharply to 25 mg L^{-1}, coincident with the decrease in nitrite concentration from day 100, suggesting that complete nitrification was recovered (Figure 4.3a). Nitrate and nitrite concentrations were transiently undetected in R2 and R3 after day 25, suggesting a decrease in AOB and NOB activity due to sludge washout (Figure 4.3a,b). However, in R3, nitrite concentration gradually increased from day 58, reaching 195 mg L^{-1} on day 100, associated with the complete ammonium oxidation, suggesting the recovery of AOB activity (Figure 4.3b). While NOB activity also recovered, it occurred to a lesser extent since nitrate concentration stabilized at circa 36 mg L^{-1}, which was 5.5 times less than nitrite concentration (Figure 4.3a). In R2, although ammonium removal efficiencies increased from day 79, nitrite and nitrate concentration remained relatively low, suggesting poor AOB and NOB activities (Figure 4.3a,b).

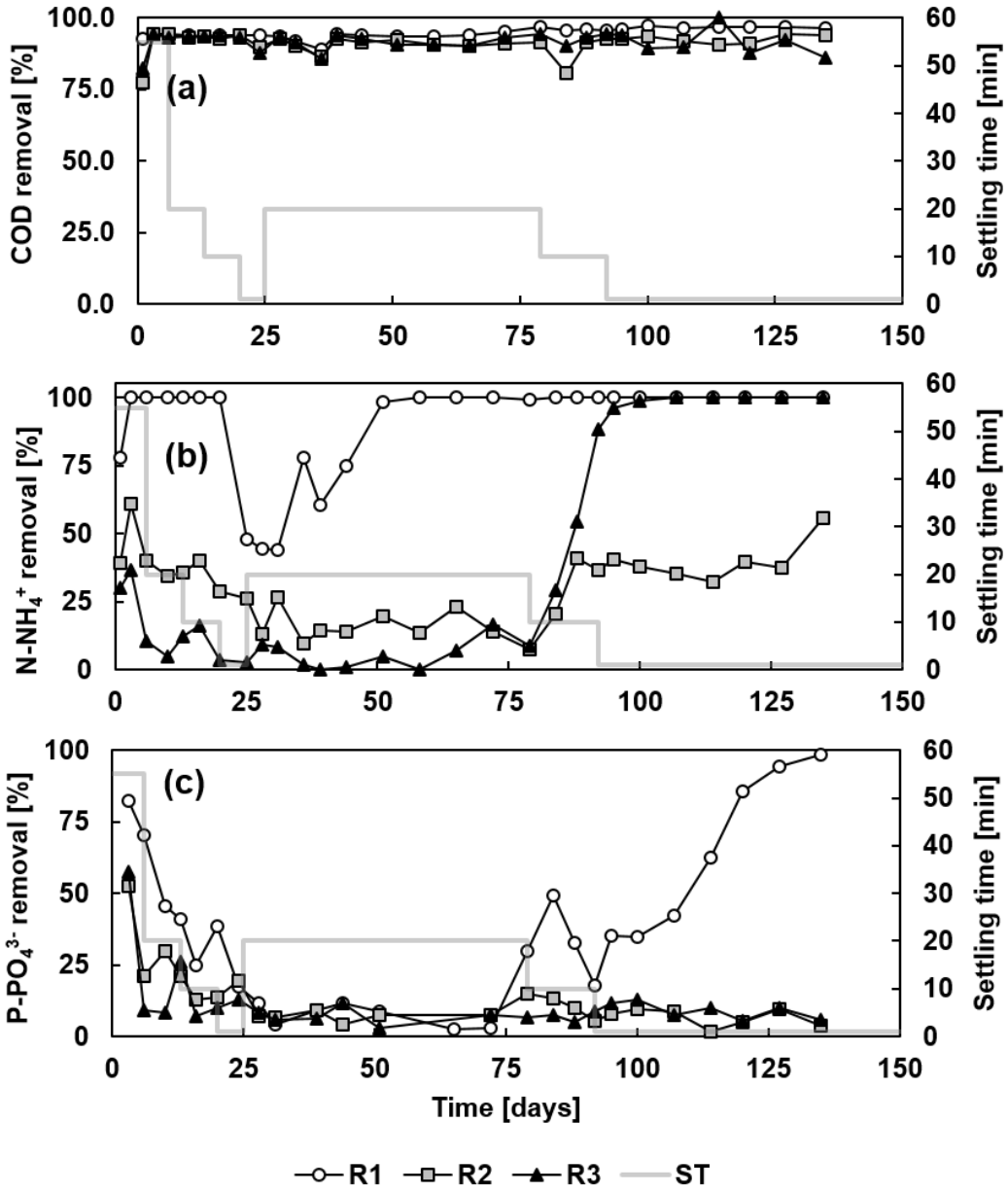


Figure 4.2 – Removal efficiencies for COD (a), N-NH_4^+ (b), and P-PO_4^{3-} (c) in R1 (—○—), R2 (—□—), and R3 (—▲—). The settling time (ST) (——) applied throughout the reactors' operation.

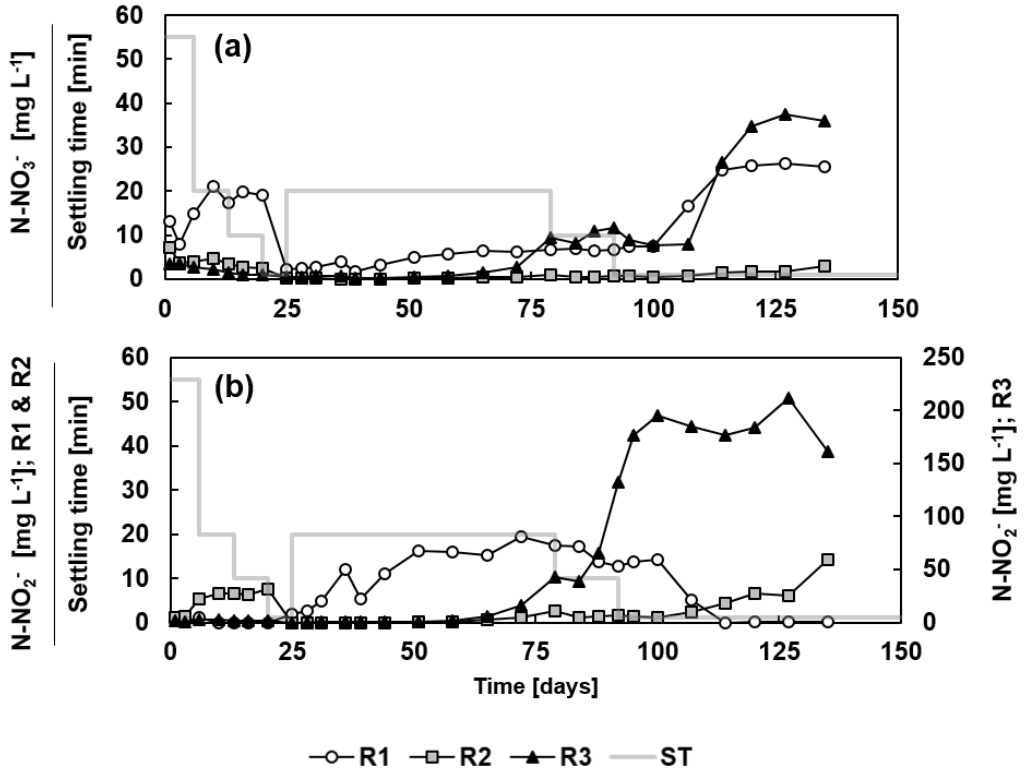


Figure 4.3 – $N\text{-}NO_3^-$ (a) and $N\text{-}NO_2^-$ (b) effluent concentration in R1 (—○—), R2 (—□—), and R3 (—▲—). The settling time (ST) (——) applied throughout the reactors' operation.

4.3.3. Morphological properties

The TA_{Flocs}/Vol varied between 0.3 and 0.4 $mm^2\ \mu L^{-1}$ in all reactors during the first 20 days, decreasing drastically after altering the settling time to 1 min (Figure 4.4a). In R1, the TA_{Flocs}/Vol reached 0.18 ± 0.04 $mm^2\ \mu L^{-1}$ on day 31, which was 4 and 6 times higher than in R2 and R3, respectively (Figure 4.4a). After sludge washout, the $TA_{Granules}$/Vol increased in all reactors, yet with a steeper increase in R1 (Figure 4.4b). The $TA_{Granules}$/Vol stabilized at 279 ± 16 $mm^2\ mL^{-1}$ on day 51 in R1, whereas in R2 and R3, the $TA_{Granules}$/Vol reached 148 ± 13 $mm^2\ mL^{-1}$ (day 51) and 100 ± 10 $mm^2\ mL^{-1}$ (day 135), respectively (Figure 4.4b). Viscous and filamentous bulking impaired further granules quantification in R2 (i.e., from day 51) and momentarily in R3 (i.e., from day 44 to 100) (Figure 4.4b). From day 51, the TL/TA_{Flocs} increased gradually from 92 ± 4 mm^{-1} to 1064 ± 11 mm^{-1} in R2, while filamentous outgrowth started from day 31 in R3, with the TL/TA_{Flocs} reaching 1303 ± 23 mm^{-1} on day 39 (Figure 4.4c). The decrease in the settling time to 1 min (from day 92) induced the TL/TA_{Flocs} decrease to 70 ± 3 mm^{-1}, 66 ± 2 mm^{-1} and 146 ± 3 mm^{-1} in R1, R2, and R3, respectively (Figure 4.4c).

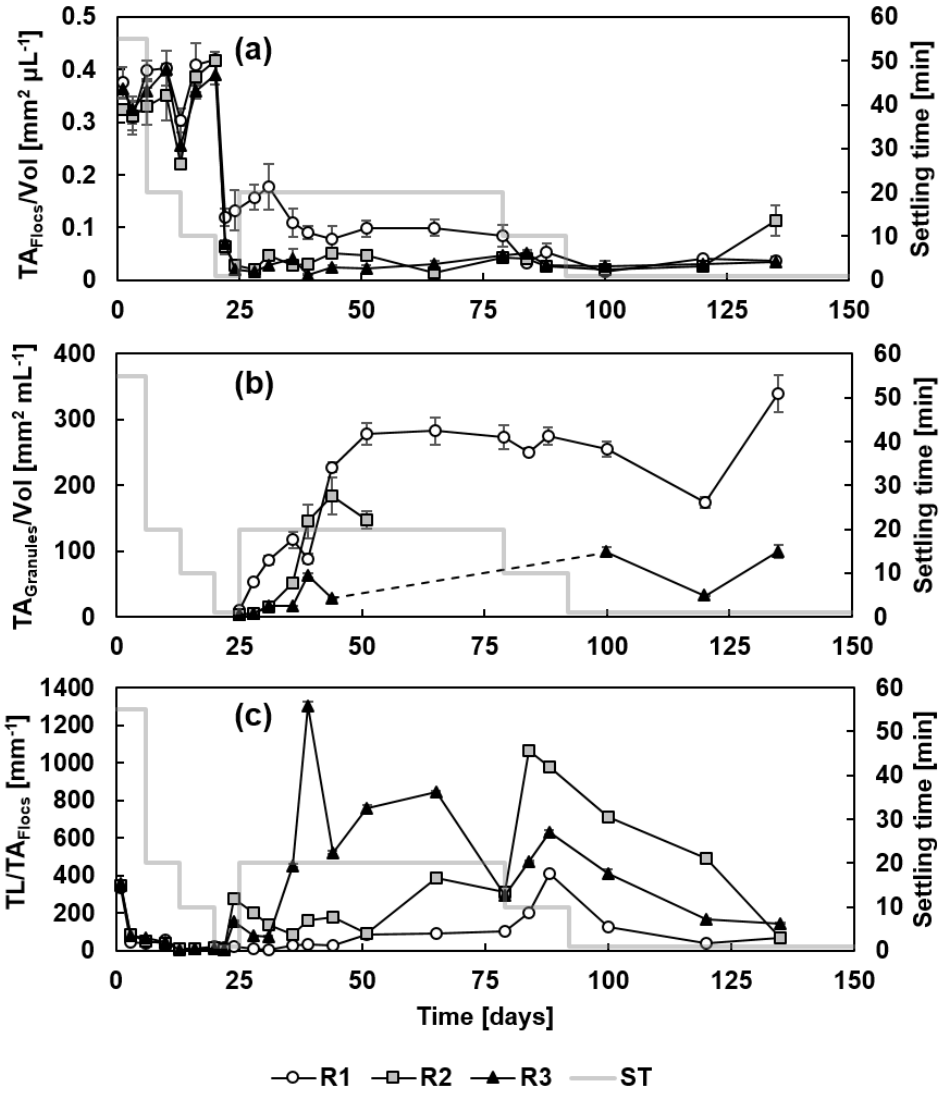


Figure 4.4 – TA_{Flocs}/Vol (a), $TA_{Granules}$/Vol (b), and TL/TA_{Flocs} (c) in R1 (—○—), R2 (—□—), and R3 (—▲—). The settling time (ST) (——) applied throughout the reactors' operation.

Microscopic observations revealed high amounts of free and protruding filaments in R2 and R3, and filamentous macrostructures after day 25 (Figure 4.5a-d). Nonetheless, the granules produced in the reactors R2 and R3 were visually distinct from R1 (Figure 4.5e-g). In R1, granules presented a dense and compact structure with variable sizes (Figure 4.5e), whereas in R2, only a few large granules with yellowish colour were observed at the end of the operation (Figure 4.5f). In R3, granules were small and compact with a reddish colour, and the coexistence of granules and filamentous macrostructures persisted until the end of the operation (Figure 4.5g).

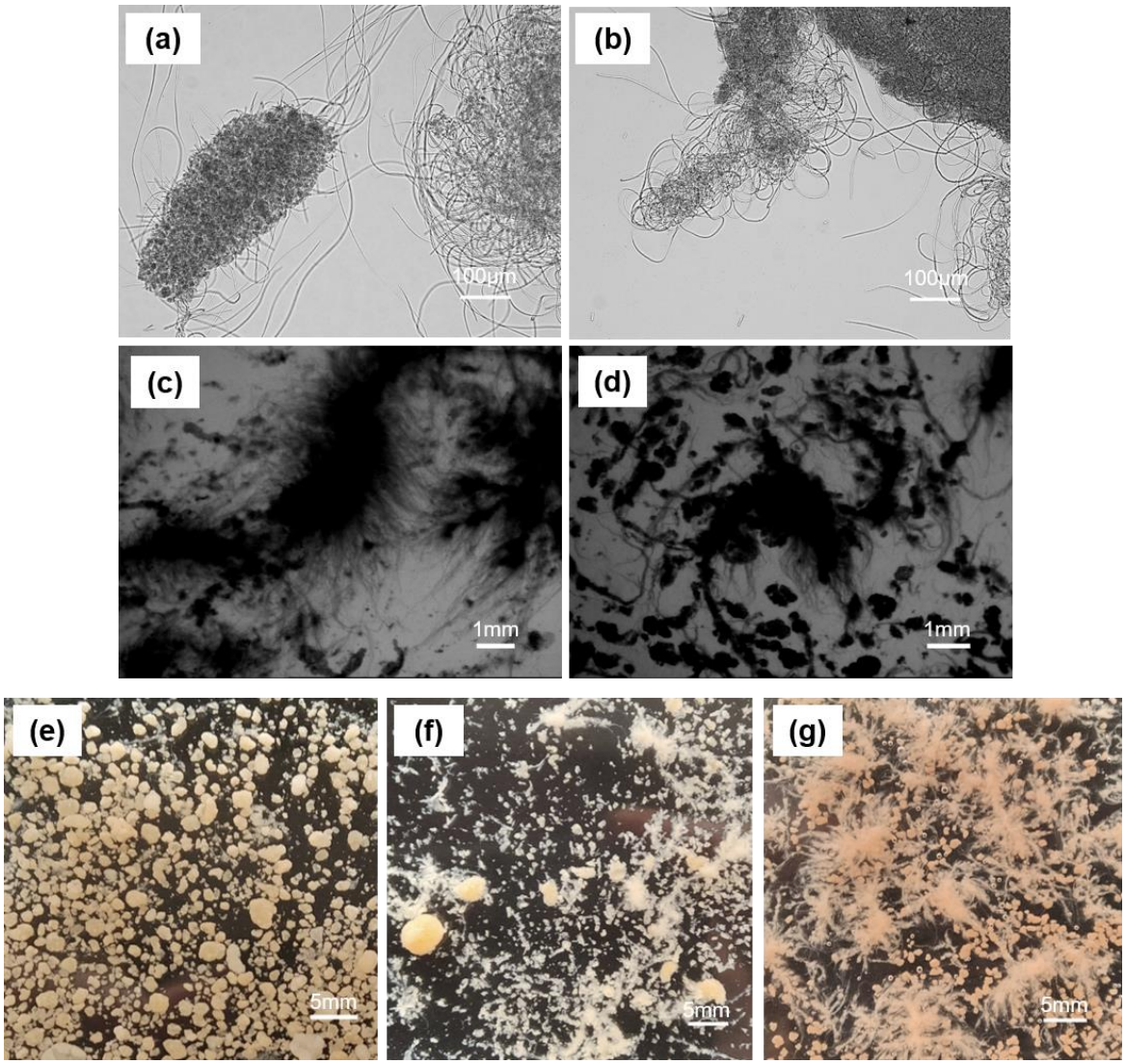


Figure 4.5 – Bright-field microscopy of flocs and filaments observed in R2 (a) and R3 (b) on day 84 and day 39, respectively. Stereomicroscopy from the granular fraction observed in R2 (c) and R3 (d) on day 79. Images of the AGS formed in R1 (e), R2 (f) and R3 (g) on day 129.

The granular fraction in R1 was further characterized regarding their size during the formation of granules, and a granulation (Gr) and maturation (Mt) period could be defined due to the evolution of the granular fraction (Figure 4.6). The Deq remained stable at around 411 ± 21 µm during the granulation period (i.e., day 25 and 51), followed by a gradual increase to 934 ± 33 µm during the maturation period (i.e., from day 51 onwards) (Figure 4.6a). The Area/Vol of Gc1 (200 µm ≤ Deq ≤ 600 µm), Gc2 (600 µm < Deq < 1000 µm) and Gc3 (Deq ≥ 1000 µm) increased during the granulation period, with a prevalence of Gc1 that reached 165 ± 3 mm^2 mL^{-1} (Figure 4.6b). During the maturation period, the Area/Vol of Gc3 increased gradually to 253 ± 33 mm^2 mL^{-1}, while Gc1 decreased to 22 ± 4 mm^2 mL^{-1} at the end of the operation.

After decreasing the settling time to 1 min (from day 92), the Volume/Vol of Gc3 increased considerably from 221 ± 22 mm^3 mL^{-1} to 806 ± 215 mm^3 mL^{-1} (Figure 4.6c).

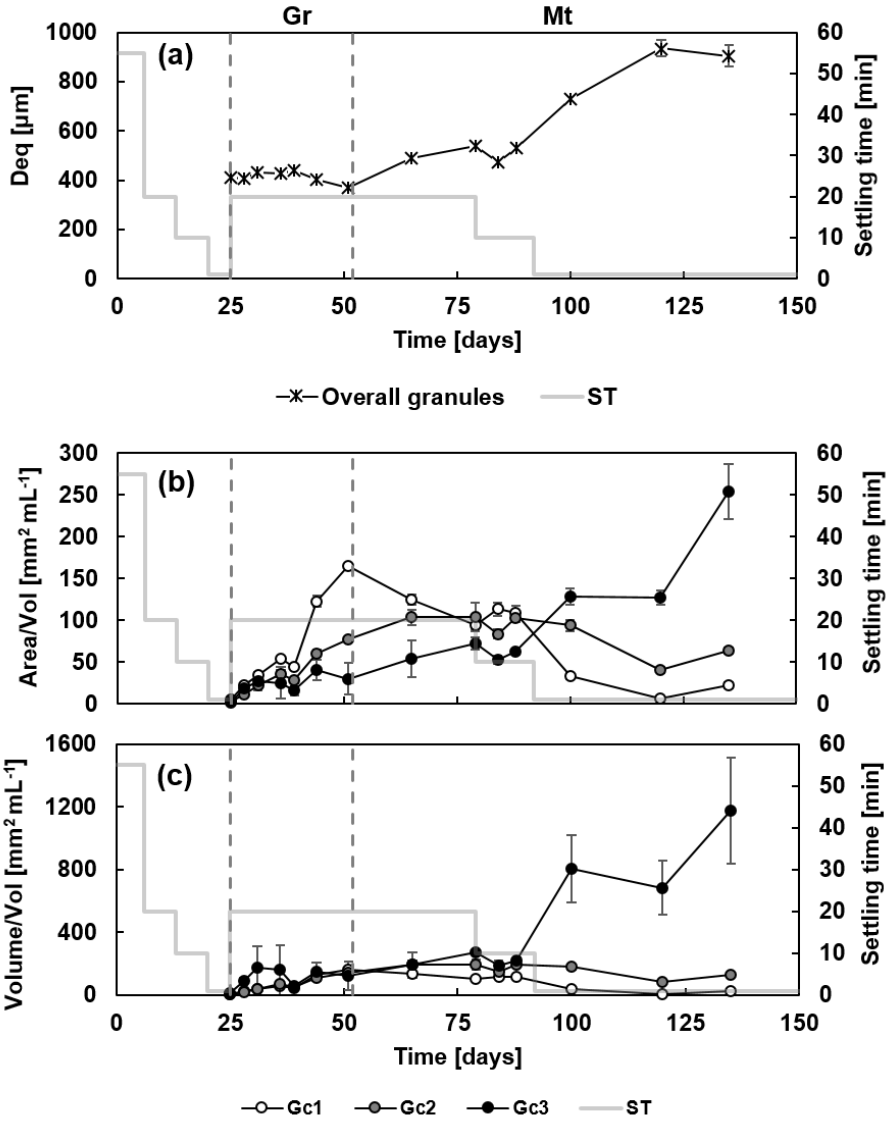


Figure 4.6 – Detailed evolution of the granules Deq (a), Area/Vol (b), and Volume/Vol (c) according to the size class: overall granules (–✳–), Gc1 (—○—), Gc2 (—●—), and Gc3 (—●—) during granulation (Gr) and maturation (Mt) periods in R1. The settling time (ST) (——) applied throughout the reactors' operation.

4.3.4. Effluent quality assessment

A PLS analysis was performed to predict the effluent quality during the granulation process in R1, using QIA parameters from the floccular and granular fractions. The correlation coefficients regression (R^2) for the training, validation, and overall set, as well as the RMSEP, RPD and observed values range for each studied variable is shown in Table 4.6. The R^2 for training and validation sets were above 0.92 and 0.89, respectively in all studied variable. The RMSEP were relatively low, representing 8.0%, 8.6%, 4.1%, and 5.3% of the values range observed for $P\text{-}PO_4^{3-}$, $N\text{-}NH_4^+$, $N\text{-}NO_2^-$, and $N\text{-}NO_3^-$, respectively. The RPD values for all PLS models were above the value 3 considered to be the threshold for a satisfactory prediction (Cozzolino et al., 2004).

Table 4.6 – PLS modelling results for each target variable

Target variable	R^2 training	R^2 validation	R^2 overall	RPD	RMSEP	Observed values mg L^{-1}	
					mg L^{-1}	Min.	Max.
$P\text{-}PO_4^{3-}$	0.92	0.92	0.90	3.46	1.60	0.326	20.2
$N\text{-}NH_4^+$	0.94	0.92	0.90	3.99	2.31	0	27
$N\text{-}NO_2^-$	0.99	0.89	0.96	9.42	0.71	0	17.4
$N\text{-}NO_3^-$	0.97	0.89	0.91	6.00	1.27	1.7	25.8

Min – minimum value measured; Max – maximum value measured

The regression analysis between the predicted and observed (measured) values revealed good prediction abilities for all studied parameters, with R^2 above 0.90 for all the PLS models (Figure 4.7). The regression between the predicted and observed $P\text{-}PO_4^{3-}$ and $N\text{-}NH_4^+$ exhibited the lowest overall R^2. The assessment of phosphate encompassed the use of variables, including flocs morphology, filamentous bacteria content, and granules distribution (Table 4.5). In contrast, the main variables for ammonium assessment included mostly granules content (4 out of the 7 variables). The regression between the predicted and observed $N\text{-}NO_2^-$ exhibited the highest R^2 of 0.96, meaning that 96% of the observed variation could be explained with QIA parameters. The assessment of nitrite and nitrate depended on a similar set of variables, comprised within the flocs morphology (5 out of the 7 variables), small and large granules (Table 4.5).

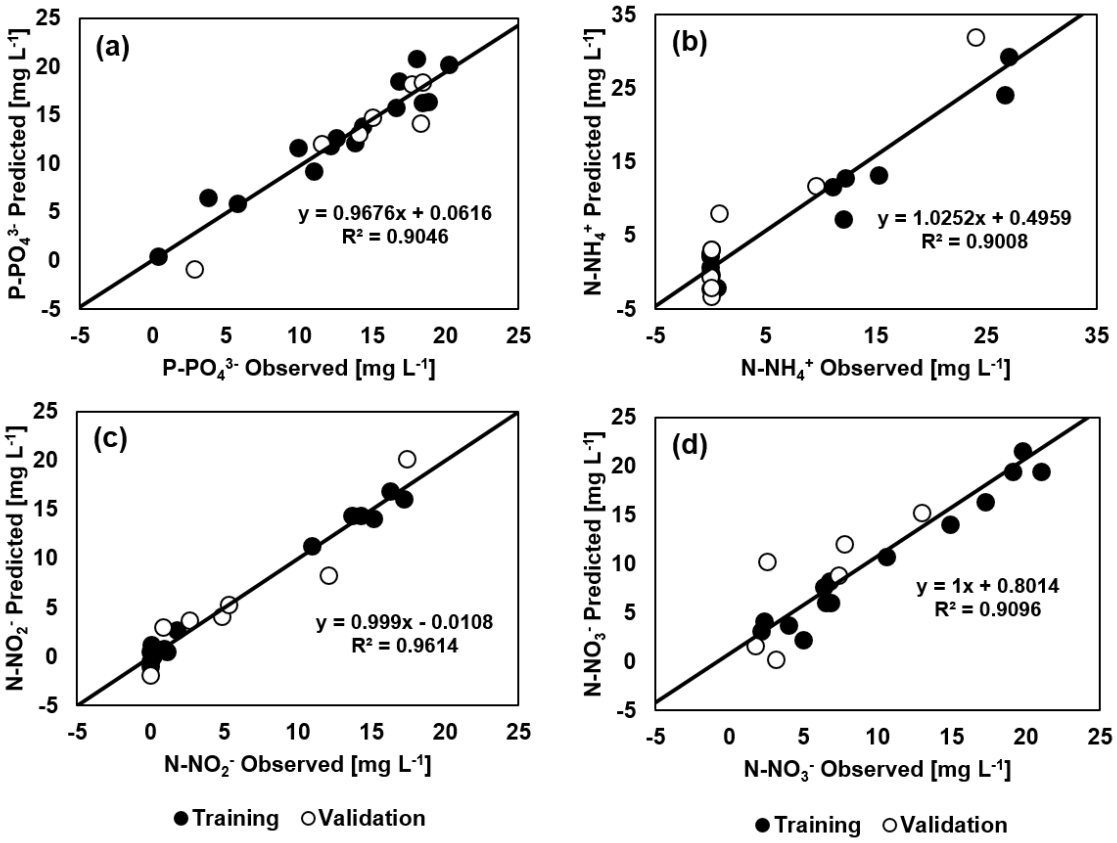


Figure 4.7 – Correlation between observed and predicted effluent concentration of: $P\text{-}PO_4^{3-}$ (a), $N\text{-}NH_4^+$ (b), $N\text{-}NO_2^-$ (c), and $N\text{-}NO_3^-$ (d). Training (●) and validation (○) data set.

4.4. DISCUSSION

The gradual decrease in the settling time is frequently used to accelerate the granulation process in SBR (Qin et al., 2004). However, this strategy, which selects for aggregates with high settling velocities, may lead to extensive sludge washout during reactors start-up periods, with consequences to biomass characteristics and treatment performances (Weissbrodt et al., 2012). This work assessed the effect of distinct ammonium concentrations during the granulation process on floccular and granular fractions morphology before and after washout conditions.

All reactors were exposed to decreasing settling time from 55 to 1 min during the first 25 days. Extensive sludge washout was only observed at the early stage of the operation and after the decrease in the settling time to 1 min, which selected aggregates with a minimum settling velocity of 5.3 m h^{-1}. Floccular sludge remained predominant under decreasing settling time, while filamentous bacteria were significantly reduced under 55 min of settling time (Figure 4.4a,c). During the first 25 days of operation, irregularly

shaped granules with distinct sizes were occasionally observed, yet their number was negligible for quantifications purposes. However, the number of granules increased after sludge washout and the increase in the settling time to 20 min (Figure 4.4b).

The sharper increase in $TA_{Granules}$/Vol evidenced a higher granulation rate in R1, most likely favoured by the higher COD/N ratio (i.e., COD/N 10), which stimulated sludge growth (Figure 4.4b). Previous work has shown that the COD/N ratio of 10 promoted rapid granulation and maintenance of granular stability (Shi and Liu, 2021). Additionally, the higher floccular sludge fraction (i.e., TA_{Flocs}/Vol) in R1 after sludge washout contributed to the faster granulation (Figure 4.1c). The lower biomass retention in R2 and R3 increased the F/M ratio to about 11 (in R2) and 4 (in R3) times higher than in R1, which impaired the increase in $TA_{Granules}$/Vol in these reactors (Figure 4.1c). While an F/M ratio of 1.1 $g_{COD}\ g_{VSS}^{-1}\ d^{-1}$ facilitate the rapid formation of large granules during reactor start-up (Li et al., 2011), the granulation process may not occur at a higher F/M ratio (Jungles et al., 2011). Although granulation rate increased in R2 and R3 after the decrease in F/M ratio, the lower granulation rate in the reactor with a COD/N ratio of 2 (i.e., R3) evidenced the negative impact of higher ammonium concentration added to the system. Luo et al. (2014) observed that the decrease in COD/N ratio resulted in SBR process instability, causing granules deterioration and decreased nitrification efficiency. Similarly, granular disintegration and the decrease in ammonium and phosphate removal efficiencies were observed in a recent work testing the stability of AGS under decreasing C/N from 20 to 2 (Wang et al., 2020). In contrast, successful granulation was achieved at COD/N ratios of 5 and 3, yet granules were significantly smaller than granules produced under higher ratios (i.e., 10 and 20) (Yang et al., 2005). In the present work, the granules initially formed in R2 and R3 after sludge washout were slowly overcome with the establishment of filamentous bacteria, which negatively impacted the settling ability (Figure 4.1d). Additionally, the reactors' bulk medium acquired viscous consistency, compromising image acquisition of the granular fraction due to the inability to manipulate the granules, which is essential for granules isolation and quantification (Costa et al., 2013).

Figueroa et al. (2015) studied the reason for filamentous growth in AGS systems. The source of filamentous bacteria was attributed to the initial inoculum when using synthetic wastewater, meaning that filamentous bacteria are not entirely washed out during the granulation process and could develop in favourable operating conditions (Figueroa et al., 2015). In our work, the TL/TA_{Flocs} showed that filaments were present in all reactors and increased under washout conditions (Figure 4.4c). However, filamentous bacteria outgrowth did not occur in R1, resulting in a successful granulation process and granules stability

overtime. Thus, the filamentous overgrowth in R2 and R3 might be related to the establishment of favourable conditions due to the poor ammonium removal efficiency. Prior to washout conditions, poor ammonium removal efficiencies were observed in R2 and R3, with the latter presenting the lowest efficiency (Figure 4.2b). Filamentous outgrowth occurred first in R3 from day 36, concomitant to the lowest granulation rate and ammonium removal efficiency. However, in R3, efficient ammonium removal at day 100 suggests the recovery of AOB activity, concomitant with the reduction in the viscosity of the medium and the formation of regular and compact shaped granules without filaments on the granules' surface. The $TA_{Granules}$/Vol in R3 were considerably lower than in R1 (Figure 4.4b), which support the results observed by Yang et al. (2005). Despite the successful formation of granules in R3, filamentous bacteria remained in the system in long filamentous macrostructures (Figure 4.5g).

Granulation failed in R2 with the observation of only a few granules surrounded by filaments embedded in a viscous medium and presenting poor nutrients removal efficiencies (Figure 4.5f). Bassin et al. (2019) observed the formation of unstable granules with filamentous outgrowth and pasty consistency during the granulation process from activated sludge. The granulation failure was attributed to the microbial community existing in the initial inoculum, which came from a sewage treatment plant designed for organic matter removal and with poor nitrifying capability (Bassin et al., 2019). Successful granulation with long term stability could be achieved after a sludge acclimation period under reduced washout conditions, which favoured granulation and suppressed filamentous bacteria (Bassin et al., 2019). In R1, the increase in ammonium removal efficiency was concomitant to the granulation period (i.e., days 25 to 51) (Figure 4.6). During this period, the size of granules remained stable (i.e., circa 400 µm), followed by a gradual increase during the maturation period induced by the transitions from Gc1 to Gc3 (Figure 4.6a,b). Complete nitrification was attained after day 100, suggesting the recovery of NOB activity, most likely associated with the sharp increase of the granular fraction volume of Gc3 (Figure 4.6c). At the same period, the phosphate removal efficiency improved from 35% to 98%, concomitant to the decrease in nitrite concentration, which has been shown to inhibit PAO activity (Bassin et al., 2011).

An apparent complex relation between the sludge morphological changes and nutrients removal occurs during a granulation process. Thus, the QIA data was further used to estimate the effluent concentration of phosphate, ammonium, nitrite, and nitrate throughout the formation of granules in R1. For this purpose, PLS models were used to correlate the QIA parameters from the floccular and granular fraction to the target variables (i.e., $P\text{-}PO_4^{3-}$, $N\text{-}NH_4^+$, $N\text{-}NO_2^-$, and $N\text{-}NO_3^-$). Good prediction (i.e., $R^2 > 0.9$) could be achieved for all target variables, using parameters from both floccular and granular fractions. Costa et

al., 2022 used QIA methodologies to estimate ammonium, nitrite and nitrate effluent concentration of an AGS systems during the treatment of industrial wastewater. Although these authors used mature AGS, the importance of both floccular and granular fractions for process monitoring was demonstrated (Costa et al., 2022).

Apart from estimating the target variable as a function of the X dataset, PLS predictions help identifying relevant parameters linked to the increase or decrease of each target variable. Concerning ammonium, nitrite and nitrate predictions, the highest VIP parameter were related to the granular faction (Table 4.5). While the most important parameter for nitrate predictions was related to the granular fraction, complete nitrification (i.e., high nitrate concentration in the effluent) was attained prior to the extensive sludge washout; thus, 5 out of the 7 parameters used to estimate nitrate concentration belonged to the floccular fraction, which prevailed at the early stage of the process. In contrast, the highest ammonium concentration in the effluent was observed after sludge washout. The recovery of AOB activity occurred during the granulation process, and consequently, 4 out of the 7 parameters used to estimate ammonium in the effluent belonged to the granular fraction. Phosphate concentration in the effluent increased at the early stage due to the gradual washout of the floccular fraction. Hence, it may be assumed that the gradual loss of flocs and their morphological changes correlated with de increase in phosphate effluent concentration, thus the floccular fraction assuming higher importance (i.e., the highest VIP). Then, the recovery of PAO activity increased during granules maturation with the transition from Gc1 to Gc3; thus, the parameters belonging to the granular faction assumed higher importance in the prediction model (Table 4.5).

Overall, PLS models allowed to identify which QIA parameter provided the most crucial information regarding each target variable, highlighting the importance of QIA data on the process performance during granulation. However, care should be taken when constructing a generalized PLS model to be applied to all granulation processes due to the complexity and diversity of AGS systems. Thus, the PLS flexibility in determining the most significant parameters in individual system can be considered an advantage (Silva et al., 2022).

4.5. CONCLUSIONS

This work evaluated the sludge's morphological changes and the biological nutrient removal performance during the granulation from activated sludge in SBR operated under different COD/N ratios and decreasing settling time. A comprehensive relationship between biological nutrient removal and sludge morphology could be established. AGS was successfully achieved in SBR operated at COD/N ratios of 10 and 2. While the nutrient removal efficiencies were negatively affected by the sludge washout, the COD/N ratio impacted the granulation rate. In SBR operated at a COD/N ratio of 10, the AOB activity recovered rapidly during granulation, whereas the NOB and PAO activity was only observed subsequently to the prevalence of larger granules. Poor ammonium removal efficiencies during granulation favoured the development of viscous bulking and filamentous bacteria in the reactors operated at a lower COD/N ratio. The increase in AOB activity led to compact and regular granules, which were concomitant to the decrease in viscosity but not for filamentous bacteria. The QIA data was successfully used to construct PLS models to estimate the effluent quality in SBR operated at a COD/N of 10 during the granulation process under extensive washout conditions. The good predictions achieved for all target variables with parameters belonging to the floccular and granular fractions indicated the potential of QIA to monitor and control the granulation process.

4.6. REFERENCES

Adav, S.S., Lee, D.J., Show, K.Y., Tay, J.H., 2008. Aerobic granular sludge: Recent advances. Biotechnol. Adv. 26, 411–423. https://doi.org/10.1016/j.biotechadv.2008.05.002

Amaral, A.L.P., 2003. Image analysis in biotechnological processes: applications to wastewater treatment. PhD thesis, University of Minho. http://hdl.handle.net/1822/4506.

APHA, 2005. Standard Methods for the Examination of Water & Wastewater 21st Edition, American Public Health Association, American Water Works Association, Water Environment Federation.

Bassin, J.P., Pronk, M., Muyzer, G., Kleerebezem, R., Dezotti, M., van Loosdrecht, M.C.M., 2011. Effect of elevated salt concentrations on the aerobic granular sludge process: Linking microbial activity with microbial community structure. Appl. Environ. Microbiol. 77, 7942–7953. https://doi.org/10.1128/AEM.05016-11

Bassin, J.P., Tavares, D.C., Borges, R.C., Dezotti, M., 2019. Development of aerobic granular sludge under tropical climate conditions: The key role of inoculum adaptation under reduced sludge washout for stable granulation. J. Environ. Manage. 230, 168–182. https://doi.org/10.1016/j.jenvman.2018.09.072

Bengtsson, S., de Blois, M., Wilén, B., Gustavsson, D., 2019. A comparison of aerobic granular sludge with conventional and compact biological treatment technologies. Environ. Technol. 40, 2769–2778. https://doi.org/10.1080/09593330.2018.1452985

Beun, J.J., Van Loosdrecht, M.C.M., Heijnen, J.J., 2000. Aerobic granulation. Water Sci. Technol. 41, 41–48. https://doi.org/10.2166/wst.2000.0423

Cai, F., Lei, L., Li, Y., Chen, Y., 2021. A review of aerobic granular sludge (AGS) treating recalcitrant wastewater: Refractory organics removal mechanism, application and prospect. Sci. Total Environ. 782, 146852. https://doi.org/10.1016/j.scitotenv.2021.146852

Costa, J.C., Mesquita, D.P., Amaral, A.L., Alves, M.M., Ferreira, E.C., 2013. Quantitative image analysis for the characterization of microbial aggregates in biological wastewater treatment: a review. Environ. Sci. Pollut. Res. 20, 5887–5912. https://doi.org/10.1007/s11356-013-1824-5

Costa, J.G., Paulo, A.M.S., Amorim, C.L., Amaral, A.L., Castro, P.M.L., Ferreira, E.C., Mesquita, D.P., 2022. Quantitative image analysis as a robust tool to assess effluent quality from an aerobic granular sludge system treating industrial wastewater. Chemosphere 291. https://doi.org/10.1016/j.chemosphere.2021.132773

Cozzolino, D., Kwiatkowski, M.J., Parker, M., Cynkar, W.U., Dambergs, R.G., Gishen, M., Herderich, M.J., 2004. Prediction of phenolic compounds in red wine fermentations by visible and near infrared spectroscopy. Anal. Chim. Acta 513, 73–80. https://doi.org/10.1016/j.aca.2003.08.066

de Kreuk, M.K., Heijnen, J.J., Van Loosdrecht, M.C.M., 2005. Simultaneous COD, nitrogen, and phosphate removal by aerobic granular sludge. Biotechnol. Bioeng. 90, 761–769. https://doi.org/10.1002/bit.20470

de Kreuk, M.K., Kishida, N., van Loosdrecht, M.C.M., 2007. Aerobic granular sludge - State of the art. Water Sci. Technol. 55, 75–81. https://doi.org/10.2166/wst.2007.244

Figueroa, M., Val Del Río, A., Campos, J.L., Méndez, R., Mosquera-Corral, A., 2015. Filamentous bacteria existence in aerobic granular reactors. Bioprocess Biosyst. Eng. 38, 841–851. https://doi.org/10.1007/s00449-014-1327-x

Franca, R.D.G., Pinheiro, H.M., van Loosdrecht, M.C.M., Lourenço, N.D., 2018. Stability of aerobic granules during long-term bioreactor operation. Biotechnol. Adv. 36, 228–246. https://doi.org/10.1016/j.biotechadv.2017.11.005

Jungles, M.K., Figueroa, M., Morales, N., Val del Río, Á., da Costa, R.H.R., Campos, J.L., Mosquera-Corral, A., Méndez, R., 2011. Start up of a pilot scale aerobic granular reactor for organic matter and nitrogen removal. J. Chem. Technol. Biotechnol. 86, 763–768. https://doi.org/10.1002/jctb.2589

Leal, C., del Río, A.V., Mesquita, D.P., Amaral, A.L., Ferreira, E.C., 2022. Prediction of sludge settleability, density and suspended solids of aerobic granular sludge in the presence of pharmaceutically active compounds by quantitative image analysis and chemometric tools. J. Environ. Chem. Eng. 10. https://doi.org/10.1016/j.jece.2022.107136

Leal, C., Val del Río, A., Ferreira, E.C., Mesquita, D., Amaral, A.L., 2021. Validation of a quantitative image analysis methodology for the assessment of the morphology and structure of aerobic granular sludge in the presence of pharmaceutically active compounds. Environ. Technol. Innov. 23, 101639. https://doi.org/10.1016/j.eti.2021.101639

Li, A.J., Li, X.Y., Yu, H.Q., 2011. Effect of the food-to-microorganism (F/M) ratio on the formation and size of aerobic sludge granules. Process Biochem. 46, 2269–2276. https://doi.org/10.1016/j.procbio.2011.09.007

Lin, H., Ma, R., Hu, Y., Lin, J., Sun, S., Jiang, J., Li, T., Liao, Q., Luo, J., 2020. Reviewing bottlenecks in aerobic granular sludge technology : Slow granulation and low granular stability. Environ. Pollut. 263, 114638. https://doi.org/10.1016/j.envpol.2020.114638

Liu, Y., Tay, J.H., 2004. State of the art of biogranulation technology for wastewater treatment. Biotechnol. Adv.

22, 533–563. https://doi.org/10.1016/j.biotechadv.2004.05.001

Luo, J., Hao, T., Wei, L., Mackey, H.R., Lin, Z., Chen, G.H., 2014. Impact of influent COD/N ratio on disintegration of aerobic granular sludge. Water Res. 62, 127–135. https://doi.org/10.1016/j.watres.2014.05.037

Pronk, M., de Kreuk, M.K., de Bruin, B., Kamminga, P., Kleerebezem, R., van Loosdrecht, M.C.M., 2015. Full scale performance of the aerobic granular sludge process for sewage treatment. Water Res. 84, 207–217. https://doi.org/10.1016/j.watres.2015.07.011

Qin, L., Liu, Y., Tay, J.H., 2004. Effect of settling time on aerobic granulation in sequencing batch reactor. Biochem. Eng. J. 21, 47–52. https://doi.org/10.1016/j.bej.2004.03.005

Shi, Y., Liu, Y., 2021. Evolution of extracellular polymeric substances (EPS) in aerobic sludge granulation: Composition, adherence and viscoelastic properties. Chemosphere 262, 128033. https://doi.org/10.1016/j.chemosphere.2020.128033

Silva, S.A., Val del Río, A., Amaral, A.L., Ferreira, E.C., Alves, M.M., Mesquita, D.P., 2022. Monitoring morphological changes from activated sludge to aerobic granular sludge under distinct organic loading rates and increasing minimal imposed sludge settling velocities through quantitative image analysis. Chemosphere 286, 131637. https://doi.org/10.1016/j.chemosphere.2021.131637

Wang, L., Yu, X., Xiong, W., Li, P., Wang, S., Fan, A., Su, H., 2020. Enhancing robustness of aerobic granule sludge under low C/N ratios with addition of kitchen wastewater. J. Environ. Manage. 265. https://doi.org/10.1016/j.jenvman.2020.110503

Weissbrodt, D.G., Lochmatter, S., Ebrahimi, S., Rossi, P., Maillard, J., Holliger, C., 2012. Bacterial selection during the formation of early-stage aerobic granules in wastewater treatment systems operated under wash-out dynamics. Front. Microbiol. 3, 1–22. https://doi.org/10.3389/fmicb.2012.00332

Wu, L., Peng, C., Peng, Y., Li, L., Wang, S., Ma, Y., 2012. Effect of wastewater COD/N ratio on aerobic nitrifying sludge granulation and microbial population shift. J. Environ. Sci. 24, 234–241. https://doi.org/10.1016/S1001-0742(11)60719-5

Yang, S.-F., Tay, J.-H., Liu, Y., 2005. Effect of Substrate Nitrogen/Chemical Oxygen Demand Ratio on the Formation of Aerobic Granules. J. Environ. Eng. 131, 86–92. https://doi.org/10.1061/(asce)0733-9372(2005)131:1(86)

Zhang, Z., Yu, Z., Dong, J., Wang, Z., Ma, K., Xu, X., Alvarezc, P.J.J., Zhu, L., 2018. Stability of aerobic granular sludge under condition of low influent C/N ratio: Correlation of sludge property and functional microorganism. Bioresour. Technol. 270, 391–399. https://doi.org/10.1016/j.biortech.2018.09.045

CHAPTER 5

Improving nutrient removal efficiencies of aerobic granular sludge by bioaugmentation with bioactive granules: Accessing the impact on the granules' morphology through quantitative image analysis

Two sequencing batch reactors (SBR) with morphological distinct aerobic granular sludge (AGS) presenting nutrient removal deficiencies were bioaugmented with bioactive granules exhibiting high nutrient removal efficiencies without altering the reactors operating conditions. Complete nitrification was successfully achieved and sustained throughout the entire operation after bioaugmentation. In the SBR inoculated with larger granules (i.e., R1), phosphate removal efficiency reached 60% after bioaugmentation but decreased to around 10% at the end of the operation. Quantitative image analysis (QIA) data revealed the fragmentation and washout of the bioactive granules. In the SBR with similar granules size to the bioactive granules (i.e., R2), phosphate was efficiently removed up to 10 mg L^{-1}. However, subsequent phosphate concentration increases in the influent led to a transient reactor performance instability, concomitant with the occurrence of protruding filaments and unstable granular structures. Bioaugmentation positively affected sludge settling ability and sludge concentration compared with the non-bioaugmented reactor (i.e., R3). After 63 days, AGS in the non-bioaugmented reactor could not perform efficient nutrient removal. The result evidenced the possibility of using bioactive granules to augment AGS in SBRs exhibiting deficiencies in nutrient removal. However, morphological differences between bioactive granules and innate AGS must be carefully considered to minimize the possibility of granules fragmentation and washout without changing reactor operating conditions.

5.1. INTRODUCTION

Wastewater treatment using aerobic granular sludge (AGS) technology may replace conventional activated sludge (CAS) systems due to higher energy efficiencies and cost-effectiveness of the AGS process (Adav et al., 2008; Pronk et al., 2015). AGS technology relies on the growth of a self-immobilizing microbial community to form granules, usually achieved through selective environmental and operational pressure (Adav et al., 2008; Rollemberg et al., 2018). Sequencing batch reactors (SBR) are typically used to produce AGS, resulting in the selection of compact and spherical-shaped aggregates with high settling velocities (Wilén et al., 2018). Furthermore, AGS has a layered structure with anoxic/aerobic zones, allowing multiple biological processes to co-occur in a single reactor (Han et al., 2022). Thus, SBRs are typically operated with alternating anaerobic/aerobic periods that favour slow-growing microorganisms, namely nitrifying bacteria, i.e., ammonium-oxidizing bacteria (AOB) and nitrite-oxidizing bacteria (NOB), and polyphosphate-accumulating organisms (PAO), which are beneficial for granulation and granule stability (de Kreuk et al., 2005; Rollemberg et al., 2018).

Limited nutrient removal efficiencies are still reported during the granulation process, and even after, granules maturation is achieved (Pishgar et al., 2019; Rollemberg et al., 2019a, 2019b). Several work reported a significant decrease in nutrient removal efficiency after toxic events in AGS systems (He et al., 2021; Jiang et al., 2020; Wei et al., 2015). In some cases, removal efficiency could not be restored even after removing the toxic compound (Ely et al., 2022; He et al., 2021; Oliveira et al., 2021). Disturbance periods may lead to alteration in the AGS microbial composition due to the washout of bacteria unable to adapt to toxic events (Amorim et al., 2018). The granules' morphology is also affected by the presence of toxic compounds, resulting in granules fragmentation, decreasing settling properties, and sludge washout (Amorim et al., 2016; Muñoz-Palazon et al., 2019; Tomar et al., 2022).

Bioaugmentation, i.e., the addition of specialized microbial strain or consortia of microorganisms (El Fantroussi and Agathos, 2005), can solve practical problems in biological wastewater treatment systems, namely by accelerating the system start-up, treatment recovery, and increasing removal capacities (Winkler et al., 2018). Successful bioaugmentation can only be achieved if the added microorganisms remain active in the system (Martín-Hernández et al., 2012). Consequently, bioaugmentation failures are often reported, mainly due to the inability to maintain adequate inoculum size within the reactors (Raper et al., 2018). AGS systems are typically operated with short settling time to select aggregates with high settling velocities; thus, effective bioaugmentation in AGS systems may require microbial immobilization (Oliveira et al., 2021) or adjusting operating conditions (Duque et al., 2011), which may be impractical

in full-scale applications (Oliveira et al., 2021). Microbial immobilization is regarded as an efficient method to improve the survival and activity of bioaugmented microorganisms (Herrero and Stuckey, 2015); however, the cost-effectiveness of bioaugmentation is still controversial for practical application (Ma et al., 2022). The addition of bioactive granules from surplus AGS systems removes the need for microbial immobilization and may be an environmentally friendly and cost-effective method to recover nutrient removal efficiencies in AGS systems after toxic events. Furthermore, the AGS morphology and stability could also be improved by adding bioactive granules. Adding crushed granules to a SBR with floccular sludge accelerated the granulation process while maintaining efficient ammonium removal capacity (Pijuan et al., 2011). However, efficient phosphate removal was not preserved, and operating conditions were adjusted to avoid sludge washout.

This work aimed to investigate the effectiveness of using bioactive granules with high nutrient removal capabilities as bioaugmenting microbial consortia to recover two SBR containing AGS with distinct morphologies and exhibiting nitrogen and phosphorus removal deficiencies. The impact of bioaugmentation on the morphology and distribution of the granules was investigated using quantitative image analysis (QIA).

5.2. MATERIAL AND METHODS

5.2.1. Reactors setup and operation

Three lab-scale SBR (R1, R2, and R3) with dimensions of 18.5 cm height and 9 cm diameter (H/D = 2) and 1L working volume were operated in cycles of 6 h as follows: 120 min anaerobic feed, 234 min aeration, 1 min sludge settling, and 5 min effluent discharge. This configuration allowed to maintain aggregates with a minimal imposed sludge settling velocity of 5.3 m h^{-1}. All reactors were operated at room temperature (22.9 ± 1.4 °C) with a hydraulic retention time of 12 h and an exchange ratio of 50%. Oxygen was supplied at the bottom during aeration to ensure good mixing and saturation with dissolved oxygen. The reactors were fed with a synthetic medium containing sodium acetate as a carbon source. The average concentrations of COD, ammonium, and phosphate applied to the reactors are described in Table 5.1. The feed was prepared with tap water supplemented with $MgSO_4.7H_2O$ (0.09 g L^{-1}), $CaCl_2.2H_2O$ (0.03 g L^{-1}), sodium bicarbonate (0.6 g L^{-1}) and a concentrated trace solution (0.75 mL L^{-1}) consisting of: $FeCl_3.6H_2O$ (6 g L^{-1}); H_3BO_3 (0.6 g L^{-1}); $CuSO_4.5H_2O$ (0.12 g L^{-1}); KI (0.72 g L^{-1}); $MnCl_2.4H_2O$ (0.48 g L^{-1}); $Na_2MoO_2.2H_2O$ (0.24 g L^{-1}); $ZnSO_4.7H_2O$ (0.48 g L^{-1}); $CoCl_2.6H_2O$ (0.6 g L^{-1}), and EDTA (40 g L^{-1}).

Table 5.1 – Acetate, ammonium and phosphate concentrations in the feed for each reactor

Components	Unit	R1	R2	R3
Acetate (as COD)	mg L^{-1}	476 ± 44	512 ± 33	505 ± 35
N-NH_4^+	mg L^{-1}	47 ± 2	49 ± 2	48 ± 2
P-PO_4^{3-}	mg L^{-1}	19.4 ± 0.5 (63)[a]	4.7 ± 0.2 (28)[a] 9.7 ± 0.1 (7) 14.4 ± 0.4 (11) 19.5 ± 0.3 (17)	4.7 ± 0.2 (63)[a]

[a] Mean ± standard deviation (number of days submitted to P-PO_4^{3-} concentration)

5.2.2. Reactors inoculum and bioactive granules sludge source

Two morphologically distinct AGS were used to inoculate three SBRs; R1 was inoculated with AGS from a 5L lab-scale SBR operated under high-strength synthetic wastewater as described in Leal et al. (2022). R2 and R3 were inoculated with the same AGS produced under high ammonium concentration (i.e., 230 ± 20 mg L^{-1}) and phosphate (i.e., 20 ± 2 mg L^{-1}) as described in Chapter 4. Surplus AGS collected from a lab-scale SBR treating synthetic wastewater, as described in Chapter 4, was used as bioactive granules for bioaugmentation. These granules were cultivated for 244 days with 500 mg L^{-1} (as COD) of acetate, 50 mg L^{-1} of ammonium, and 20 mg L^{-1} of phosphate, presenting removal efficiencies of 96 ± 1%, 99 ± 1%, and 95 ± 3%, respectively. The removal efficiencies were obtained as an average of 5 analyses for 13 days before collecting granules for bioaugmentation.

5.2.3. Bioaugmentation

Images of the bioactive granules and the AGS used to inoculate R1, R2, and R3 are shown in Figure 5.1. Before bioaugmentation, the bioactive granules and the AGS in R1, R2, and R3 were characterized in relevant morphological characteristics and granules size distribution using QIA, as described in Table 5.2. Details on QIA methodology are described in section 5.2.5. Bioaugmentation experiments were conducted in R1 and R2, and after ten days, both reactors were bioaugmented with bioactive granules concentration of 1.4 g L^{-1} and 0.7 g L^{-1}, respectively, corresponding to an MLVSS content of 23% for each reactor. No bioaugmentation was performed in R3.

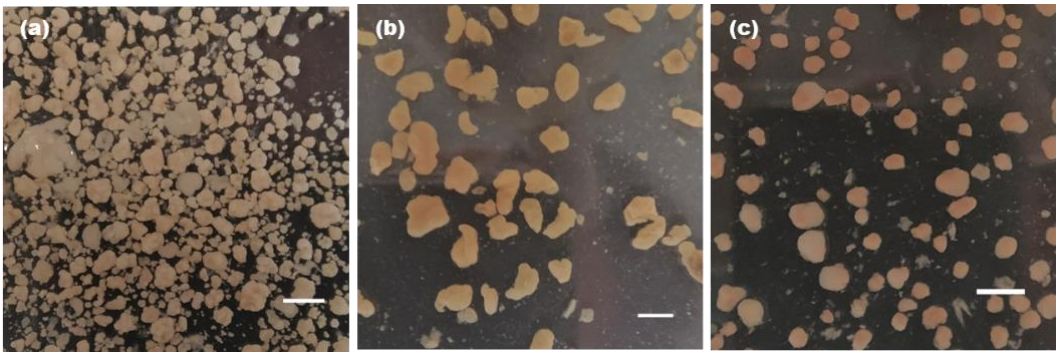


Figure 5.1 – Images of the granules morphology. Bioactive granules (a). AGS used to inoculate: R1 (b), R2 and R3 (c). The scale bar equal to 5 mm.

Table 5.2 – Characterization of bioactive granules and innate granules present in R1, R2 and R3, before bioaugmentation

		Parameter			
	Size class	**Number (%)**	**Area (%)**	**Volume (%)**	**Deq (μm)**
Bioactive granules[1]	Deq < 1000μm	67 ± 3	19 ± 4	7 ± 2	573 ± 8
	Deq ≥ 1000μm	33 ± 3	81 ± 4	93 ± 2	1664 ± 146
	Overall[3]	100	100	100	914 ± 41
R1[2]	Deq < 1000μm	33 ± 4	1 ± 0	0 ± 0	456 ± 20
	Deq ≥ 1000μm	67 ± 4	99 ± 0	100 ± 0	3484 ± 258
	Overall[3]	100	100	100	2483 ± 310
R2[2]	Deq < 1000μm	88 ± 3	36 ± 5	13 ± 2	518 ± 13
	Deq ≥ 1000μm	12 ± 3	64 ± 5	87 ± 2	1842 ± 69
	Overall[3]	100	100	100	656 ± 31
R3[2]	Deq < 1000μm	91 ± 2	41 ± 14	16 ± 9	487 ± 8
	Deq ≥ 1000μm	9 ± 2	59 ± 14	84 ± 9	1818 ± 317
	Overall[3]	100	100	100	590 ±43

(1) Bioactive granules were characterized before bioaugmentation; (2) AGS on R1, R2 and R3 was characterized on day 10; (3) Overall refers to the characterization of all granules.

5.2.4. Analytical methods

Volatile suspended solids in the reactor mixed liquor (MLVSS) were determined according to standard methods (APHA, 2005) . Sludge settling ability was monitored by determining the sludge volume index after 5 minutes (SVI_5) and 30 minutes (SVI_{30}) according to standard methods (APHA, 2005). In all reactors, samples of the influent and effluent were filtered with a syringe membrane filter (0.45 µm pore size). The concentrations of chemical oxygen demand (COD), ammonium nitrogen ($N\text{-}NH_4^+$), nitrite ($N\text{-}NO_2^-$), nitrate ($N\text{-}NO_3$), and phosphate ($P\text{-}PO_4^{3-}$) were determined spectrophotometrically using a cuvette test kit (Hach-Lange GmbH, Dusseldorf, Germany) and a DR2800™ spectrophotometer (Hach-Lange, GmbH). The amount of COD available for the aeration phase was quantified at the transition between anaerobic feeding and the aeration phase. The total inorganic nitrogen (TIN) concentration in the effluent was assumed as the sum of ammonium, nitrite and nitrate concentration (Long et al., 2014).

5.2.5. Quantitative image analysis

5.2.5.1. Sludge sampling

To characterise the granules, a sample volume of 10 mL was taken at the beginning of the aeration phase when the sludge was completely mixed. The samples were washed with phosphate buffered saline (PBS) and the supernatant was discarded after the granules had settled. The granules were resuspended with a mixture of 1:1 PBS and absolute ethanol (≥ 99.8%) and stored (-20 °C) until analysis. Prior to image acquisition, the granules were washed with distilled water to remove the PBS-ethanol mixture and resuspended to their original volume.

5.2.5.2. Image acquisition, processing, and analysis

Images of granules were taken using an Olympus SZ-40 stereomicroscope (Olympus, Shinjuku, Japan), at 15× magnification. A fixed volume was placed in a Petri dish, and all granules present in that particular volume were captured. This procedure was performed in triplicate. The number of granules analysed per sample averaged 469 ± 215, 381 ± 89 and 422 ± 164, for R1, R2 and R3, respectively. Images were acquired with a CCD AVC D5CE Sony video camera (Sony, Tokyo, Japan) and Image-Pro Plus software (Media Cybernetics, MD, USA), in 768 × 576 pixels and 8-bit format. Image processing, including pre-treatment, segmentation, and debris removal steps, was performed as described in Amaral (2003). Binary

images were created with the detected aggregate, which enabled the subsequent determination of the morphological parameters.

Only aggregates with an equivalent diameter (Deq) ≥ 200 μm were considered granules, determined by the Area parameter as shown in Chapter 3. Granules distribution was accessed by dividing granules into two size classes based on their equivalent diameter, namely Deq < 1000 μm and Deq ≥ 1000 μm. The percentage of granules for each size class was determined by the ratio between the sum of the number of granules within that size class and the total number of quantified granules:

$$\text{Number} = \frac{\sum_{i=1}^{n} N}{TN} \times 100$$

Where, *N* is the number of each *i* granule belonging to *n* size class, and *TN* is the total number of granules present in the sample. The percentage of area for each size class was determined by the ratio between the sum of the area of granules within that size class and the total area of granules (TA):

$$\%\text{Area} = \frac{\sum_{i=1}^{n} A}{TA} \times 100$$

where, *A* is the area of each *i* granule belonging to *n* size class, and *TA* is the total area of granules present in the sample. TA, expressed in mm^2 mL^{-1}, was calculate as shown in Chapter 4. The total volume of granules per unit of volume, expressed in mm^3 mL^{-1}, was calculated using the equation:

$$TV_{Granules}/Vol = \frac{\sum V}{Vol}$$

where V is the volume of each *i* granule (mm^3) and Vol is the volume of sample analysed (mL). Granules apparent density (MLVSS/TV) was calculated by dividing the MLVSS concentration by the $TV_{Granules}$. The convexity and solidity morphological parameter depends on the creation of the convex hull, i.e. the smaller convex polygon enclosing the granules and determined by the vectorization of the granules contour (Amaral, 2003). The granules convexity and solidity were determined as shown in Chapter 3. More information on the calculation of these parameters can be found in Amaral (2003). Image processing and analysis routines were performed in Matlab™ 8.5 (the MathWorks Inc, USA).

5.3. RESULTS

5.3.1. The effect of bioaugmentation on nutrient removal performance

The effluent concentrations of ammonium, nitrite, and nitrate are shown in Figure 5.2. In all reactors and before bioaugmentation, ammonium was primarily oxidized to nitrite, which was present in the effluent in higher concentrations than nitrate, indicating that the nitrification process was not complete. After adding the bioactive granules in R1 and R2 on day 10, nitrite concentration in the effluent decreased until day 21, remaining undetected until the end of the operation, while nitrate concentration increased (Figure 5.2a,b). Partial nitrification remained unaltered in R3, although a decreasing trend in nitrite concentration was observed during the operation (Figure 5.2c). Generally, TIN concentrations in the effluent were lower in R2 and R3, evidencing higher nitrogen removal via denitrification. TIN removal efficiency in R2 and R3 reached 70%, whereas only 45% was observed in R1.

Phosphate concentrations in the influent and effluent are shown in Figure 5.3. In the first ten days, influent and effluent phosphate concentrations were similar (i.e., ≈ 20 mg L^{-1}) in R1, revealing a low phosphate uptake capacity of the initial AGS (Figure 5.3a). Interestingly, the effluent concentration decreased drastically from 17 mg L^{-1} to 8 mg L^{-1} immediately after adding the bioactive granules (Figure 5.3a). However, the improved phosphate uptake capacity was not permanent since the effluent concentration increased to similar values as before bioaugmentation (Figure 5.3a). R2 and R3 were initially fed with a phosphate concentration of 5 mg L^{-1}, which was lower than that used in the granulation process (see chapter 4). Nevertheless, no increase in the capacity of phosphate uptake was observed in the first ten days in either reactor (Figure 5.3b,c).

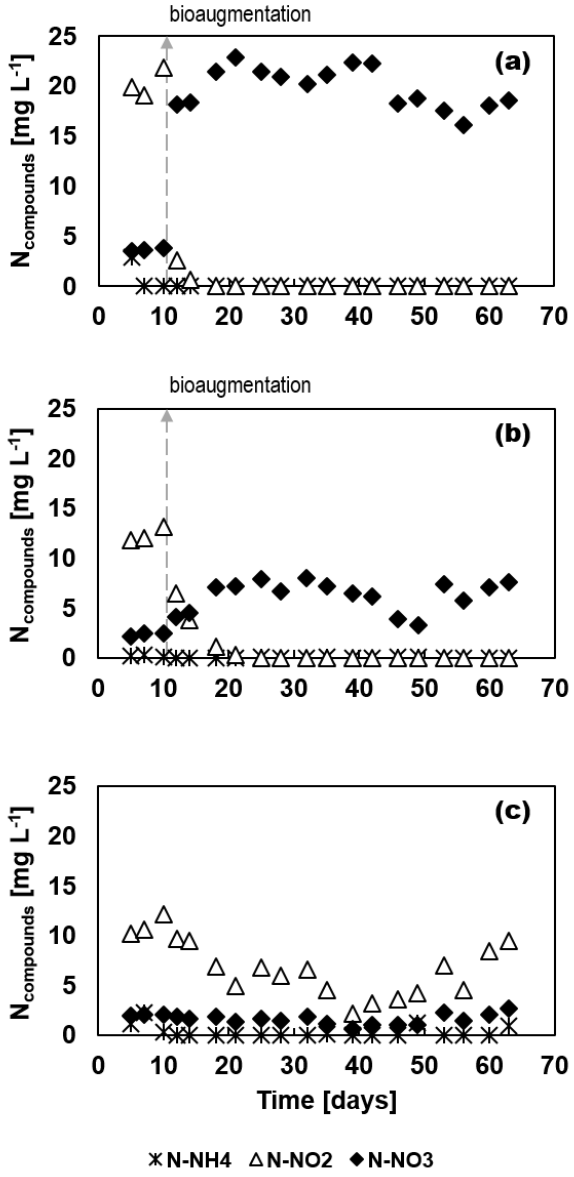


Figure 5.2 – Effluent ammonium (✱), nitrite (△) and nitrate (◆) concentration profiles in: R1 (a), R2 (b) and R3 (c). Dashed arrow mark bioaugmentation day.

After bioaugmentation in R2, effluent concentration gradually decreased and remained below 0.15 mg L^{-1} until day 28 (Figure 5.3b). From this day onwards, phosphate concentration in the feed was gradually increased from 5 to 20 mg L^{-1}. Unstable phosphate uptake was observed at 15 mg L^{-1} and 20 mg L^{-1}, resulting in an increase in the effluent concentration up to 24 mg L^{-1}. Nevertheless, phosphate concentration in the effluent stabilized at around 10 mg L^{-1}, corresponding to a removal efficiency of 50%. In R3, phosphate uptake was relatively low, and both influent and effluent phosphate concentrations remained stable during the reactor operation (Figure 5.3c).

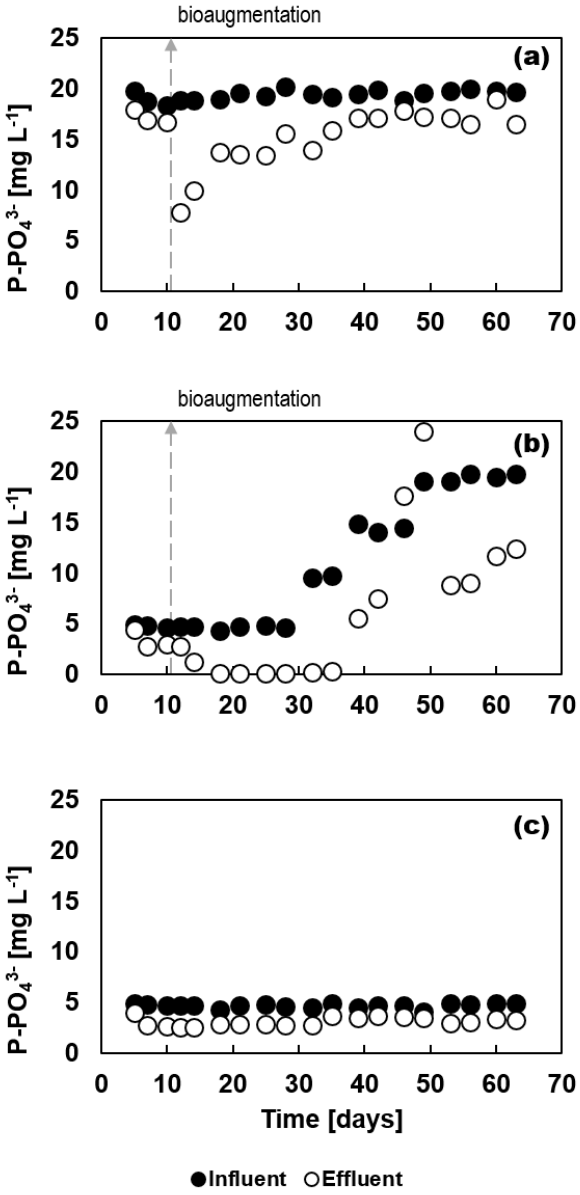


Figure 5.3 – Influent (●) and effluent (○) phosphate concentration profiles in: R1 (a), R2 (b) and R3(c). Dashed arrow mark bioaugmentation day.

High COD removal efficiency was observed in all reactors (Table 5.3). In R1, most of the COD was consumed during the anaerobic feeding phase, while in R2 and R3, approximately 230 mg L^{-1} was still available for the aerobic phase. The effluent COD concentration was slightly lower in R1 and R2 than in R3, possibly due to the addition of the bioactive granules.

Table 5.3 – COD concentrations and overall removal efficiency in each reactor

Substrate	R1	R2	R3
Aeration (mg L^{-1})	50 ± 35	229 ± 39	226 ± 33
Effluent (mg L^{-1})	20 ± 12	21 ± 12	31 ± 9
Removal (%)	96 ± 3	96 ± 2	94 ± 2

5.3.2. The effect of bioaugmentation in sludge concentration and settling properties

R2 and R3 were inoculated with the same AGS but differed from R1, resulting in different MLVSS concentrations at the beginning of the SBRs operation (Figure 5.4a,c,e). After bioaugmentation, MLVSS gradually increased and reached 12 g L^{-1} and 10 g L^{-1} in R1 and R2, respectively (Figure 5.4a,c). On the other hand, the MLVSS concentration in the non-bioaugmented reactor (i.e., R3) remained quite stable and did not exceed 6 g L^{-1}, which was 1.5 times lower than the sludge concentration achieved in R2 (Figure 5.4e). A decrease in the MLVSS/MLSS ratio was observed in both bioaugmented reactors but was more pronounced in R2, decreasing from 0.95 to 0.75, while it did not decrease below 0.85 in R1 (Figure 5.4a,c).

The development of the AGS settling properties was evaluated using SVI_5 and SVI_{30} measurements (Figure 5.4b,d,f). In R1, AGS exhibited excellent settling properties prior to bioaugmentation, with SVI_5 and SVI_{30} values below 45 mL g^{-1} and an SVI_{30}/SVI_5 ratio equal to unit. Both SVI_5 and SVI_{30} remained quite stable (i.e. 22 ± 3 mL g^{-1}) following bioaugmentation (Figure 5.4b). In contrast, increasing SVI_5 and SVI_{30} values were observed in R2 and R3 during the first ten days, attributed to the unstable AGS after inoculation (Figure 5.4d,f). However, in R2, both SVI_5 and SVI_{30} gradually decreased from 82 to 35 mL g^{-1} after adding the bioactive granules (Figure 5.4d). A transient deterioration of the settling ability was observed in R2 from day 35, and although SVI_5 and SVI_{30} resumed decreasing, the SVI_{30}/SVI_5 ratio was still lower than the unit (Figure 5.4d). In contrast, the settling ability of AGS continued to deteriorate in R3, with SVI_5 and SVI_{30} exceeding 100 mL g^{-1} on day 14, followed by a decreasing trend to 55 mL g^{-1} and 46 mL g^{-1}, respectively, at the end of the SBR operation (Figure 5.4f). Although settling ability improved over time in R3, SVI_{30}/SVI_5 deteriorated from day 43 onwards.

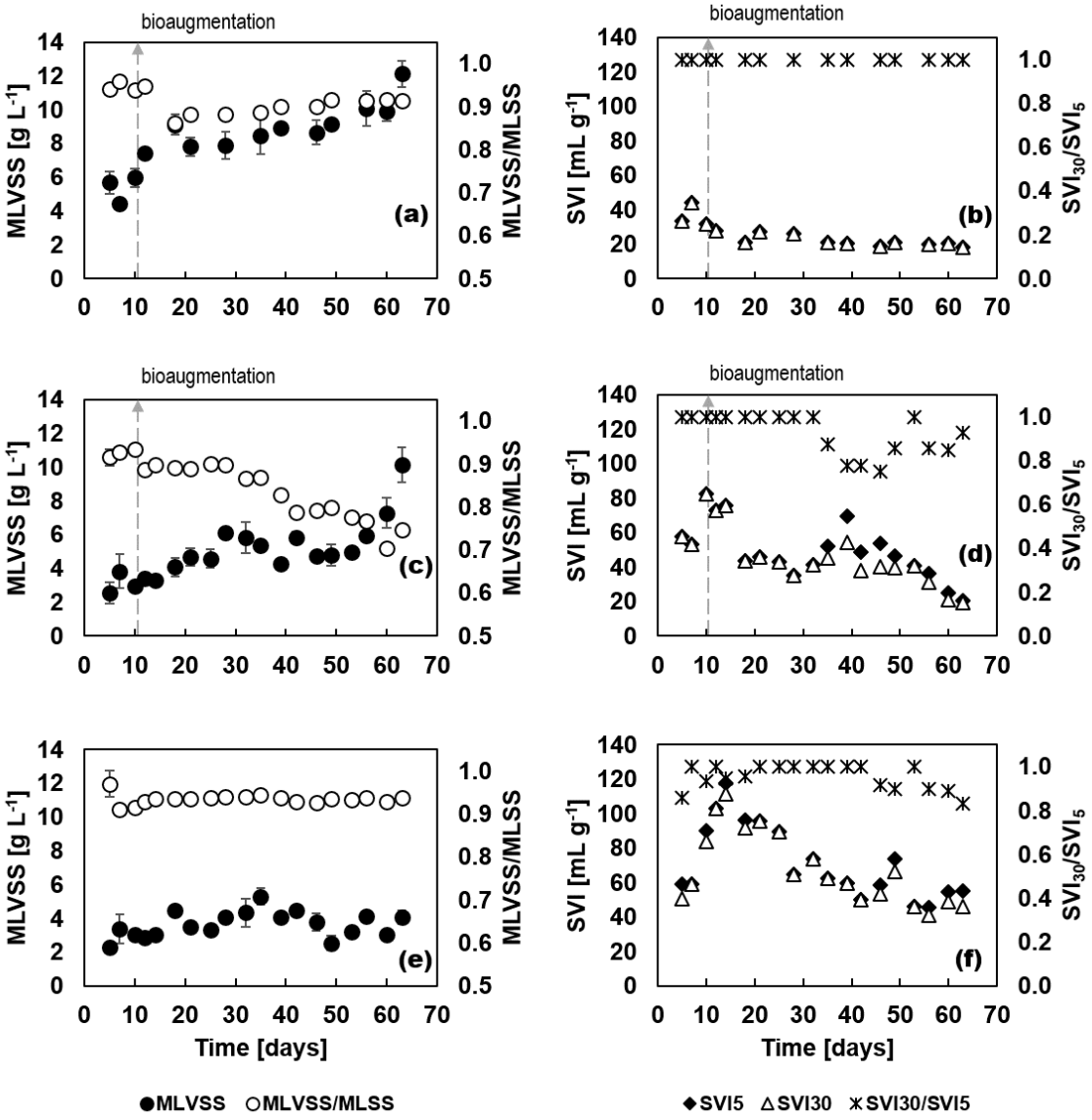


Figure 5.4 – MLVSS (●), MLVSS/MLSS (○), SVI_5 (◆), SVI_{30} (△) and SVI_{30}/SVI_5 (✱) profiles: in R1 (a,b), R2 (c,d) and R3 (e,f). Dashed arrow mark bioaugmentation day.

5.3.3. Granules distribution and morphology

The granules distribution in terms of area (%) and number (%) before and after bioaugmentation was investigated using QIA (Figure 5.5). In R1, granules with a Deq ≥ 1000 µm were initially predominant in terms of area and number (i.e., 99% and 70%, respectively) (Figure 5.5a,b). After bioaugmentation, a disturbance in the granules distribution was observed, with the frequency of granules with a Deq < 1000 µm increasing from 33 to 66%, while the area increased from 1 to 9%. Granules with a Deq < 1000 µm

continued to outnumber larger granules and accounted for 87% of the total number of granules and 20% of the granule area on day 18, however, followed by a decreasing trend until the end of the operation (Figure 5.5a,b).

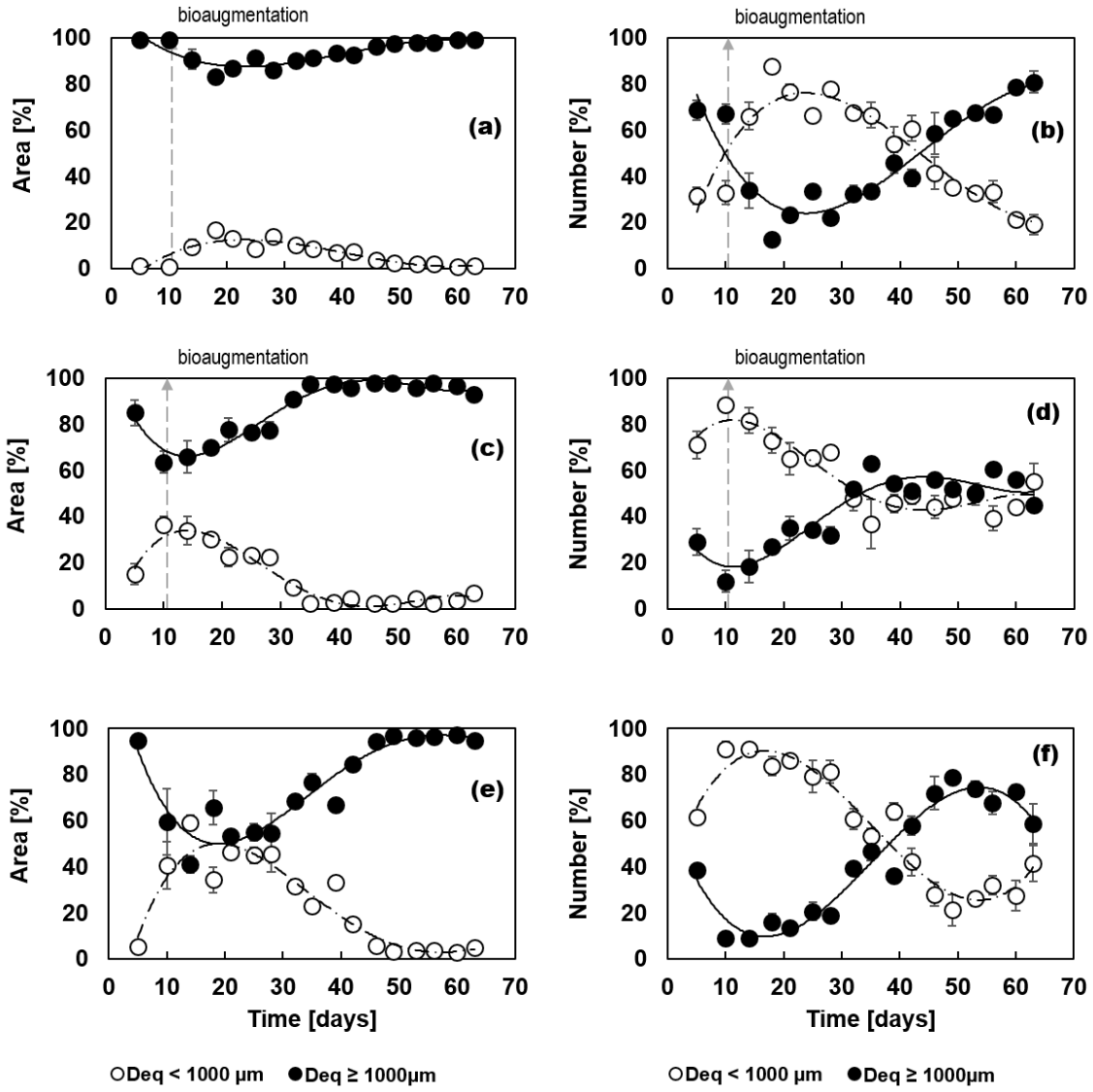


Figure 5.5 – Area and number distribution profiles for granules with Deq < 1000 µm (○) and Deq ≥ 1000 µm (●) in: R1 (a,b), R2 (c,d) and R3 (e,f). Dashed arrow mark bioaugmentation day.

During the first ten days, a significant decrease in the area of granules with Deq ≥ 1000 µm was observed in R2 and R3, from 85 to 63% and from 94 to 60%, respectively, suggesting that a steady-state was not reached (Figure 5.5c,e). In the same period, granules with Deq ≥ 1000 µm were outnumbered by smaller granules, accounting for 11 and 9% in R2 and R3, respectively (Figure 5.5d,f). The prevalence of granules with Deq ≥ 1000 µm in terms of area increased significantly in R2 after bioaugmentation, reaching values of over 90% on day 32 (Figure 5.5c). In the non-bioaugmented reactor (i.e R3), the predominance of granules with Deq ≥ 1000 µm also occurred, however, at a slower pace, eventually reaching 94% of total granules area on day 46, which was 14 days later than in R2 (Figure 5.5c,e). In R2, the frequency of small and large granules reached a steady-state at day 32, which remained until the end of the operation (Figure 5.5d). In R3, granules with Deq ≥ 1000 µm outnumbered smaller granules at day 42, representing more than 60% of the total AGS (Figure 5.5f).

The evolution of the granules Deq and solidity before and after bioaugmentation were evaluated by QIA (Figure 5.6). Before bioaugmentation, granules were relatively large, with a Deq of 2483 ± 310 µm, being 2.7 times larger than the bioactive granules (Figure 5.6a, Table 5.2). Eight days after bioaugmentation, the Deq decreased to 682 ± 10 µm, which was lower than the average size of the bioactive granules (i.e., 914 ± 41 µm), suggesting that fragmentation occurred, reducing the overall solidity of the granules (Figure 5.6a). Images of the typical granules observed on day 21 revealed the coexistence of large intact granules with smaller granules and fragments with an irregular shape (Figure 5.6b-d), which contributed to the decrease in the apparent solidity (Figure 5.6a). After this day, both Deq and solidity showed an increasing trend, returning to values similar to those before bioaugmentation (Figure 5.6a) and the prevalence of large granules with a regular structure (Figure 5.6e-g).

The granules' apparent density and convexity in R2 were evaluated before and after bioaugmentation (Figure 5.7a). As mentioned previously, AGS seemed not to have reached a steady-state before bioaugmentation, supported by the decrease in apparent density of granules from 0.011 to 0.005 g cm^{-3} at day 10 (Figure 5.7a). In contrast, the convexity, which measures the roughness of the granules' edges, was quite sable. After bioaugmentation, both parameters exhibited an oscillatory behaviour, underlining the occurrence of disturbance and recovery periods during operation (Figure 5.7a). The convexity of granules decreased from 0.91 to 0.79 on days 21 and 46, respectively, most likely due to the appearance of protruding filaments as observed on day 39 (Figure 5.7d,e). At the end of the operation, the apparent density of granules increased to 0.012 g cm^{-3} (Figure 5.7a), which was concomitant with the increase in convexity and the exclusion of protruding filaments in the granules' surface (Figure 5.7f,g).

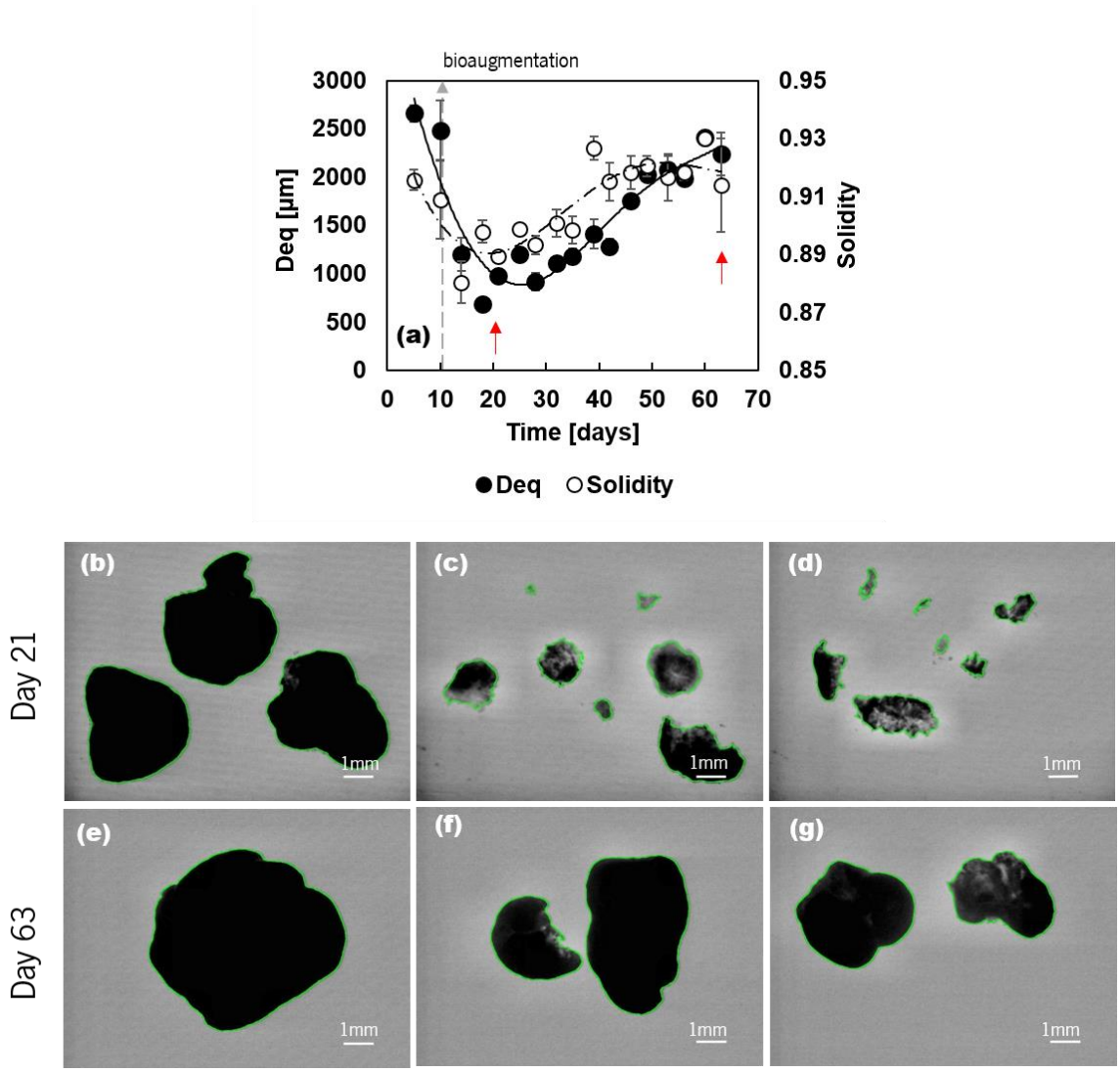


Figure 5.6 – The average Deq (●) and solidity (○) profiles of AGS in R1 (a). Dashed arrow mark bioaugmentation day. Red arrows marks the granules observation on day 21 and 63. Images of typical granules recognized by the software on day 21 (b-d) and on day 63 (e-g), acquired at 15x magnification. The scale is equal to 1mm.

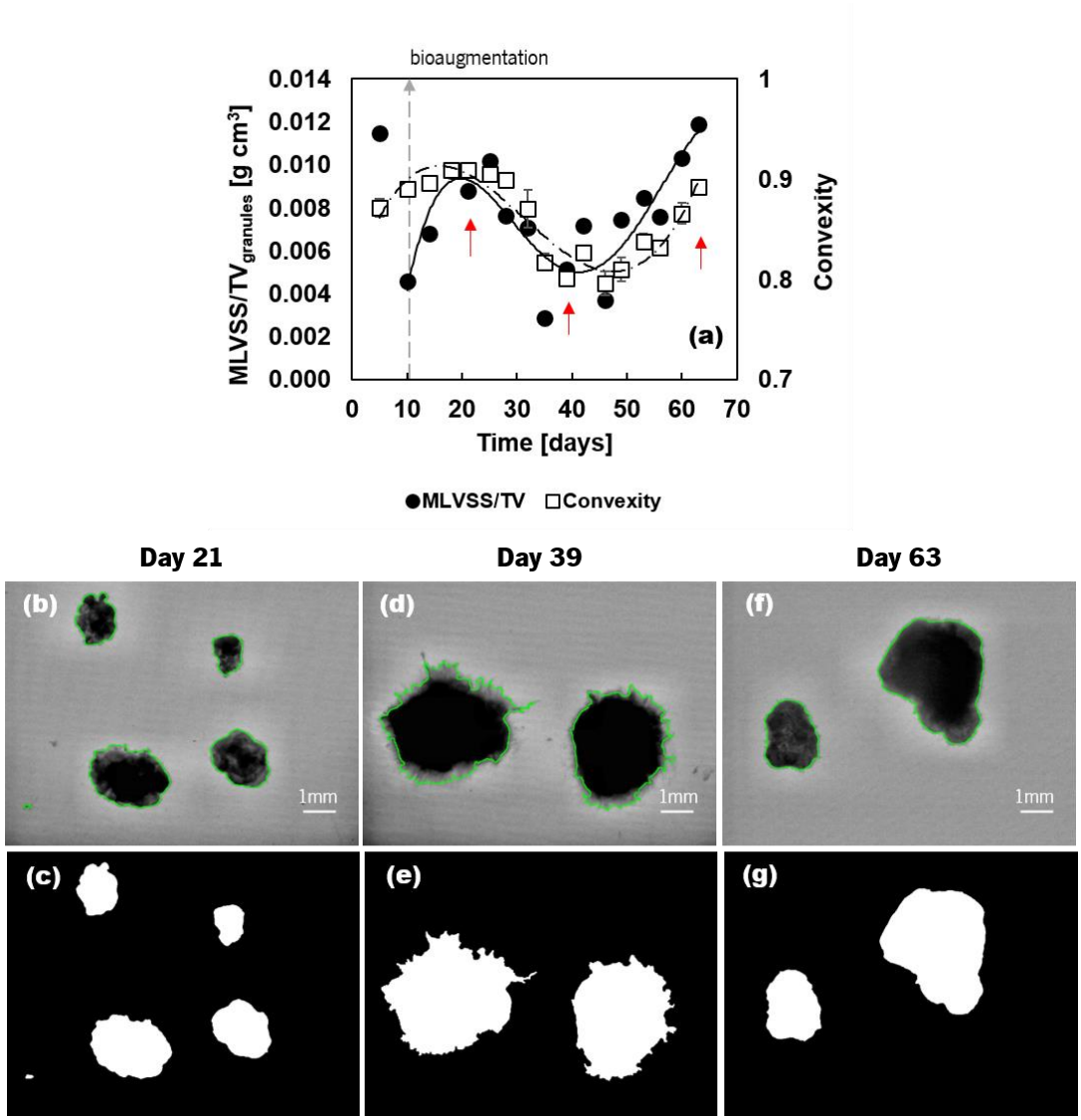


Figure 5.7 – MLVSS/TV (●) and convexity (□) profiles of AGS in R2 (a). Dashed arrow mark bioaugmentation day. Red arrows marks the granules observation on day 21, 39 and 63. Images of typical granules recognized by the software and the respective binary image created on day 21 (b,c), day 39 (d,e) and day 63 (f,g), acquired at 15x magnification. The scale is equal to 1mm.

The evolution of the granules' convexity and solidity was monitored by QIA in the non-bioaugmented reactor (Figure 5.8). The granules' convexity and solidity showed an increasing trend, indicating that granules' morphology was not stable, possibly influenced by the applied conditions that differed from the one used during the granulation process (Chapter 4). From day 25 to 46, both morphological parameters reached a steady-state, followed by a decrease until the end of the operation (Figure 5.8a). Images of the

typical granules on day 32 revealed spherical and regular shape granules (Figure 5.8b,c) instead of the larger, irregular shape granules with protruding filaments on the surface observed on day 63 (Figure 5.8d,e), leading to a decrease in both shape descriptors (Figure 5.8a).

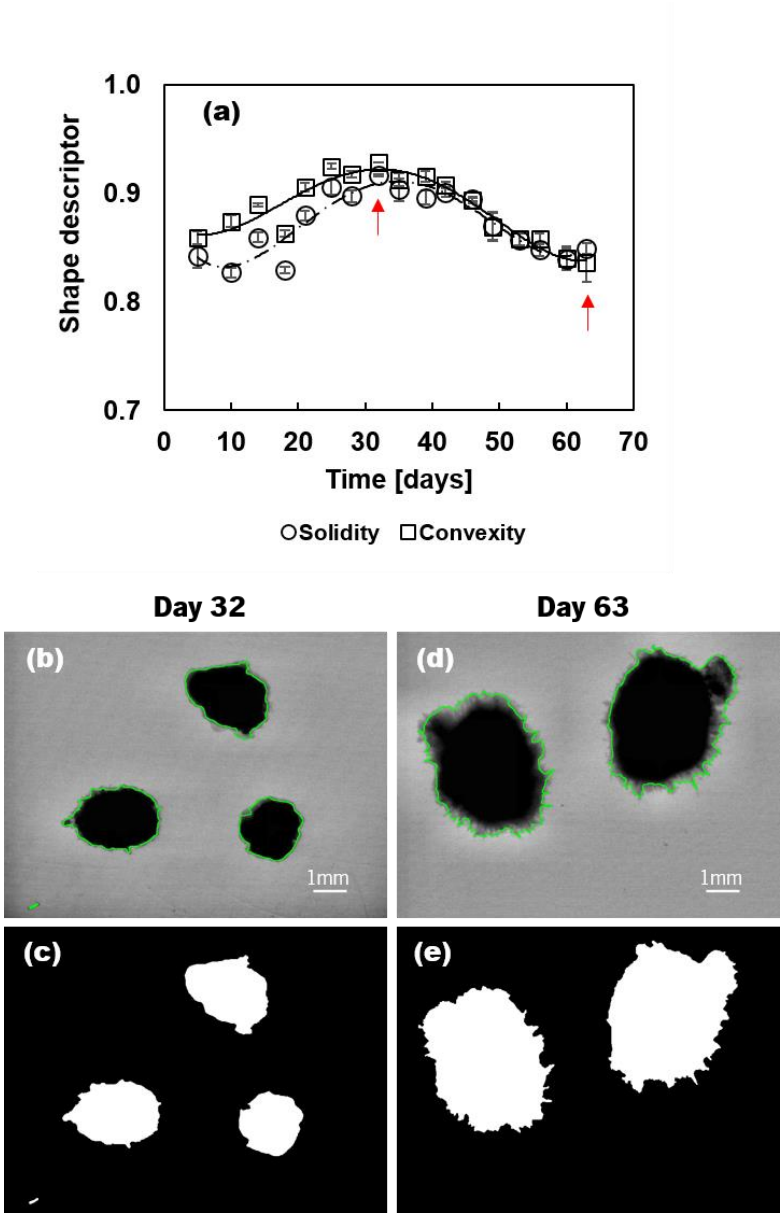


Figure 5.8 – The solidity (O) and convexity (☐) profiles of AGS in R3 (a). Dashed arrow mark bioaugmentation day. Red arrows marks the granules observation on day 32 and 63. Images of typical granules recognized by the software and the respective binary image created on day 32 (b,c) and on day 63 (d,e), acquired at 15x magnification. The scale is equal to 1mm.

5.4. DISCUSSION

The interest in using AGS for biological wastewater treatment has increased over the years, which allows for simultaneous carbon, nitrogen, and phosphorus removal in a single unit (de Kreuk et al., 2005). However, limited nutrient removal efficiencies are still reported during granulation even after obtaining mature granules (Pishgar et al., 2019; Rollemberg et al., 2019a), which relies on the establishment of slow-growing microorganisms (de Kreuk et al., 2005). Among nitrifiers, NOB are considered more sensitive to several operational factors (Rollemberg et al., 2018), and when suppressed, leads to nitrite accumulation in SBR systems, affecting phosphate removal as nitrite was found to inhibit PAO activity (Bassin et al., 2011).

Bioaugmentation can solve several practical problems, such as accelerating system recovery (Winkler et al., 2018). However, bioaugmentation failures are often reported due to the inability of the bioaugmented strain/or microbial consortia to remain in the system (Raper et al., 2018). AGS is characterized by a compact and layered structure with good settling properties without the need for carrier material (Pronk et al., 2015), which are advantages in bioaugmentation strategies (Winkler et al., 2018). In this work, two morphologically distinct AGS with nutrient removal deficiencies (i.e., low NOB and PAO activity) were used to inoculate two SBR (i.e. R1 and R2) and bioaugmented with bioactive granules presenting high nitrification and phosphate removal capabilities. In a separate SBR (i.e., R3), the effect of decreasing nutrient concentration without bioaugmentation was also accessed. In all reactors, the evolution in the morphology of granules was monitored through QIA.

5.4.1. The influence of granules morphology on the bioaugmentation efficacy

In R1, the nitrification process, which was only partial before bioaugmentation, was stimulated by the addition of bioactive granules. Nitrite concentration was no longer detected eight days after adding the bioactive granules, suggesting that NOB activity was enhanced after bioaugmentation (Figure 5.2a). Phosphate uptake was also enhanced after bioaugmentation, resulting in a significant reduction in phosphate concentration in the effluent (Figure 5.3a). However, phosphate removal decreased over time, suggesting that PAO activity could not endure, which was associated with the differences in size between the bioactive granules and the innate AGS. On average, bioactive granules were 2.7 times smaller than the innate AGS in R1. The granules area and number distributions showed the increase of smaller granules (i.e., Deq < 1000 μm) after bioaugmentation, which continued to increase afterward, suggesting

granules fragmentation (Figure 5.5a,b). The average Deq decreased to 682 ± 10 μm, which was 3.6 times and 1.3 times lower than the innate AGS and the bioactive granules, respectively. Granules fragmentation contributed to the decrease of granules solidity, which followed the same trend as the Deq (Figure 5.6). In an upwards fed reactor, substrate uptake is more likely to occur through larger granules, as these remain at the bottom of the reactor due to their higher settling velocity (van Dijk et al., 2020). Therefore, substrate limitation might have contributed to the bioactive granules fragmentation in R1, gradually washout as perceived by the decrease in the percentage of small granules and increase in the average Deq, concomitant with the decline in the capacity of phosphate uptake.

Despite the apparent washout of the bioactive granules shown by QIA, NOB activity continued throughout the operation, indicating that these microorganisms endured in the systems. Nitrifiers have been shown to reside in the aerobic layer of the granules, which depends on oxygen concentration and oxygen consumption by the microbial community (Winkler et al., 2015). Therefore, it is likely that the innate AGS outer layer might have been colonized by nitrifiers, particularly NOB, released during the fragmentation of the bioactive granules, thus remaining in the reactor and maintaining microbial activity. However, this was not the case for PAO activity. Generally, PAOs are located in the anoxic inner layer of the granules (Wilén et al., 2018; Winkler et al., 2013), which hinders the establishment of these microorganisms on the innate AGS during the bioactive granules fragmentation. Furthermore, before bioaugmentation in R1, the substrate was mainly consumed during the anaerobic feeding period (Table 5.3); thus, other polyhydroxyalkanoates (PHA) accumulating bacteria, such as glycogen accumulating organisms (GAO), outcompeted PAO for carbon uptake during anaerobic feeding.

5.4.2. The influence of bioactive granules in the morphological stability of AGS

The AGS used to inoculate R2 and R3 was produced using a synthetic medium containing 230 mg L^{-1} N-NH_4^+ and 20 mg L^{-1} P-PO_4^{3-} which were 4.6 and 4 times higher than the ammonium and phosphate concentration initially applied to both reactors. However, reducing ammonium and phosphate concentrations did not enhance the conversion of nitrite to nitrate nor the phosphate uptake, as observed in both reactors during the first ten days (Figure 5.2b,c; Figure 5.3b,c). The short operation period (i.e., ten days) was probably not sufficient to promote the growth of slow-growing microorganisms and improve nutrient removal, and as such, operation in R3 continued with the same operating conditions while in R2, bioaugmentation was performed.

Nutrient removal capability was enhanced after adding the bioactive granules in R2; ammonium was removed via complete nitrification, which increased nitrate concentration in the effluent, while phosphate removal efficiency exceeded 90% eight days after bioaugmentation (Figure 5.2b; Figure 5.3b). In contrast, in the non-bioaugmented reactor (i.e., R3), ammonium continued to be removed via partial or incomplete nitrification with nitrite accumulation observed throughout the operation (Figure 5.2c; Figure 5.3c). Furthermore, phosphate uptake did not improve over time, despite the low influent concentration (i.e., 5 mg L^{-1}). The accumulation of nitrite in R3 might have limited phosphate removal since the presence of nitrite was found to be inhibitory to phosphate uptake in SBR systems (Bassin et al., 2011; Pijuan et al., 2011).

R2 and R3 exhibited the same area and number distribution tendency over time, suggesting that nutrient removal was not directly related to the granules distribution in both systems (Figure 5.5c,d,e,f). However, bioaugmentation accelerated the granules distribution in R2, with 90% of the granules area belonging to large granules (Deq ≥ 1000 μm) 22 days after bioaugmentation, and equilibrium in the number of small (Deq < 1000 μm) and large granules was reached in the same period, which was faster than in the non-bioaugmented reactor that culminated with the prevalence of larger granules (Figure 5.5c,d,e,f). It has been found that the addition of crushed granules in SBR start-up accelerated the granulation process and improved system performances (Coma et al., 2012; Pijuan et al., 2011). Similarly, bioaugmentation promoted faster sludge stabilization, which improved sludge settling ability and promoted sludge growth (Figure 5.4c,d).

The subsequent increase in phosphate concentration in R2 led to deteriorating phosphate uptake and sludge settling properties. The convexity values revealed protruding filaments on the granular surface, often associated with process instability (Moura et al., 2018). The presence of filaments on the granular surface was concomitant with the decrease in the apparent granular density revealed by QIA (Figure 5.7) and was associated with the COD availability during the aerobic phase (Table 5.3). As phosphate uptake recovered to around 50% removal efficiency, the granules' convexity and apparent density increased as filaments on the granular surface disappeared. Protruding filaments were also observed in the non-bioaugmented reactor (Figure 5.8). The decrease in convexity and solidity of AGS exposed the unstable conditions in R3 at the end of the operation, concomitant with the predominance of larger granules, lower settling abilities, and lower sludge concentration. Filaments outgrowth can deteriorate the settling sludge velocities, leading to granules washout and decreased sludge concentration in AGS systems (Haaksman et al., 2020; van Dijk et al., 2020).

5.5. CONCLUSIONS

In this work, complete nitrification was achieved and maintained in SBR bioaugmented with bioactive granules, regardless of the morphology of the innate AGS. The establishment of efficient phosphate removal depended on the influent concentration and the morphology of the innate AGS. The morphological differences between the innate AGS and the bioactive granules led to a transient phosphate removal efficiency due to fragmentation and gradual washout of bioactive granules. While phosphate removal up to 10 mg L^{-1} was successfully maintained using morphologically similar innate and bioactive granules, successive increases in phosphate concentration in the feed led to a transient decrease in the granules' apparent density and prompted protruding filaments on the granular surface. Decreasing nutrient concentration alone did not stimulate complete nitrification or phosphate uptake, resulting in protruding filaments and unstable granules morphology over time. Bioaugmentation improved the sludge settling ability and increased sludge concentration compared to the non-bioaugmented reactor.

5.6. REFERENCES

Adav, S.S., Lee, D.J., Show, K.Y., Tay, J.H., 2008. Aerobic granular sludge: Recent advances. Biotechnol. Adv. 26, 411–423. https://doi.org/10.1016/j.biotechadv.2008.05.002

Amaral, A.L.P., 2003. Image analysis in biotechnological processes: applications to wastewater treatment. PhD thesis, University of Minho. http://hdl.handle.net/1822/4506.

Amorim, C.L., Alves, M., Castro, P.M.L., Henriques, I., 2018. Bacterial community dynamics within an aerobic granular sludge reactor treating wastewater loaded with pharmaceuticals. Ecotoxicol. Environ. Saf. 147, 905–912. https://doi.org/10.1016/j.ecoenv.2017.09.060

Amorim, C.L., Moreira, I.S., Ribeiro, A.R., Santos, L.H.M.L.M., Delerue-Matos, C., Tiritan, M.E., Castro, P.M.L., 2016. Treatment of a simulated wastewater amended with a chiral pharmaceuticals mixture by an aerobic granular sludge sequencing batch reactor. Int. Biodeterior. Biodegrad. 115, 277–285. https://doi.org/10.1016/j.ibiod.2016.09.009

APHA, 2005. Standard Methods for the Examination of Water & Wastewater 21st Edition, American Public Health Association, American Water Works Association, Water Environment Federation.

Bassin, J.P., Pronk, M., Muyzer, G., Kleerebezem, R., Dezotti, M., van Loosdrecht, M.C.M., 2011. Effect of elevated salt concentrations on the aerobic granular sludge process: Linking microbial activity with microbial community structure. Appl. Environ. Microbiol. 77, 7942–7953. https://doi.org/10.1128/AEM.05016-11

Coma, M., Verawaty, M., Pijuan, M., Yuan, Z., Bond, P.L., 2012. Enhancing aerobic granulation for biological nutrient removal from domestic wastewater. Bioresour. Technol. 103, 101–108. https://doi.org/10.1016/j.biortech.2011.10.014

de Kreuk, M.K., Heijnen, J.J., Van Loosdrecht, M.C.M., 2005. Simultaneous COD, nitrogen, and phosphate removal by aerobic granular sludge. Biotechnol. Bioeng. 90, 761–769.

https://doi.org/10.1002/bit.20470

Duque, A.F., Bessa, V.S., Carvalho, M.F., de Kreuk, M.K., van Loosdrecht, M.C.M., Castro, P.M.L., 2011. 2-Fluorophenol degradation by aerobic granular sludge in a sequencing batch reactor. Water Res. 45, 6745–6752. https://doi.org/10.1016/j.watres.2011.10.033

El Fantroussi, S., Agathos, S.N., 2005. Is bioaugmentation a feasible strategy for pollutant removal and site remediation? Curr. Opin. Microbiol. 8, 268–275. https://doi.org/10.1016/j.mib.2005.04.011

Ely, C., Moreira, I.S., Bassin, J.P., Dezotti, M.W.C., Mesquita, D.P., Costa, J., Ferreira, E.C., Castro, P.M.L., 2022. Treatment of saline wastewater amended with endocrine disruptors by aerobic granular sludge: Assessing performance and microbial community dynamics. J. Environ. Chem. Eng. 10. https://doi.org/10.1016/j.jece.2022.107272

Haaksman, V.A., Mirghorayshi, M., van Loosdrecht, M.C.M., Pronk, M., 2020. Impact of aerobic availability of readily biodegradable COD on morphological stability of aerobic granular sludge. Water Res. 187, 116402. https://doi.org/10.1016/j.watres.2020.116402

Han, X., Jin, Y., Yu, J., 2022. Rapid formation of aerobic granular sludge by bioaugmentation technology: A review. Chem. Eng. J. 437, 134971. https://doi.org/10.1016/j.cej.2022.134971

He, Q., Xie, Z., Fu, Z., Wang, M., Xu, P., Yu, J., Ma, J., Gao, S., Chen, L., Zhang, W., Song, J., Wang, H., 2021. Interaction and removal of oxytetracycline with aerobic granular sludge. Bioresour. Technol. 320. https://doi.org/10.1016/j.biortech.2020.124358

Herrero, M., Stuckey, D.C., 2015. Bioaugmentation and its application in wastewater treatment: A review. Chemosphere 140, 119–128. https://doi.org/10.1016/j.chemosphere.2014.10.033

Jiang, Y., Liu, Y., Zhang, H., Yang, K., Li, J., Shao, S., 2020. Aerobic granular sludge shows enhanced resistances to the long-term toxicity of Cu(II). Chemosphere 253, 126664. https://doi.org/10.1016/j.chemosphere.2020.126664

Leal, C., del Río, A.V., Mesquita, D.P., Amaral, A.L., Ferreira, E.C., 2022. Prediction of sludge settleability, density and suspended solids of aerobic granular sludge in the presence of pharmaceutically active compounds by quantitative image analysis and chemometric tools. J. Environ. Chem. Eng. 10. https://doi.org/10.1016/j.jece.2022.107136

Long, B., Yang, C. zhu, Pu, W. hong, Yang, J. kuan, Jiang, G. sheng, Dan, J. feng, Li, C. yang, Liu, F. biao, 2014. Rapid cultivation of aerobic granular sludge in a pilot scale sequencing batch reactor. Bioresour. Technol. 166, 57–63. https://doi.org/10.1016/j.biortech.2014.05.039

Ma, H., Zhao, Y., Yang, K., Wang, Y., Zhang, C., Ji, M., 2022. Application oriented bioaugmentation processes: Mechanism, performance improvement and scale-up. Bioresour. Technol. 344, 126192. https://doi.org/10.1016/j.biortech.2021.126192

Martín-Hernández, M., Suárez-Ojeda, M.E., Carrera, J., 2012. Bioaugmentation for treating transient or continuous p-nitrophenol shock loads in an aerobic sequencing batch reactor. Bioresour. Technol. 123, 150–156. https://doi.org/10.1016/j.biortech.2012.07.014

Moura, L.L., Duarte, K.L.S., Santiago, E.P., Mahler, C.F., Bassin, J.P., 2018. Strategies to re-establish stable granulation after filamentous outgrowth: Insights from lab-scale experiments. Process Saf. Environ. Prot. 117, 606–615. https://doi.org/10.1016/j.psep.2018.06.005

Muñoz-Palazon, B., Rodriguez-Sanchez, A., Hurtado-Martinez, M., de Castro, I.M., Juarez-Jimenez, B., Gonzalez-Martinez, A., Gonzalez-Lopez, J., 2019. Performance and microbial community structure of an aerobic granular sludge system at different phenolic acid concentrations. J. Hazard. Mater. 376, 58–67. https://doi.org/10.1016/j.jhazmat.2019.05.015

Oliveira, A.S., Amorim, C.L., Zlopasa, J., van Loosdrecht, M., Castro, P.M.L., 2021. Recovered granular sludge extracellular polymeric substances as carrier for bioaugmentation of granular sludge reactor. Chemosphere 275, 130037. https://doi.org/10.1016/j.chemosphere.2021.130037

Pijuan, M., Werner, U., Yuan, Z., 2011. Reducing the startup time of aerobic granular sludge reactors through seeding floccular sludge with crushed aerobic granules. Water Res. 45, 5075–5083. https://doi.org/10.1016/j.watres.2011.07.009

Pishgar, R., Dominic, J.A., Sheng, Z., Tay, J.H., 2019. Influence of operation mode and wastewater strength on aerobic granulation at pilot scale: Startup period, granular sludge characteristics, and effluent quality. Water Res. 160, 81–96. https://doi.org/10.1016/j.watres.2019.05.026

Pronk, M., de Kreuk, M.K., de Bruin, B., Kamminga, P., Kleerebezem, R., van Loosdrecht, M.C.M., 2015. Full scale performance of the aerobic granular sludge process for sewage treatment. Water Res. 84, 207–217. https://doi.org/10.1016/j.watres.2015.07.011

Raper, E., Stephenson, T., Anderson, D.R., Fisher, R., Soares, A., 2018. Industrial wastewater treatment through bioaugmentation. Process Saf. Environ. Prot. 118, 178–187. https://doi.org/10.1016/j.psep.2018.06.035

Rollemberg, S.L. de S., Barros, A.R.M., de Lima, J.P.M., Santos, A.F., Firmino, P.I.M., dos Santos, A.B., 2019a. Influence of sequencing batch reactor configuration on aerobic granules growth: Engineering and microbiological aspects. J. Clean. Prod. 238. https://doi.org/10.1016/j.jclepro.2019.117906

Rollemberg, S.L. de S., de Oliveira, L.Q., Barros, A.R.M., Melo, V.M.M., Firmino, P.I.M., dos Santos, A.B., 2019b. Effects of carbon source on the formation, stability, bioactivity and biodiversity of the aerobic granule sludge. Bioresour. Technol. 278, 195–204. https://doi.org/10.1016/j.biortech.2019.01.071

Rollemberg, S.L., Mendes Barros, A.R., Milen Firmino, P.I., Bezerra dos Santos, A., 2018. Aerobic granular sludge: Cultivation parameters and removal mechanisms. Bioresour. Technol. 270, 678–688. https://doi.org/10.1016/j.biortech.2018.08.130

Silva, S.A., Val del Río, A., Amaral, A.L., Ferreira, E.C., Alves, M.M., Mesquita, D.P., 2022. Monitoring morphological changes from activated sludge to aerobic granular sludge under distinct organic loading rates and increasing minimal imposed sludge settling velocities through quantitative image analysis. Chemosphere 286, 131637. https://doi.org/10.1016/j.chemosphere.2021.131637

Tomar, S.K., Kumar, R., Chakraborty, S., 2022. Simultaneous biodegradation of pyridine, indole, and ammonium along with phenol and thiocyanate by aerobic granular sludge. J. Hazard. Mater. 422, 126861. https://doi.org/10.1016/j.jhazmat.2021.126861

van Dijk, E.J.H., Pronk, M., van Loosdrecht, M.C.M., 2020. A settling model for full-scale aerobic granular sludge. Water Res. 186, 116135. https://doi.org/10.1016/j.watres.2020.116135

Wei, D., Wang, Y., Wang, X., Li, M., Han, F., Ju, L., Zhang, G., Shi, L., Li, K., Wang, B., Du, B., Wei, Q., 2015. Toxicity assessment of 4-chlorophenol to aerobic granular sludge and its interaction with extracellular polymeric substances. J. Hazard. Mater. 289, 101–107. https://doi.org/10.1016/j.jhazmat.2015.02.047

Wilén, B.M., Liébana, R., Persson, F., Modin, O., Hermansson, M., 2018. The mechanisms of granulation of activated sludge in wastewater treatment, its optimization, and impact on effluent quality. Appl. Microbiol. Biotechnol. 102, 5005–5020. https://doi.org/10.1007/s00253-018-8990-9

Winkler, M.K.H., Kleerebezem, R., De Bruin, L.M.M., Verheijen, P.J.T., Abbas, B., Habermacher, J., Van Loosdrecht, M.C.M., 2013. Microbial diversity differences within aerobic granular sludge and activated sludge flocs. Appl. Microbiol. Biotechnol. 97, 7447–7458. https://doi.org/10.1007/s00253-012-4472-7

Winkler, M.K.H., Le, Q.H., Volcke, E.I.P., 2015. Influence of Partial Denitrification and Mixotrophic Growth of NOB on Microbial Distribution in Aerobic Granular Sludge. Environ. Sci. Technol. 49, 11003–11010.

https://doi.org/10.1021/acs.est.5b01952

Winkler, M.K.H., Meunier, C., Henriet, O., Mahillon, J., Suárez-Ojeda, M.E., Del Moro, G., De Sanctis, M., Di Iaconi, C., Weissbrodt, D.G., 2018. An integrative review of granular sludge for the biological removal of nutrients and recalcitrant organic matter from wastewater. Chem. Eng. J. 336, 489–502. https://doi.org/10.1016/j.cej.2017.12.026

CHAPTER 6

The effect of LCFA on the performance and stability of aerobic granular sludge in a sequencing batch reactor

The effect of long-chain fatty acids (LCFA) in the removal of soluble chemical oxygen demand (COD), nitrogen and phosphorus by aerobic granular sludge (AGS) in a sequencing batch reactor (SBR) was evaluated. At an oleate concentration of 61.3 ± 2.0 mg L^{-1}, oleate accumulated in the reactor, resulting in an increasing volatile suspended solids concentration in the effluent. Quantitative image analysis (QIA) data revealed that small granules (< 1000 μm) were washed out due to their larger specific surface area for oleate adsorption. This selective sludge washout increased the average granule size inside the reactor, which had a positive effect on total inorganic nitrogen (TIN) removal. However, under the highest oleate concentration tested (i.e., 113.8 ± 3.8 mg L^{-1}), ammonium removal efficiency decreased from 100% to 80%, while phosphate was no longer efficiently removed due to the availability of soluble COD during the aeration phase, which favoured filaments outgrowth. Principal component analysis (PCA) showed that oleate had a negative impact on the morphology and stability of aerobic granules, associated with decreasing reactor performances. Nevertheless, these results demonstrate the feasibility of using AGS system in the treatment of oleate-containing wastewater treatment in concentrations below 60 mg L^{-1}. Limiting oleate adsorption appeared essential for the stability and performance of AGS system; thus, selecting large granules could minimize oleate adsorption onto AGS, preventing sludge washout and maintaining reactor performance.

6.1. INTRODUCTION

The increasing worldwide consumption of fats, oils and grease leads to the generation of large amounts of lipid-rich domestic and industrial wastewater. Lipids represent 30% to 40% of the chemical oxygen demand (COD) present in wastewaters (Dueholm et al., 2001). In domestic wastewaters specifically, lipids can be found in concentrations varying between 40 to 100 mg L^{-1} (Forster, 2007; Quéméneur and Marty, 1994), which are easily converted into long-chain fatty acids (LCFA) that retain most of the lipid energy. The presence of LCFA contributes to several operational problems in biological wastewater treatment systems. The negative effect of LCFA in anaerobic digesters has been extensively reported in the literature (Alves et al., 2009; Holohan et al., 2022). Among typical operational problems are sludge flotation (Singh et al., 2019) and inhibition (Chen et al., 2014) due to LCFA adsorption onto the biomass (Pereira et al., 2005). While at lower concentrations, the presence of LCFA in conventional activated sludge systems is associated with filamentous outgrowth, which induces several sludge settling problems (Rossetti et al., 2005).

AGS technology for wastewater treatment could replace conventional activated sludge systems due to the process's higher energy efficiency and cost-effectiveness (Bengtsson et al., 2019). Since aerobic granules are denser and more compact than activated sludge, higher biomass concentration and better biomass retention are achieved in AGS systems, which enables treatment of higher loads and confers greater tolerance to recalcitrant compounds (Cai et al., 2021). Thus, AGS systems have been studied for the treatment of complex wastewater, including petrochemical (Campo and Di Bella, 2019), fish cannery (Carrera et al., 2021), pulp mill (Vashi et al., 2019), textile dyes (Sarvajith et al., 2018), and pharmaceutical (Amorim et al., 2016). However, the aerobic granules instability has significantly limited the further widespread use of this technology and is still considered a bottleneck of AGS systems (Franca et al., 2018; Lin et al., 2020). The effect of LCFA in AGS systems has never been evaluated in concentrations typical of domestic wastewaters. Besides, in liquid digestates provided from anaerobic digesters treating lipid-rich industrial effluents, LCFA can also occur in concentrations that may negatively influence the long-term AGS integrity.

The main objective of this work was to evaluate the impact of low LCFA concentration, yet still relevant in the domestic wastewater context, on the removal of soluble COD, nitrogen and phosphorus in AGS systems. Oleate (oleic acid; C18:1) is an unsaturated LCFA and was the model LCFA used in this work because it is commonly found in a variety of raw products, sewage grease deposits, and consequently in

wastewater treatment plants (Long et al., 2012; Viswanathan et al., 1962; Williams et al., 2012). The effects on the granule's distribution and morphology were also evaluated through QIA.

6.2. MATERIAL AND METHODS

6.2.1. Experimental setup

A 1L working volume sequencing batch reactor (SBR) with dimensions of 18.5 cm height and 9 cm diameter (H/D = 2) was operated in cycles of 6 h as follows: 120 min anaerobic feed, 234 min aeration, 1 min sludge settling, and 5 min effluent discharge. The peristaltic pumps were controlled by automatic timers to regulate the inflow and outflow times of the system. The reactor was operated at room temperature (21.3 ± 2.3 °C) with a hydraulic retention time of 12 h and an exchange ratio of 50%. Oxygen was added to the bottom of the reactor during aeration to ensure good mixing and saturation with dissolved oxygen. The reactor was inoculated with AGS produced from activated sludge in a previous experiment treating a synthetic medium containing sodium acetate as the sole carbon source (see Chapter 4). The initial mixed liquor volatile suspended solids (MLVSS) was 6.9 ± 0.2 g L^{-1}. The sludge retention time (SRT) was not controlled during the operating period.

The reactor was fed with sodium acetate 476 ± 45 mg L^{-1} (in COD), 48 ± 3 mg L^{-1} of N-NH_4^+ and 20 ± 1 mg L^{-1} P-PO_4^{3-}. The feed was prepared with tap water supplemented with $MgSO_4.7H_2O$ (0.09 g L^{-1}), $CaCl_2.2H_2O$ (0.03 g L^{-1}), sodium bicarbonate (0.6 g L^{-1}) and a concentrated trace solution (0.75 mL L^{-1}) consisting of: $FeCl_3.6H_2O$ (6 g L^{-1}); H_3BO_3 (0.6 g L^{-1}); $CuSO_4.5H_2O$ (0.12 g L^{-1}); KI (0.72 g L^{-1}); $MnCl_2.4H_2O$ (0.48 g L^{-1}); $Na_2MoO_2.2H_2O$ (0.24 g L^{-1}); $ZnSO_4.7H_2O$ (0.48 g L^{-1}); $CoCl_2.6H_2O$ (0.6 g L^{-1}), and EDTA (40 g L^{-1}). After 28 days of reactor operation, sodium oleate (≥ 82 % as oleic acid, Riedel-de-Häen, Seelze, Germany) was added to the feed at concentrations ranging from 0.9 ± 0.03 mg L^{-1} to 113.8 ± 3.8 mg L^{-1} (Table 6.1). During the aeration period, 2 mL of the reactor contents were collected and stored for quantification of oleate (-20 °C).

Table 6.1 – Oleate concentration in the influent throughout the SBR operation

Operation period (days)	Time of exposure (days)	Oleate concentration in SBR feed (mg L^{-1})
29 – 38	9	0.9 ± 0.03
39 – 49	10	4.4 ± 0.1
50 – 59	9	8.8 ± 0.3
60 – 70	10	21.9 ± 0.7
71 – 80	9	35.0 ± 1.2
81 – 91	10	48.1 ± 1.6
92 – 101	9	61.3 ± 2.0
102 – 112	10	87.5 ± 2.9
113 – 147	34	113.8 ± 3.8

6.2.2. Analytical methods

Chemical oxygen demand (COD), ammonium nitrogen ($N\text{-}NH_4^+$), nitrite ($N\text{-}NO_2^-$), nitrate ($N\text{-}NO_3^-$), and phosphate ($P\text{-}PO_4^{3-}$) were determined spectrophotometrically using a cuvette test kit (Hach-Lange GmbH, Dusseldorf, Germany) and a DR2800™ spectrophotometer (Hach-Lange, GmbH). Prior to analysis, samples were filtered using a syringe membrane filter (0.45 μm pore size). The amount of soluble COD available for the aeration phase ($COD_{aeration}$) was quantified at the transition between anaerobic feeding and the aeration phase. The amount of $P\text{-}PO_4^{3-}$ released to the bulk medium during the anaerobic feeding phase was also quantified before aeration started. The mixed liquor suspended solids and volatile suspended solids (MLSS and MLVSS) in the reactor, and the total and volatile suspended solids in the effluent ($TSS_{effluent}$ and $VSS_{effluent}$), were determined according to standard methods (APHA, 2005). Sludge settleability was monitored by determining the sludge volume index after 5 minutes (SVI_5) and 30 minutes (SVI_{30}) according to standard methods (APHA, 2005). Oleate concentration was determined according to Neves et al. 2009. Free saturated and unsaturated LCFA from C12 to C18 were esterified with HCl:1-propanol at 100 °C for 3.5 h, extracted with dichloromethane, and quantified by gas chromatography with a flame ionization detector (GC-FID). LCFA were separated using a Teknokroma TRB-WAX column (30 m x 0.25 mm x 0.25 μm) with helium as the carrier gas, at 1 mL min^{-1}. The injector and detector temperatures were 220 °C and 250 °C, respectively. The initial oven temperature was 50 °C, which was

maintained for 2 min, followed by a 10 °C min^{-1} ramp up to 225 °C, and finally, isothermal conditions were maintained for 10 min.

6.2.3. Quantitative image analysis

6.2.3.1. Sludge sampling

For granules characterization, a sample volume of 10 mL was collected at the beginning of the aeration phase when complete mixing of the sludge was achieved. The samples were washed with phosphate-buffered saline solution (PBS). The granules were allowed to settle and the supernatant was discarded. The granules were re-suspended with a mixture of 1:1 PBS and absolute ethanol (≥ 99.8%) and stored (-20 °C) until analysis. Prior to image acquisition, granules were washed with distilled water to remove the PBS-ethanol and re-suspended to its initial volume.

6.2.3.2. Image acquisition, processing, and analysis

Images of granules were taken using an Olympus SZ-40 stereomicroscope (Olympus, Shinjuku, Japan), at 15× magnification. A fixed volume was placed in a Petri dish, and all granules present in this volume were captured. This procedure was performed in triplicate so that at least 250 granules could be quantified. Images were acquired with a CCD AVC D5CE Sony video camera (Sony, Tokyo, Japan) and Image-Pro Plus software (Media Cybernetics, MD, USA), in 768 × 576 pixels and 8-bit format. Image processing, including pre-treatment, segmentation, and debris removal steps, was performed as described in Amaral (2003). Binary images were created with the recognized granules, allowing the subsequent determination of morphological parameters (Figure 6.1). Only aggregates with an equivalent diameter (Deq) ≥ 200 μm were considered granules (de Kreuk et al., 2007), determined by the Area parameter as shown in Chapter 3.

Granules distribution was assessed by dividing granules into three size classes (Gc) based on their Deq, namely Gc1 (200 μm ≤ Deq ≤ 600 μm), Gc2 (600 μm < Deq < 1000 μm), and Gc3 (Deq ≥ 1000 μm). The percentage of granules (%Nb) for each size class (i.e., Gc1, Gc2, and Gc3) was determined by the ratio between the sum of the number of granules within that size class and the total number of quantified granules per volume ($TN_{granules}$/Vol). Total area of granules ($TA_{Granules}$/Vol), expressed in (mm^2 mL^{-1}) and the total granules volume ($TV_{Granules}$/Vol), expressed in mm^3 mL^{-1}, were calculated as shown in Chapter 4

and Chapter 5, respectively. The surface-area-to-volume ratio (SA:V), expressed in mm^{-1}, was determined by the ratio between the $TA_{Granules}$ and the $TV_{Granules}$. The morphological parameter convexity, depends on the creation of the convex hull, i.e. the smaller convex polygon enclosing the granules and determined by the vectorization of the granules contour (Amaral, 2003). The convexity of granules was calculated as shown in Chapter 3. More information on the calculation of these parameters can be found in Amaral (2003). Image processing and analysis routines were performed in Matlab™ 8.5 (the MathWorks Inc, USA).

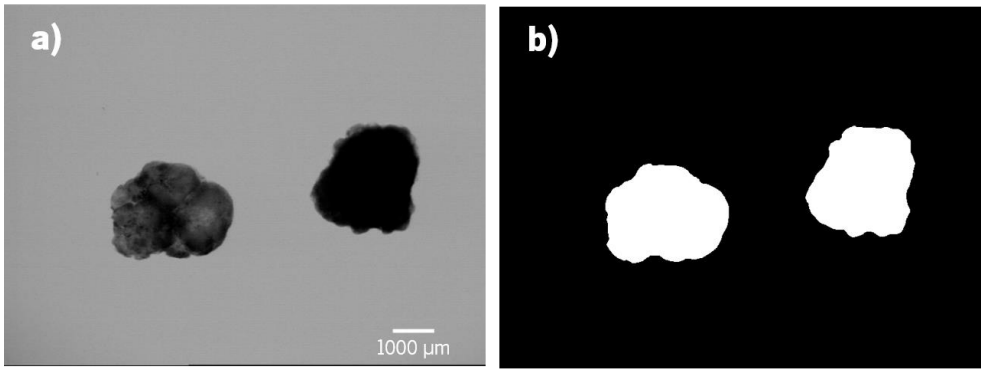


Figure 6.1 – Original image (a) of granules, and the binary image (b) created.

6.2.4. Principal Component Analysis

Principal component analysis (PCA) aims to determine hidden and complex relationships between parameters that compose an X dataset. PCA was performed using the morphological data determined by QIA (Annexe Table A1) and the reactor operational data. The X dataset was composed of 26 parameters and 12 observations. Before PCA, each variable was scaled as described in Chapter 3. PCA was performed in Microsoft Excel using the XLSTAT statistical software.

6.3. RESULTS

6.3.1. Organic matter and nutrients removal efficiencies

No oleate was added during the first 28 days to stabilize the granules. Since AGS were produced using acetate as the sole carbon source and oleate increases the total concentration of COD, only the soluble COD (i.e., acetate) was monitored to understand the effect of oleate on the efficiency of COD removal.

Nutrient removal and granules morphology were also monitored to understand the effects of oleate on AGS systems.

The oleate concentration in the reactor was monitored throughout the experiment (Figure 6.2a). Before increasing the oleate concentration, the accumulation of oleate in the reactor was examined. The result showed that oleate accumulation was not observed until day 94, when AGS were exposed to a concentration of 61.3 ± 2.0 mg L^{-1} (Figure 6.2a). However, the subsequent increase in oleate concentration in the feed did not result in an increase in oleate concentration inside the reactor, suggesting that adsorption of oleate onto AGS was limited.

The soluble COD in the effluent was quite stable during SBR operation and remained mostly below 30 mg L^{-1}, corresponding to a COD removal efficiency of 96.2 ± 1% (Figure 6.2b). The soluble COD available for the aeration phase was quite low, ranging from 19 to 57 mg L^{-1}, indicating that most of the soluble COD was consumed during the anaerobic feeding phase. However, a change in the SBR consumption pattern was observed from day 112 onward, as most of the soluble COD was removed during the aeration phase. When the SBR was fed with an oleate concentration of 87.5 ± 2.9 mg L^{-1} and 113.8 ± 3.8 mg L^{-1}, the soluble COD available for the aeration phase increased dramatically to values above 215 mg L^{-1} (Figure 6.2b).

Phosphate concentration after anaerobic feeding was 5 to 6 times higher than that present in the feed (i.e. 100 – 120 mg L^{-1}), indicating that the amount of phosphate released to the bulk medium varied between 80 and 100 mg L^{-1}. However, the phosphate concentration in the effluent was less than 1 mg L^{-1} during 126 days, representing a phosphate removal efficiency between 90 and 99% (Figure 6.2c). When the highest oleate concentration was applied to the SBR system (i.e., on day 113), the amount of phosphate released during anaerobic feeding decreased sharply to values around 30 mg L^{-1}. Nevertheless, the phosphate concentration in the effluent remained below 1 mg L^{-1}. From day 129, the phosphate concentration in the effluent increased to values above 20 mg L^{-1} (Figure 6.2c).

The total inorganic nitrogen (TIN) concentration in the SBR influent was assumed to be equal to the ammonium concentration since no other nitrogen sources were added to the influent. AGS showed high ammonium removal as the concentration in the effluent was below the detection limit (0.015 mg L^{-1}). However, a decrease in ammonium oxidation was observed from day 129 when the concentration in the effluent increased to 10 mg L^{-1} (Figure 6.2d).

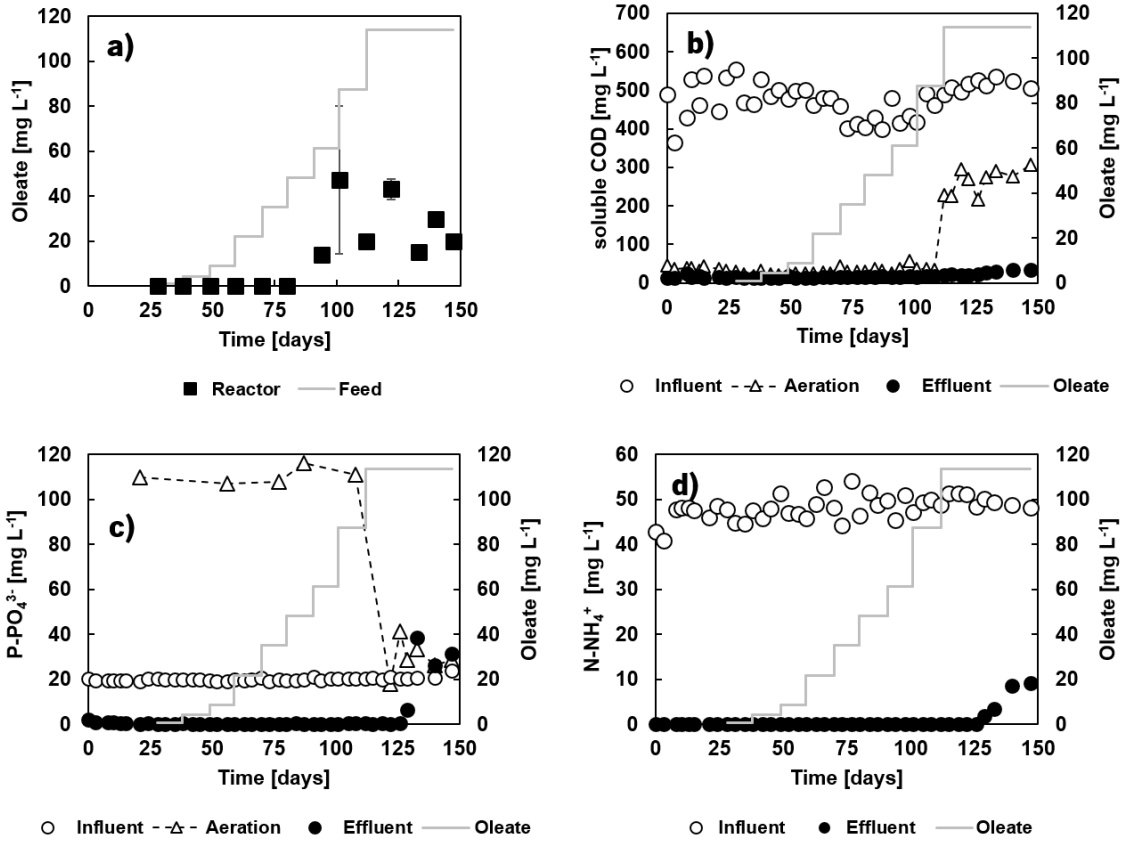


Figure 6.2 – Concentration profiles during the SBR operation: Oleate (a), soluble COD (b), $P\text{-}PO_4^{3-}$ (c) and $N\text{-}NH_4^+$ (d). Oleate concentration in the reactor (■) and in the feed (—). Soluble COD, $P\text{-}PO_4^{3-}$ and $N\text{-}NH_4^+$ concentration in the influent (○) and effluent (●). Soluble COD and $P\text{-}PO_4^{3-}$ at the beginning of the aeration phase (- -△- -).

Cycle analyses for COD, ammonium, and phosphate removal were performed on days 126 and 147, when the highest concentration of oleate was added and SBR instability was observed (Figure 6.3). In both cycles analysed, most of the soluble COD was consumed during the aerobic phase (Figure 6.3a). However, on day 126, a steeper COD degradation was observed and most of it was degraded 30 minutes after the start of aeration. In addition, a higher COD accumulation rate was observed during the anaerobic feeding phase on day 147, indicating a decrease in anaerobic COD consumption. Most of the phosphate accumulated in AGS was released under aerobic conditions in both cycles, showing the deterioration of phosphate removal efficiency (Figure 6.3b). On day 126, phosphate concentration reached 120 mg L^{-1} after 30 minutes of aeration, which was completely removed in the remaining cycle time. On day 147, phosphate release lasted longer, followed by a less steep phosphate uptake rate. However, a phosphate concentration of 30 mg L^{-1} remained at the end of the cycle. In both cycles, ammonium was removed

during the aeration phase (Figure 6.3c). However, a sharper ammonium degradation rate was observed on day 126, which was completely removed by the end of the cycle. The aeration time was not sufficient to remove the ammonium on day 147. The cycle started with a higher ammonium concentration due to accumulation from the previous cycle. After the anaerobic feeding period, the ammonium concentration reached 30 mg L^{-1}, which was 2 times higher than on day 126 (Figure 6.3c).

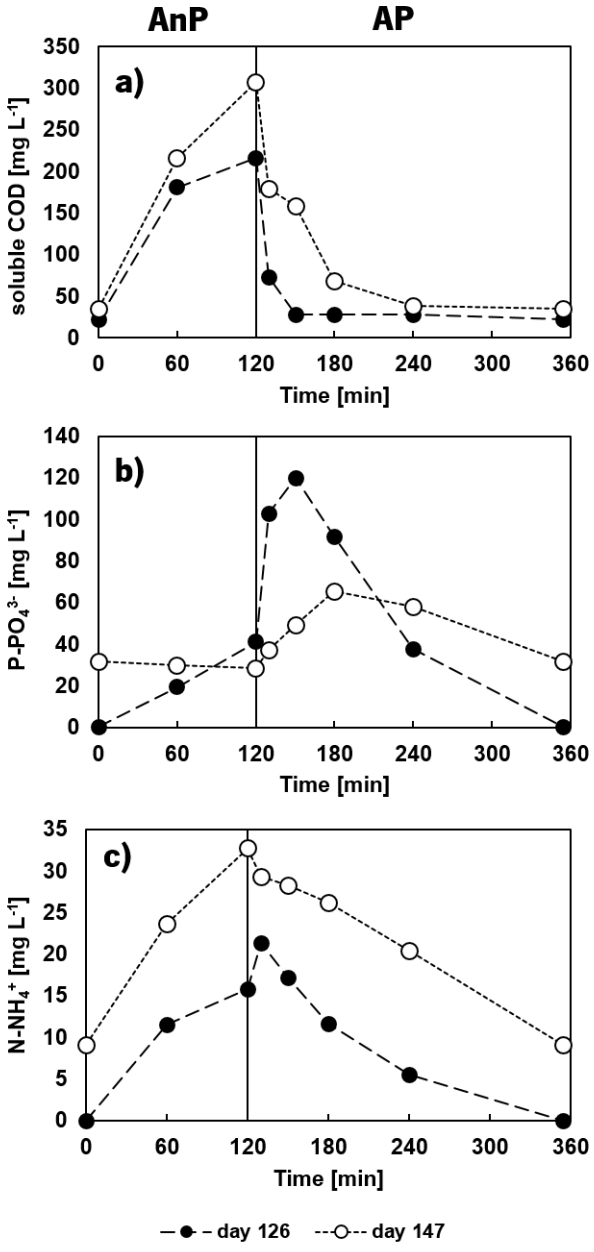


Figure 6.3 – Concentration profiles of soluble COD (a), $P\text{-}PO_4^{3-}$ (b), and $N\text{-}NH_4^+$ (c) during anaerobic feeding phase (AnP) and aeration phase (AP) in the SBR cycle analysis at day 126 (—●—) and day 147 (---○---).

TIN in the effluent was considered as the sum of ammonium, nitrite and nitrate. During the first 28 days of operation, most of the ammonium was converted to nitrate and only a low concentration of nitrite (i.e., < 1 mg L^{-1}) was detected in the effluent (Figure 6.4a). The nitrate concentration increased before the addition of oleate, indicating a decrease in the denitrification capacity of the AGS. However, the nitrate concentration in the effluent decreased steadily when oleate was added to the feed, increasing the TIN removal efficiency up to 94%. A clear negative correlation (R^2 = 0.977) was observed between the nitrate concentration in the effluent and the oleate concentration in the feed (Figure 6.4b).

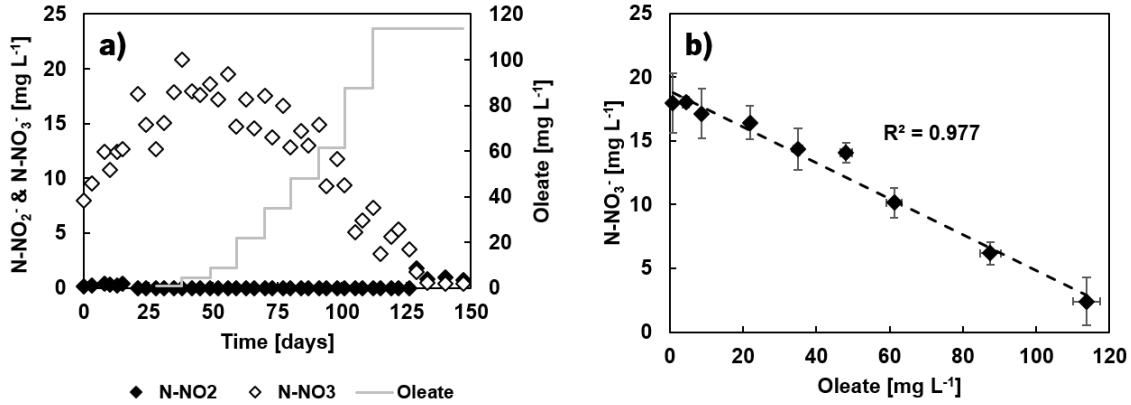


Figure 6.4 – $N\text{-}NO_{2}^{-}$ (◆) and $N\text{-}NO_{3}^{-}$ (◇) concentrations in the effluent and oleate concentration in the feed (—) during SBR operation (a), and correlation analysis between nitrate concentration in the effluent and oleate concentration in the feed (b).

6.3.2. Sludge concentration and settling properties

The MLSS and MLVSS concentrations in the reactor were quite unstable during the first 28 days of operation (Figure 6.5a). In this period, the MLVSS concentration fluctuated between 5.3 ± 0.2 g L^{-1} and 7.9 ± 0.2 g L^{-1}. MLSS and MLVSS exhibited an increasing trend after oleate was added to the feed. However, both MLSS and MLVSS decreased considerably when the highest concentration of oleate (i.e., 113.8 ± 3.8 mg L^{-1}) was added to the reactor. MLVSS decreased from 9.0 ± 0.4 g L^{-1} to 5.7 ± 0.6 g L^{-1}, corresponding to a 36% decrease in biomass concentration. Additionally, a steeper decline in MLSS was observed due to the loss of inert suspended solids associated with the polyphosphate (poly-P) storage polymer, increasing the MLVSS/MLSS ratio in the reactor at the end of operation (Figure 6.5a).

The $TSS_{effluent}$ and $VSS_{effluent}$ were rather stable in the first 75 days of operation (Figure 6.5b). The average $VSS_{effluent}$ was 77 ± 10 mg L^{-1} when exposed to an oleate concentration up to 35 ± 1.2 mg L^{-1}. However, at a higher oleate concentration, the $VSS_{effluent}$ increased considerably, reaching 496 ± 55 mg L^{-1} on day 126 (Figure 6.5b). From this day the $VSS_{effluent}$ decreased but remained above 200 mg L^{-1}.

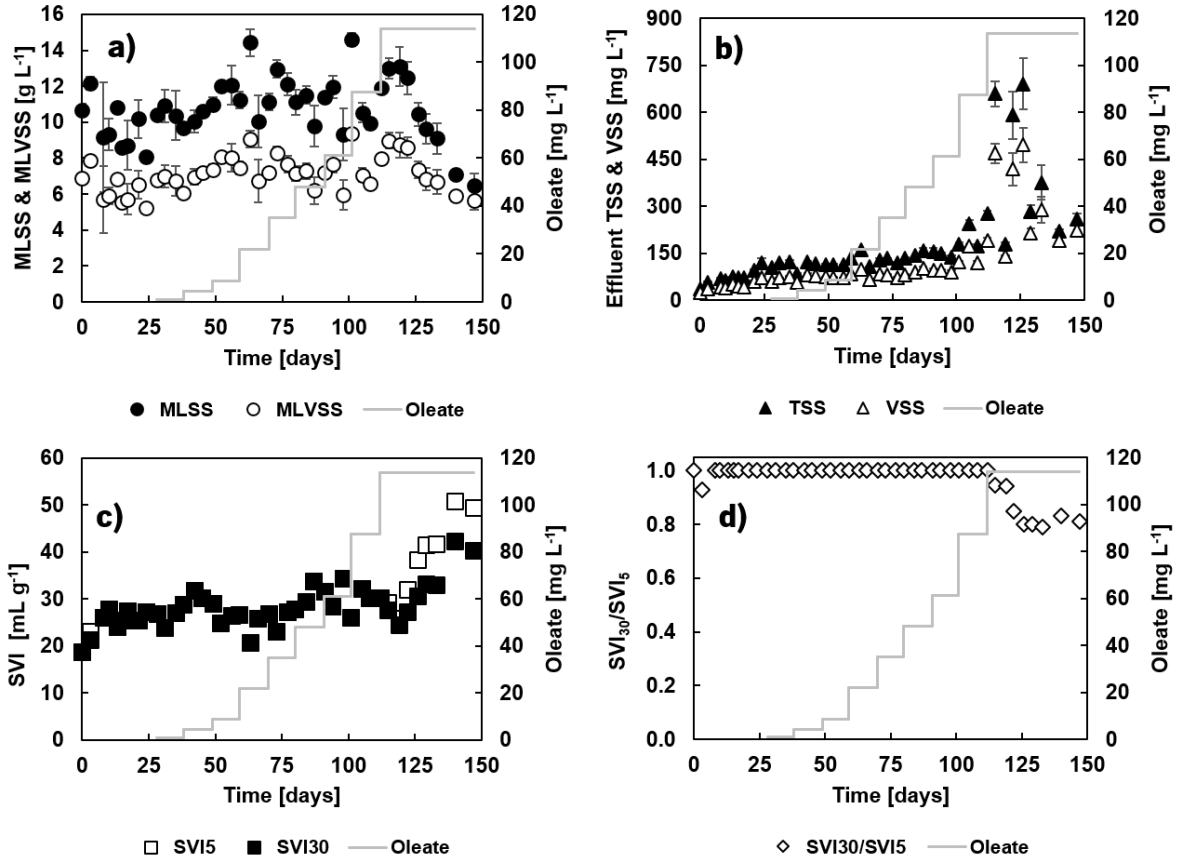


Figure 6.5 – Profiles during the SBR operation: MLSS (●) and MLVSS (○) concentration in the reactor (a), TSS (▲) and VSS (△) concentration in the effluent (b), SVI_5 (□) and SVI_{30} (■) (c), and SVI_{30}/SVI_5 (◇) ratio (d). Oleate concentration in the feed (—).

The sludge exhibited good settling ability properties with values of SVI_5 and SVI_{30} below 35 mL g^{-1} by day 120 (Figure 6.5c). SVI values reached 50 and 40 mL g^{-1} for SVI_5 and SVI_{30}, respectively, when sludge was exposed to the highest oleate concentration. Although the SVI values were still quite low, a deterioration in the sludge settling ability was confirmed as the SVI_{30}/SVI_5 ratio decreased considerably, indicating a decrease in the terminal settling velocity of the granules (Figure 6.5d).

6.3.3. Distribution and morphology of aerobic granular sludge

The morphological changes of AGS due to the increase in oleate concentration were evaluated by QIA. Before the addition of oleate, both $\%Nb_{Gc1}$ and $\%Nb_{Gc2}$ represented 70% of the AGS (i.e., Deq < 1000 µm), while $\%Nb_{Gc3}$ accounted for the remaining 30% of granules (Deq ≥ 1000 µm) (Figure 6.6a). The granules distribution changed when AGS was exposed to the highest concentration of oleate. On day 122, the prevalence of granules with Deq < 1000 µm decreased to 25% and granules with Deq ≥ 1000 µm became predominant in the system. The $TN_{granules}$/Vol decreased considerably from day 112, consistent with the biomass washout observed during this period (Figure 6.6b). In addition, the overall granules Deq (Deq_{ovr}) increased considerably from 802 ± 31 µm (at day 80) to 2006 ± 234 µm (at day 147), indicating that larger granules were able to endure in the system (Figure 6.6b). The estimated granules SA:V decreased during reactor operation, which can be attributed to a decrease in the total number of granules and an increase in granules size (Figure 6.6c).

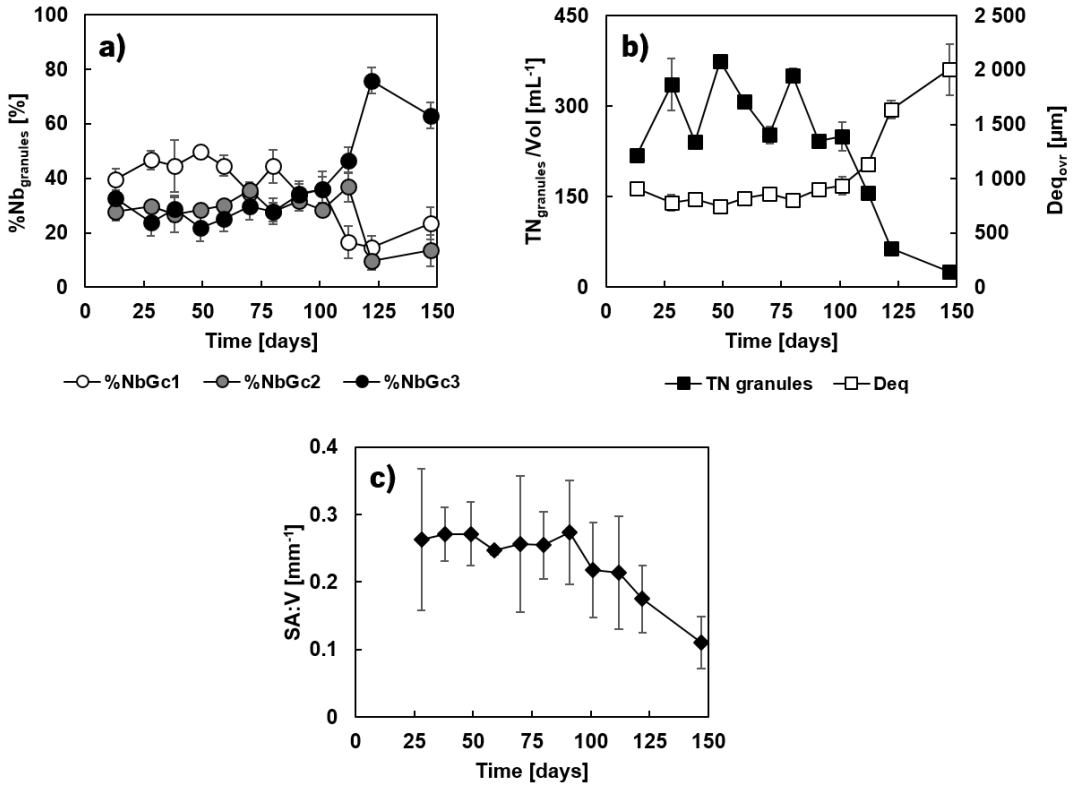


Figure 6.6 – AGS profile during SBR operation: $\%NB_{Gc1}$ (-○-), $\%NB_{Gc2}$ (-●-), and $\%NB_{Gc3}$ (-●-) (a), $TN_{granules}$/Vol (-■-) and Deq_{ovr} (-□-) (b), and SA:V (-◆-) ratio (c).

The AGS morphology was observed while they were exposed to an increasing concentration of oleate. The morphological parameter convexity describes the smoothness of the granule boundary. The convexity values of the overall granules ($Conv_{ovr}$) were stable throughout the process and remained above 0.9 (Figure 6.7a). However, on day 147, the $Conv_{ovr}$ value decreased to 0.75 when the process became unstable due to AGS exposure to oleate. The granules were surrounded by protruding filaments that increased the roughness of the boundaries and consequently decreased the $Conv_{ovr}$ values (Figure 6.7b).

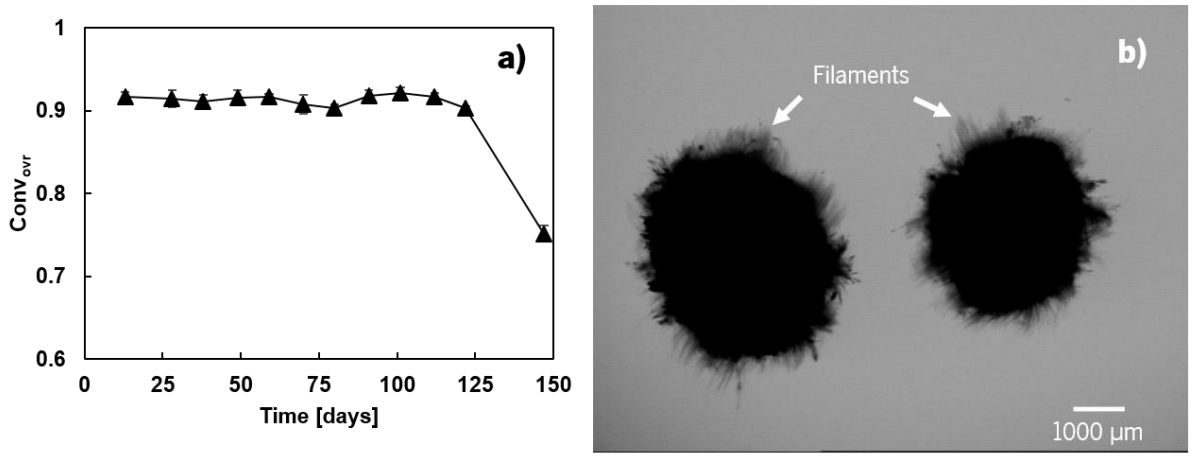


Figure 6.7 – The $Conv_{ovr}$ (—▲—) of AGS during the SBR operation (a), and image of granules with protruding filaments at day 147 with 15x magnification (b).

A PCA was accomplished to compute the scores and loadings for each principal component (PC), showing how the sample points are related and how much each variable affects the PC (Figure 6.8). The two most significant PC (PC1 and PC2) explained 91.3% of the dataset variance. Three main clusters obtained were related to the variation in AGS morphology and operational parameters caused by the increase oleate concentration throughout the reactor's operation (Figure 6.8a). The first cluster (C1), located at the top left quadrant, with negative scores in PC1 and positive scores in PC2, incorporates the initial 80 days of reactor operation subjected to oleate concentration up to 35 mg L^{-1}. The second (C2) cluster, located at the left bottom quadrant with negative scores in PC1 and PC2, encompassed the reactor operation subjected to oleate concentration from 48.1 to 61.3 mg L^{-1}. The third (C3) cluster, located in the bottom right quadrant, with positive scores in PC1 and negative scores in PC2, encompassed day 112 and day 122 exposed to an oleate concentration of 87.5 mg L^{-1} to 113.8 mg L^{-1}, respectively. The lasting

observation (i.e. day 147), located in the top right quadrant with positive scores in both PC1 and PC2, was the last operational day exposed to an oleate concentration of 113.8 mg L^{-1}.

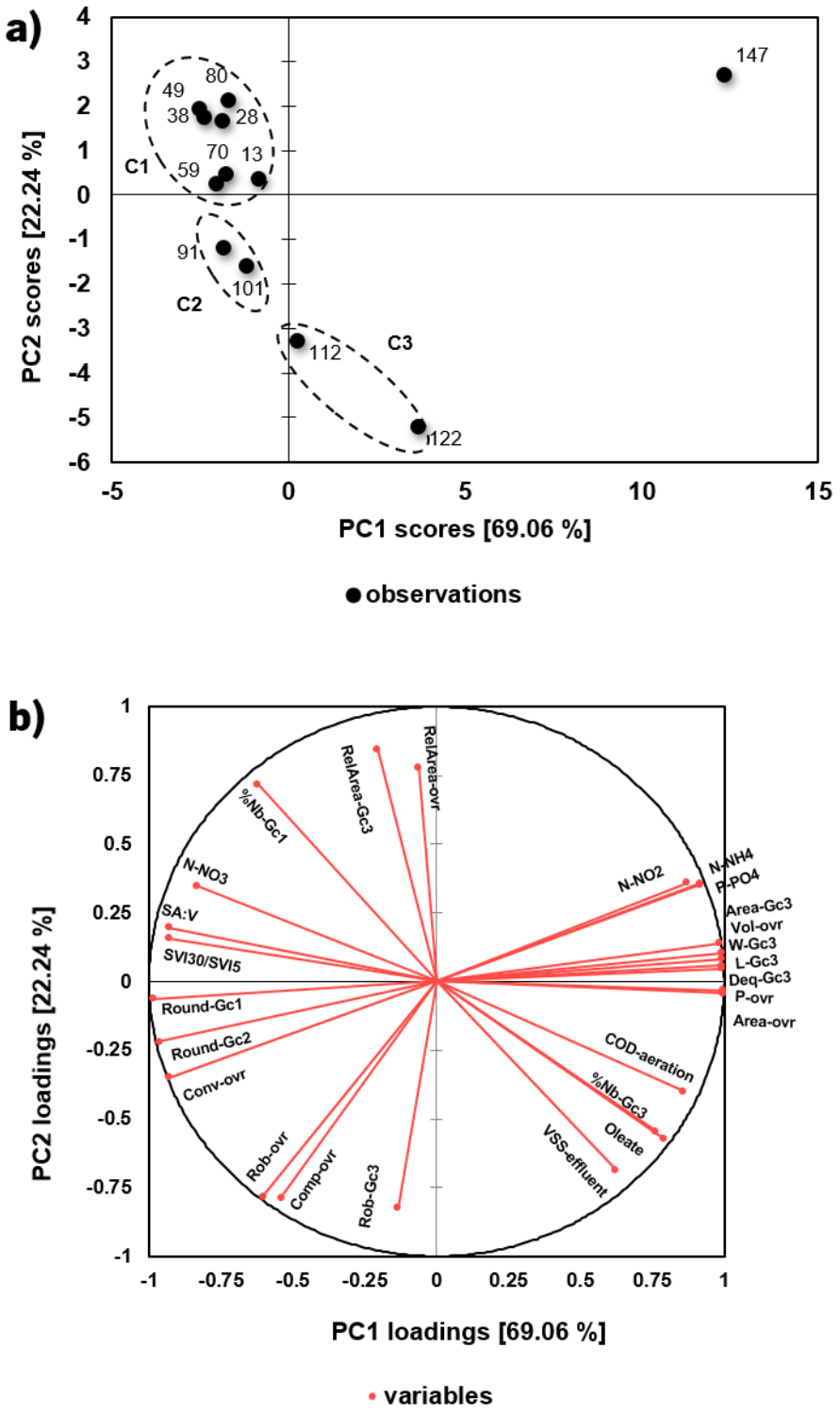


Figure 6.8 – PCA of the dataset: scores (a) and loadings (b) plots of PC1 vs PC2.

PC2 allowed to distinguish C1 from C2, whereas PC1 allowed to discriminate C1 and C2 from C3 and the remaining observation (day 147). The C2 cluster is negatively influenced by the morphological changes in the overall AGS robustness (Rob_{ovr}) and compactness ($Comp_{ovr}$) (Figure 6.8b). The C3 cluster was positively impacted by the concentrations of $VSS_{effluent}$, oleate, $COD_{aeration}$, and contents in large granules ($\%Nb_{Gc3}$). The observation of day 147 was positively influenced by the morphology of the overall and large granules and increasing effluent $N\text{-}NO_{2}^{-}$, $N\text{-}NH_{4}^{+}$, and $P\text{-}PO_{4}^{-3}$ concentrations (Figure 6.8b).

6.4. DISCUSSION

Oleate had an obvious negative effect on anaerobic uptake of soluble COD, but not on removal efficiency, since most soluble COD could be degraded during the aeration phase (Figure 6.2b). Since the reactor feed was static, the accumulation of oleate in the settled sludge bed possibly led to substrate limitation, which reduced the anaerobic uptake of soluble COD. Oleate accumulation in the reactor (solid and liquid fractions) was detected when a concentration of circa 60 mg L^{-1} was added to the feed (Figure 6.2a). At oleate concentrations above 60 mg L^{-1}, the $VSS_{effluent}$ increased considerably, resulting in a lower sludge retention time.

The presence of a high COD concentration during the aeration phase had a negative effect on the efficiency of phosphate removal. Recent work with AGS has shown that incomplete uptake of readily biodegradable COD during anaerobic periods reduces aerobic phosphate uptake rates (Haaksman et al., 2020). Phosphate release into the medium was observed immediately after aeration began, and phosphate uptake occurred after most of the soluble COD had been consumed (Figure 6.3ab). Phosphate release during aeration eventually reduced the subsequent uptake rate, resulting in an increase in effluent concentrations and a deterioration in removal efficiency (Figure 6.2c). In biological phosphorus removal processes, the simultaneous presence of acetate and oxygen results in the release of phosphate from the sludge and uptake is limited by the polyhydroxybutyrate (PHB) and poly-P content of the cells (Brdjanovic et al., 1998).

Stable ammonium removal was observed during most of the reactor operation. However, at the highest oleate concentration, ammonium-oxidizing bacteria (AOB) and nitrite-oxidizing bacteria (NOB) were somewhat affected at oleate concentrations of 113.8 ± 3.8 mg L^{-1}, resulting in a 20% decrease in ammonium removal and residual nitrite concentration in the effluent (< 1 mg L^{-1}). Quoc et al. 2021 found that small granules (331μm) had a higher ammonium oxidation rate than larger granules. In our work,

the size distribution of AGS showed that the percentage of small granules (i.e., with Deq < 1000 μm) decreased considerably and was dominated by granules with Deq ≥ 1000 μm at higher oleate concentrations (Figure 6.6a). Simultaneous nitrification/denitrification (SND) was achieved in the system as the nitrate concentration in the effluent decreased without ammonium or nitrite accumulation (Figure 6.4a). Nitrogen removal is favoured by the decrease in oxygen concentration (Mosquera-Corral et al., 2005). The size of the granules increased considerably at higher oleate concentration, limiting oxygen diffusion to the inner layers of the granules where denitrifying organism are present (Franca et al., 2018; Winkler et al., 2013). Also oleate accumulation in the reactor could restrict the oxygen diffusion, thus promoting nitrate degradation by denitrifiers (Figure 6.4b).

As mentioned previously, at oleate concentration above 60 mg L^{-1}, sludge washout was observed, concomitant to the decrease in the total number of granules shown through QIA. However, sludge washout has predominantly consisted of small granules (Deq < 1000 μm), while larger granules could endure in the system. The specific surface area of AGS decreased as small granules were washed out, and the granule's average size increased in the reactor. Oleate adsorption was limited owing to the size increase of granules, resulting in a decrease in $VSS_{effluent}$ at the end of the reactor operation (Figure 6.5b). Although the granules in the SBR were larger at higher oleate concentrations, the sludge settling ability declined. At the highest oleate concentration, the $Conv_{ovr}$ showed a deterioration of the granule structure. This fact was due to protruding filamentous bacteria around the granules induced by the presence of soluble COD during the aeration phase and the reduction of phosphate removal, which was shown to favour the filamentous growth on the granule's surface (Haaksman et al., 2020).

PCA has already been used to identify several disturbances in anaerobic bioreactors by combining morphological and operational data (Costa et al., 2010). Here, PCA allowed elucidating the influence of oleate on the morphology of AGS and the reactor performance parameters. Three main clusters associated with the different reactor operational periods were exposed to distinct oleate concentrations (Figure 6.8a). Cluster C1 encompassed the initial observations from the reactor operation with oleate addition up to 35.0 ± 1.2 mg L^{-1}; thus, it is possible to infer that the stability of AGS was not impacted during this period. The distinction between clusters C1 and C2 reflected mostly AGS morphological changes (Rob_{ovr} and $Comp_{ovr}$), driven by the increase in oleate concentration up to 87.5 ± 2.9 mg L^{-1}. Oleate had a clear impact on the size distribution of AGS since it was inversely proportional to the percentage of small granules ($\%Nb_{Gc1}$) and directly proportional to the percentage of large granules ($\%Nb_{Gc3}$) (Figure 6.8b). Also, the oleate concentration was directly proportional to the increase in $VSS_{effluent}$

and $COD_{aeration}$ concentrations. The distinction between C2 and C3 mainly reflected the changes in these parameters (Figure 6.8ab). In contrast, the distinction between C3 and the final observation was mainly related to the morphological changes of the AGS, and to some extent, to the increase of $N\text{-}NO_2^-$, $N\text{-}NH_4^+$, and $P\text{-}PO_4^{3-}$ concentrations in the effluent. The $Conv_{ovr}$ and the roundness of smaller granules ($Round_{Gc1}$ and $Round_{Gc2}$) were inversely proportional to the nutrients concentrations in the effluent, meaning that the reactor decreasing performance was concomitant to the morphological changes of granular sludge. Hence, the PCA result clearly demonstrated the influence of oleate concentration on the morphology and stability of aerobic granules, which are associated with decreasing reactor performance.

6.5. CONCLUSIONS

Treatment of oleate-containing wastewater by AGS in an SBR was possible at oleate concentrations below 60 mg L^{-1}. Higher oleate concentrations had a negative effect on SBR performance due to the accumulation of oleate in the reactor. Adsorption of oleate had a negative effect on anaerobic COD consumption, resulting in a decrease in phosphate removal. Granules with Deq < 1000 µm were selectively removed from the systems due to their larger specific surface area, while larger granules remained in the system. The ammonium removal efficiency was also affected but remained above 80%. Furthermore, TIN removal efficiency increased due to the higher denitrification capacity of large granules. While AGS maintained a good settling capacity (< 50 mL g^{-1}), the SVI_{30}/SVI_5 ratio decreased due to the appearance of protruding filamentous bacteria on the surface of the granules. Ensuring anaerobic COD uptake and limiting oleate adsorption appeared to be key factors in maintaining AGS stability and reactor performance in the presence of oleate-containing wastewaters. In this sense, the impact of oleate adsorption onto AGS could be limited through the selective use of large granules (i.e., Deq ≥ 2000 µm), preventing sludge washout and maintaining nutrient removal efficiencies.

6.6. REFERENCES

Alves, M.M., Pereira, M.A., Sousa, D.Z., Cavaleiro, A.J., Picavet, M., Smidt, H., Stams, A.J.M., 2009. Waste lipids to energy: How to optimize methane production from long-chain fatty acids (LCFA). Microb. Biotechnol. 2, 538–550. https://doi.org/10.1111/j.1751-7915.2009.00100.x

Amaral, A.L.P., 2003. Image analysis in biotechnological processes: applications to wastewater treatment. PhD thesis, University of Minho. http://hdl.handle.net/1822/4506.

Amorim, C.L., Moreira, I.S., Ribeiro, A.R., Santos, L.H.M.L.M., Delerue-Matos, C., Tiritan, M.E., Castro, P.M.L.,

2016. Treatment of a simulated wastewater amended with a chiral pharmaceuticals mixture by an aerobic granular sludge sequencing batch reactor. Int. Biodeterior. Biodegrad. 115, 277–285. https://doi.org/10.1016/j.ibiod.2016.09.009

APHA, 2005. Standard Methods for the Examination of Water & Wastewater 21st Edition, American Public Health Association, American Water Works Association, Water Environment Federation.

Bengtsson, S., de Blois, M., Wilén, B., Gustavsson, D., 2019. A comparison of aerobic granular sludge with conventional and compact biological treatment technologies. Environ. Technol. 40, 2769–2778. https://doi.org/10.1080/09593330.2018.1452985

Brdjanovic, D., Slamet, A., Van Loosdrecht, M.C.M., Hooijmans, C.M., Alaerts, G.J., Heijnen, J.J., 1998. Impact of excessive aeration on biological phosphorus removal from wastewater. Water Res. 32, 200–208. https://doi.org/10.1016/S0043-1354(97)00183-8

Cai, F., Lei, L., Li, Y., Chen, Y., 2021. A review of aerobic granular sludge (AGS) treating recalcitrant wastewater: Refractory organics removal mechanism, application and prospect. Sci. Total Environ. 782, 146852. https://doi.org/10.1016/j.scitotenv.2021.146852

Campo, R., Di Bella, G., 2019. Petrochemical slop wastewater treatment by means of aerobic granular sludge: effect of granulation process on bio-adsorption and hydrocarbons removal. Chem. Eng. J. 378, 122083. https://doi.org/10.1016/j.cej.2019.122083

Carrera, P., Casero-Díaz, T., Castro-Barros, C.M., Méndez, R., Val del Río, A., Mosquera-Corral, A., 2021. Features of aerobic granular sludge formation treating fluctuating industrial saline wastewater at pilot scale. J. Environ. Manage. 296. https://doi.org/10.1016/j.jenvman.2021.113135

Chen, J.L., Ortiz, R., Steele, T.W.J., Stuckey, D.C., 2014. Toxicants inhibiting anaerobic digestion: A review. Biotechnol. Adv. 32, 1523–1534. https://doi.org/10.1016/j.biotechadv.2014.10.005

Costa, J.C., Alves, M.M., Ferreira, E.C., 2010. A chemometric tool to monitor high-rate anaerobic granular sludge reactors during load and toxic disturbances. Biochem. Eng. J. 53, 38–43. https://doi.org/10.1016/j.bej.2008.12.006

de Kreuk, M.K., Kishida, N., van Loosdrecht, M.C.M., 2007. Aerobic granular sludge - State of the art. Water Sci. Technol. 55, 75–81. https://doi.org/10.2166/wst.2007.244

Dueholm, T.E., Andreasen, K.H., Nielsen, P.H., 2001. Transformation of lipids in activated sludge. Water Sci. Technol. 43, 165–172. https://doi.org/10.2166/wst.2001.0040

Forster, C.F., 2007. Oils, fats and greases in wastewater treatment. J. Chem. Technol. Biotechnol. 55, 402–404. https://doi.org/10.1002/jctb.280550420

Franca, R.D.G., Pinheiro, H.M., van Loosdrecht, M.C.M., Lourenço, N.D., 2018. Stability of aerobic granules during long-term bioreactor operation. Biotechnol. Adv. 36, 228–246. https://doi.org/10.1016/j.biotechadv.2017.11.005

Haaksman, V.A., Mirghorayshi, M., van Loosdrecht, M.C.M., Pronk, M., 2020. Impact of aerobic availability of readily biodegradable COD on morphological stability of aerobic granular sludge. Water Res. 187, 116402. https://doi.org/10.1016/j.watres.2020.116402

Holohan, B.C., Duarte, M.S., Szabo-Corbacho, M.A., Cavaleiro, A.J., Salvador, A.F., Pereira, M.A., Ziels, R.M., Frijters, C.T.M.J., Pacheco-Ruiz, S., Carballa, M., Sousa, D.Z., Stams, A.J.M., O'Flaherty, V., van Lier, J.B., Alves, M.M., 2022. Principles, Advances, and Perspectives of Anaerobic Digestion of Lipids. Environ. Sci. Technol. 56, 4749–4775. https://doi.org/10.1021/acs.est.1c08722

Lin, H., Ma, R., Hu, Y., Lin, J., Sun, S., Jiang, J., Li, T., Liao, Q., Luo, J., 2020. Reviewing bottlenecks in aerobic granular sludge technology : Slow granulation and low granular stability. Environ. Pollut. 263, 114638.

https://doi.org/10.1016/j.envpol.2020.114638

Long, J.H., Aziz, T.N., Reyes, F.L.D.L., Ducoste, J.J., 2012. Anaerobic co-digestion of fat, oil, and grease (FOG): A review of gas production and process limitations. Process Saf. Environ. Prot. 90, 231–245. https://doi.org/10.1016/j.psep.2011.10.001

Mosquera-Corral, A., De Kreuk, M.K., Heijnen, J.J., Van Loosdrecht, M.C.M., 2005. Effects of oxygen concentration on N-removal in an aerobic granular sludge reactor. Water Res. 39, 2676–2686. https://doi.org/10.1016/j.watres.2005.04.065

Neves, L., Pereira, M.A., Mota, M., Alves, M.M., 2009. Detection and quantification of long chain fatty acids in liquid and solid samples and its relevance to understand anaerobic digestion of lipids. Bioresour. Technol. 100, 91–96. https://doi.org/10.1016/j.biortech.2008.06.018

Pereira, M.A., Pires, O.C., Mota, M., Alves, M.M., 2005. Anaerobic biodegradation of oleic and palmitic acids: Evidence of mass transfer limitations caused by long chain fatty acid accumulation onto the anaerobic sludge. Biotechnol. Bioeng. 92, 15–23. https://doi.org/10.1002/bit.20548

Quéméneur, M., Marty, Y., 1994. Fatty acids and sterols in domestic wastewaters. Water Res. 28, 1217–1226. https://doi.org/10.1016/0043-1354(94)90210-0

Quoc, B.N., Wei, S., Armenta, M., Bucher, R., Sukapanpotharam, P., Stahl, D.A., Stensel, H.D., Winkler, M.K.H., 2021. Aerobic granular sludge: Impact of size distribution on nitrification capacity. Water Res. 188, 116445. https://doi.org/10.1016/j.watres.2020.116445

Rossetti, S., Tomei, M.C., Nielsen, P.H., Tandoi, V., 2005. " Microthrix parvicella ", a filamentous bacterium causing bulking and foaming in activated sludge systems: a review of current knowledge. FEMS Microbiol. Rev. 29, 49–64. https://doi.org/10.1016/j.femsre.2004.09.005

Sarvajith, M., Reddy, G.K.K., Nancharaiah, Y.V., 2018. Textile dye biodecolourization and ammonium removal over nitrite in aerobic granular sludge sequencing batch reactors. J. Hazard. Mater. 342, 536–543. https://doi.org/10.1016/j.jhazmat.2017.08.064

Singh, S., Rinta-Kanto, J.M., Kettunen, R., Tolvanen, H., Lens, P., Collins, G., Kokko, M., Rintala, J., 2019. Anaerobic treatment of LCFA-containing synthetic dairy wastewater at 20 °C: Process performance and microbial community dynamics. Sci. Total Environ. 691, 960–968. https://doi.org/10.1016/j.scitotenv.2019.07.136

Vashi, H., Iorhemen, O.T., Tay, J.H., 2019. Extensive studies on the treatment of pulp mill wastewater using aerobic granular sludge (AGS) technology. Chem. Eng. J. 359, 1175–1194. https://doi.org/10.1016/j.cej.2018.11.060

Viswanathan, C. V, Bai, B.M., Pillai, S.C., 1962. Fatty Matter in Aerobic and Anaerobic Sewage Sludges. J. Water Pollut. Control Fed. 34, 189–194.

Williams, J.B., Clarkson, C., Mant, C., Drinkwater, A., May, E., 2012. Fat , oil and grease deposits in sewers : Characterisation of deposits and formation mechanisms. Water Res. 46, 6319–6328. https://doi.org/10.1016/j.watres.2012.09.002

Winkler, M.K.H., Kleerebezem, R., De Bruin, L.M.M., Verheijen, P.J.T., Abbas, B., Habermacher, J., Van Loosdrecht, M.C.M., 2013. Microbial diversity differences within aerobic granular sludge and activated sludge flocs. Appl. Microbiol. Biotechnol. 97, 7447–7458. https://doi.org/10.1007/s00253-012-4472-7

CHAPTER 7

GENERAL CONCLUSION AND SUGGESTION FOR FUTURE WORKS

7.1. GENERAL CONCLUSION

Aerobic granular sludge (AGS) technology has the potential to replace conventional activated sludge (AS) systems. However, long granulation periods and granules instability are critical issues of AGS technology. Monitoring the dynamic biomass changes under defined operating conditions is fundamental to increase the knowledge about the granulation rates and stability of the aerobic granules. For that purpose, quantitative image analysis (QIA) methods were applied to remove the subjectivity of morphological and structural changes from flocs to granules, providing objective and quantitative research on the formation and stability of aerobic granules in bioreactors. The work presented in this thesis contributed to a better understanding of the morphological changes from flocs to granules and their activity for carbon, nitrogen and phosphorus removal and stability occurring under several operational conditions.

Aerobic granules formation was successfully achieved in a sequencing batch reactor (SBR) with a height to diameter (H/D) ratio of 2 (Chapter 3 and Chapter 4). Under the conditions tested, the granulation rate depended on the substrate concentration and the minimal imposed sludge settling velocity (Chapter 3). The morphology (solidity, eccentricity, and convexity) of early granules (≤ 650 μm) reflected the degree of sludge aggregation and could be used as indicators to anticipate process instability. Also, a comprehensive relationship between biological nutrient removal and sludge morphology could be established (Chapter 4). Chemical oxygen demand (COD)-to-nitrogen ratio (COD/N) determined the granulation rate and granules morphology. Nutrient removal efficiencies decreased during the formation of early granules, owing to the washout of slow settling floccular sludge. Poor nitrogen removal efficiencies during sludge washout and the development of early granules favoured the growth of viscous bulking and filamentous bacteria. The recovery of ammonium-oxidizing bacteria (AOB) activity followed the establishment of small granules (≤ 600 μm), while nitrite-oxidizing bacteria (NOB) and phosphate accumulating organisms (PAO) activity correlated with the transition to large granules (≥ 1000 μm). Bioactive granules with nutrient removal capabilities as bioaugmenting microbial consortia were successfully applied to recover the nutrients removal capability of AGS systems (Chapter 5). While complete nitrification could be achieved after bioaugmentation, the establishment of effective phosphate

removal was contingent on the morphological similarity between the innate and bioactive granules. Granular structure instability is a bottleneck of AGS systems, limiting the widespread use of aerobic granules. Oleate, a long-chain fatty acid (LCFA) commonly found in wastewaters, was detrimental to the stability and morphology of AGS at concentrations above 60 mg L^{-1} (Chapter 6). Small granules (< 1000 µm) were selectively washed-out from the SBR due to oleate adsorption, while oleate accumulation in the reactor limited substrate and oxygen transfer to AGS, which impaired anaerobic COD uptake and phosphate removal efficiency.

The application of chemometrics tools was fundamental to extract important information from the datasets generated during this thesis. Principal component analysis (PCA) with the QIA data allowed to follow the granulation process and establish the granulation status over time (Chapter 3). Also, the correlation between AGS morphological and reactor performance parameters could be determined using PCA (Chapter 6). The PCA result clearly demonstrated the influence of oleate concentration on the morphology and stability of aerobic granules, which were associated with decreasing the reactor performance. The sludge morphological data were successfully used to predict the sludge settling properties (SVI_5 and SVI_{30}) by partial least square (PLS) regression, with a correlation coefficient of 0.964 and 0.842 for SVI_5 and SVI_{30}, respectively (Chapter 3). Additionally, morphological parameters belonging to the floccular and granular fractions were successfully used to construct PLS models, estimating the effluent quality in terms of phosphate (R^2 = 0.905), ammonium (R^2 = 0.901), nitrite (R^2 = 0.961) and nitrate (R^2 = 0.910) concentrations (Chapter 4).

Overall, aerobic granules formation and stability were successfully monitored using QIA data, which, with the help of PCA and PLS models, could be used for timely detection of potential problems, underlining the potential of QIA to monitor and control AGS systems.

7.2. SUGGESTION FOR FUTURE WORKS

The work described in this thesis underlined the importance of monitoring the morphological change in AGS systems to predict granulation rate and granule stability under defined conditions, thus offering the possibility to improve process control. Consequently, further QIA studies should be performed to collect precise and quantitative morphological information about the rates and morphology of AGS under different operating conditions (i.e., reactors geometry and operating mode, organic and nutrients loads, and substrate type (simple or complex)). Furthermore, reactor performance relies on the establishment of an

efficient microbial community within AGS, influencing granular structure and stability. Thus, additional studies should also evaluate the relationship between the main microbial species with the morphology, structure, and distribution of flocs, filaments and granules in the AGS system.

QIA studies should also be performed in both pilot-scale and full-scale systems to validate the adequateness of the proposed morphological parameters to monitor the granulation and stability of AGS. Furthermore, with the current technological advances in image quality and computational power, optimizing QIA methodologies and developing an online image acquisition system would decrease the time and effort in QIA procedures. The application of QIA data in the development of data-driven decision-making would be of utmost importance in real-case scenarios since the operation of AGS bioreactors demands a complex automation system and specialized operators for decision-making in a full-scale system.

SCIENTIFIC OUTPUTS

Papers in journals with peer review:

1. Silva, S.A., Val del Río, A., Amaral, A.L., Ferreira, E.C., Alves, M.M., Mesquita, D.P. (2022) Monitoring morphological changes from activated sludge to aerobic granular sludge under distinct organic loading rates and increasing minimal imposed sludge settling velocities through quantitative image analysis. Chemosphere 286. https://doi.org/10.1016/j.chemosphere.2021.131637

Papers in preparation for submission to peer reviewed journals:

1. Characterization of aerobic granular sludge formation under washout dynamics through quantitative image analysis: The influence of COD/N.
2. Improving nutrient removal efficiencies of aerobic granular sludge by bioaugmentation with bioactive granules: Accessing the impact on the granules' morphology through quantitative image analysis.
3. The effect of LCFA on the performance and stability of aerobic granular sludge in a sequencing batch reactor.

Abstracts and posters in conferences

1. Silva, S.A., Val del Rio, A., Alves, M.M., Mesquita, D.P. (2019) Monitoring morphological changes of suspended sludge during aerobic granulation process. MicroBiotec 19 - Congress of Microbiology and Biotechnology 2019 (Book of Abstracts). No. P80, Coimbra, Portugal, Dec 5-7, 144.

ANNEXE

Table A1 – QIA parameters determined from each sludge fraction

Descriptor group	Parameter Abbreviation	Description	Units (BFM)	Units (STM)
Size[a]	Deq_i	Equivalent diameter of aggregates[b]	(µm)	(µm)
	P_i	Perimeter of aggregates[b]	(µm)	(µm)
	L_i	Length of aggregates[b]	(µm)	(µm)
	W_i	Width of aggregates[b]	(µm)	(µm)
	$Area_i$	Area of aggregates[b]	($µm^2$)	(mm^2)
	Vol_i	Volume of granules[c]	-	(mm^3)
Shape[a]	FF_i	Form factor of aggregates[b]	-	-
	$Conv_i$	Convexity of aggregates[b]	-	-
	$Comp_i$	Compactness of aggregates[b]	-	-
	$Round_i$	Roundness of aggregates[b]	-	-
	Sol_i	Solidity of aggregates[b]	-	-
	Ext_i	Extent of aggregates[b]	-	-
	Ecc_i	Eccentricity of aggregates[b]	-	-
	Rob_i	Robustness of aggregates[b]	-	-
	$LrgC_i$	Largest concavity of aggregates[b]	-	-
	$RelArea_i$	Ratio between hole and object area of aggregates[b]	-	-
Contents	Nb_i/Vol	Number of aggregates per volume[b]	($µL^{-1}$)	(mL^{-1})
	$Area_i/Vol$	Area of aggregates per volume[b]	(mm^2 $µL^{-1}$)	(mm^2 mL^{-1})
	$\%Nb_i$	Distribution by number of aggregates[b]	(%)	(%)
	$\%Area_i$	Distribution by Area of aggregates[b]	(%)	(%)
	TNb/Vol	Total Number of aggregates per volume[b]	($µL^{-1}$)	(mL^{-1})
	TA/Vol	Total Area of aggregates per volume[b]	(mm^2 $µL^{-1}$)	(mm^2 mL^{-1})
	TV/Vol	Total Volume of granules per volume[c]	-	(mm^3 mL^{-1})
Free and protruding filaments	TL/Vol	Total filament length per volume[d]	(mm $µL^{-1}$)	-
	Nb_{fil}/Vol	Number of filaments per volume[d]	($µL^{-1}$)	-
	Nb_{int}/Vol	Number of intersections per volume[d]	($µL^{-1}$)	-
	TL/TA_{Flocs}	Total filament length per total area of flocs[d]	(mm^{-1})	-

(a) – Parameters determined for each "i" size class and overall aggregates; (b) – parameter determined from the floccular and granular fraction separately; (c) – parameter determined solely from the granular faction; (d) – parameter determined from floccular fraction for the protruding and free filaments quantification; (e) – parameters units from bright-field microscopy (BFM) and stereomicroscopy (STM) methodologies; Information about the calculation of these parameters can be found in (Amaral, 2003).